European Journal of Technical and Natural Sciences

№ 4–5 2021

PREMIER Publishing

Vienna
2021

European Journal of Technical and Natural Sciences

Scientific journal

№ 4–5 2021

ISSN 2414-2352

Proofreading Kristin Theissen

Cover design Andreas Vogel

Additional design Stephan Friedman

Editorial office Premier Publishing s.r.o. Praha 8 – Karlín, Lyčkovo nám. 508/7, PSČ 18600

E-mail: pub@ppublishing.org

Homepage: ppublishing.org

European Journal of Technical and Natural Sciences is an international, German/English/Russian language, peer-reviewed journal. It is published bimonthly with circulation of 1000 copies.

The decisive criterion for accepting a manuscript for publication is scientific quality. All research articles published in this journal have undergone a rigorous peer review. Based on initial screening by the editors, each paper is anonymized and reviewed by at least two anonymous referees. Recommending the articles for publishing, the reviewers confirm that in their opinion the submitted article contains important or new scientific results.

Premier Publishing s.r.o. is not responsible for the stylistic content of the article. The responsibility for the stylistic content lies on an author of an article.

Instructions for authors

Full instructions for manuscript preparation and submission can be found through the Premier Publishing s.r.o. home page at: http://www. ppublishing.org

Material disclaimer

The opinions expressed in the conference proceedings do not necessarily reflect those of the Premier Publishing s.r.o., the editor, the editorial board, or the organization to which the authors are affiliated.

Premier Publishing s.r.o. is not responsible for the stylistic content of the article. The responsibility for the stylistic content lies on an author of an article.

Included to the open access repositories:

The jurnal has Index Copernicus Value (ICV) 80.97 for 2018.

Typeset in Berling by Ziegler Buchdruckerei, Linz, Austria.
Printed by Premier Publishing s.r.o., Vienna, Austria on acid-free paper.

Section 1. Information technology

https://doi.org/10.29013/EJTNS-21-4.5-3-12

Zijie Liu,
RDF International School, Shenzhen, Guangdong, China
E-mail: jenniferliuzijie@gmail.com

ROBOTIC GESTURE RECOGNITION USING MACHINE LEARNING AND ARTIFICIAL INTELLIGENCE

Abstract. To improve overall accuracy and efficiency of surgery, demand of using robotic arms with sensors attached has increased significantly. Since error-tolerant rate of surgeries is extremely low, robotic arms can provide increased flexibility and accuracy. Many current surgical robotics arms use machine learning algorithms to make predictions. Subtle deviations in surgery may have unintended consequences. Compared to machine learning models, Artificial Neural Networks provides higher prediction accuracy. In this paper, the usage of Artificial Neural networks to increase predictive power of robotic gesture recognition is explored. Six machine learning models are used as a benchmark and applied to a robotic arm with 8 sensors attached. Their performances are evaluated. Artificial Neural Networks are applied to the same dataset and give higher accuracies than all of the machine learning models. This study highlights the utilization of neural networks in robotic arms and its potential development in the future.

Keywords: Robotics, sensors, machine learning, artificial intelligence, supervised learning.

1. Introduction

Along with the rapid development of computer technology, human-computer interaction has become more prevalent [1]. Robotics have already been used skillfully in factories, space exploration, agriculture and underwater exploration [2]. The term "robot" was first used in the early 20th century. Many decades later, the concept of robots in surgery has been widely applied due to the emergence of virtual reality and telepresence technologies. Despite its brief history in surgery, robotic technology has already shown its capabilities in terms of reduced downtime, better dexterity, and more accurate results. Currently, the main system used in surgery is the Da Vinci by Intuitive Surgical [3]. The da Vinci surgical system is a robotic-assist system that enables a surgeon to perform complex procedures using a small incision. The surgeon uses a console to control the robot arm [4]. To ensure the surgery is successful, increasing its command execution accuracy is a high priority goal. This project aims to increase the accuracies of segmenting a sequence of surgical procedures into a set of gestures, such as a positioning needle and an orientation needle [5].

The use of robotic tools during surgery enables surgeons to perform complex tasks with ease. They can also reduce the number of instruments needed for the procedures by using the robotic tools' portability and ease of use [6]. However, the primary drawbacks of such robotic systems are their heavy

weight, high cost, and inability to reconfigure to meet the demands of individual patients [7]. Even though deep-learning algorithms have produced excellent results and, in some cases, exceeded human skills, the creation of robotic system intelligence to a human level is currently infeasible owing to the difficulty of building one [8].

Machine learning was used to evaluate surgeon performance in robot-assisted minimally invasive surgery in a paper presented at the 2016 World Congress on Engineering and Computer Science. In this study, six essential movement features, namely completion time, path length, depth perception, speed, smoothness, and curvature-were evaluated. Expert and rookie surgeons are distinguished using machine learning algorithms. According to reports, the experimental evaluation method correctly evaluated surgical abilities in about 85 percent of trials [9; 10].

In order to achieve a higher prediction accuracy, there is another study that aims to offer a machine learning technique for analyzing automated performance measures (APMs) and predicting clinical outcomes of robot-assisted radical prostatectomy (RARP). Radical prostatectomy is a surgery that removes the prostate gland and tissues around it [11]. The study used APMs to train three machine learning algorithms directly from robot system data (training material) and hospital duration of stay (training label) (2 days and >2 days) from 78 RARP instances, and then chose the optimal algorithm. The data were classified as "Predicted as anticipated LOS (pExp-LOS)" and "Predicted as extended LOS (pExt-LOS)" using the chosen algorithm. As a result, the "Random Forest-50" (RF-50) algorithm performed best, predicting LOS (73 cases as "pExp-LOS" and 5 cases as "pExt-LOS") with an accuracy of 87.2 percent [12].

Recently, neural networks are gradually being applied on a much wider scale. In fact, deep neural networks have been developed since the 1980s, but they gained scientists' attention and acceptance in recent years. The explosion of data on the internet combined with cloud computing resources allowed neural network models to outperform more "formally analyzable" approaches like kernel methods in prediction. One of the examples is ImageNet [13]. It is a vast collection of over 14 million annotated photos and it is designed for computer vision research [14; 15]. In 2020, the image classification on ImageNet has achieved an impressive accuracy: 91.12% [16].

In this paper, six machine learning algorithms are first applied to the muscle activity data obtained from Kaggle [23] and their prediction accuracies are evaluated. Then, to improve the accuracies, Artificial Neural Networks are applied on the same dataset and the resulted accuracy are compared to the former accuracies. This paper proposes that Artificial Neural Networks can build robotic gesture recognition models with higher accuracies than Machine learning models.

2. Methodology

2.1. The Dataset

The dataset that is used in this paper is created by Kirill Yashuk, on Kaggle [23]. They build a system that connects muscular activity (EMG – Electromyography) sensors to a user app. The app takes data, after which a server creates a Tensorflow model tailored to this user. The model may then be downloaded and run on the device to control motors or other attachments. With the aid of the App, four types of motion were captured from the MYO armband in this dataset. The MYO armband includes eight sensors on the skin surface, each of which detects the electrical activity produced by the muscles beneath it. After each gesture is held, the MYO armband records 8 consecutive readings of all 8 sensors. As a result, there are 64 columns of EMG data, with the last column representing a gesture made while the data was being recorded (classes 0–3). The gesture classes are: rock-0, scissors-1, paper-2 and ok-3. Rock, paper and scissors gestures are like the gestures performed in rock paper and scissors game, and the OK sign is made up of the index finger touching the thumb and the rest of the fingers stretched out. Table 1 show a sample of the data collected using the original dataset.

Table 1 Group 8 Sensor recordings subset for rock gesture (0)

sensor1	sensor2	sensor3	sensor4	sensor5	sensor6	sensor7	sensor8	
47	6	6	5	13	21	111	15	0
7	7	1	–8	7	21	114	48	0
–11	4	7	11	33	39	119	43	0
–35	–8	2	6	–13	–24	–112	–69	0
–2	–4	–3	0	–7	–7	1	2	1
–13	–8	1	1	–7	2	–5	–11	1
–10	3	3	1	15	10	0	–4	1
–9	–10	–4	–4	–8	0	2	15	1
–14	–2	–3	–4	–21	7	–8	–12	2
–5	–2	0	–4	–7	5	6	9	2
0	2	3	–8	19	20	0	–8	2
–2	16	6	9	1	31	16	4	2
–15	–6	–3	3	20	25	1	1	3
11	–4	–5	–4	3	–8	–7	–3	3
2	1	3	–1	1	9	4	4	3
–3	–1	–1	–3	0	–3	4	3	3

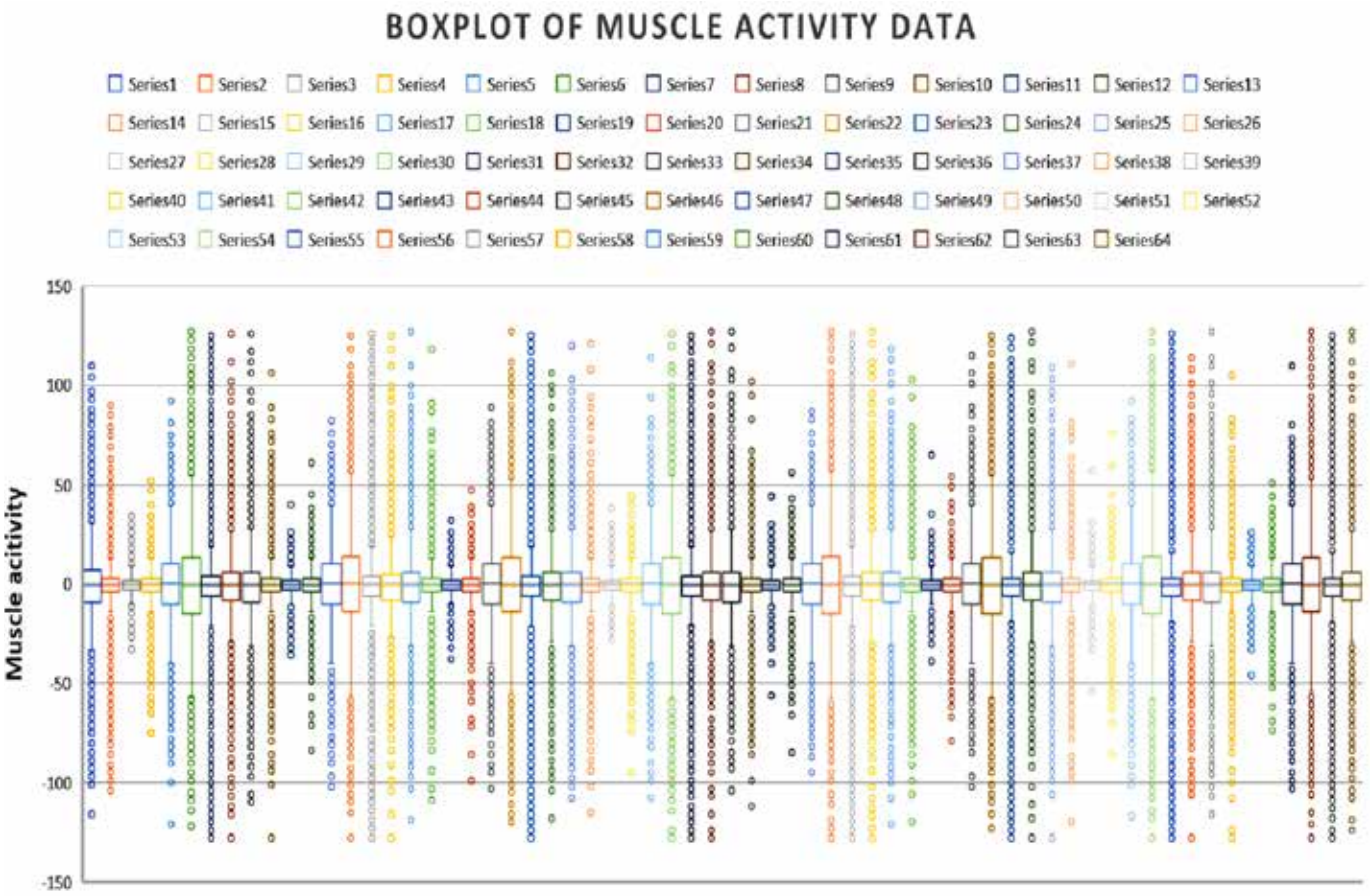

Figure 2. Boxplot of muscle activity data

Each motion was captured six times for a total of 20 seconds. Each time, the motion was previously planned and held when the recording began. While the motion was still being held, the recording comes to a halt. Each motion is kept in a fixed posture for a total of 120 seconds. In a short period of time, they are all recorded from the same right forearm. Every recording of a certain gesture class was compiled into a.csv file with a unique name (0–3) [17].

Figure 2 shows a boxplot of the muscular activity captured. There are 64 series in the boxplot of muscle activity data, which represents the 64 columns of the muscle activity dataset. The hollow circles represent the outliers in each sensor.

The range of muscle activity readings are from –128 to 127 and the means of muscle activity are around 0. From sensor 1 to sensor 8, the muscle activity of sensor 3 is the most compacted, with 50% of muscle activity data fall within –35 and 35. The muscle activity of sensor 6 are the most spread out, since the distance between its lower quartile and upper quartile are longer compared to other sensors.

2.2. Software tools

In terms of AI research, Google is extremely active. Google spent years developing TensorFlow, an AI framework, and Colaboratory, a development platform. TensorFlow is now open-source, and Google has made Colaboratory free to use since 2017. Google Colab, or just Colab, is the new name for Colaboratory [14]. On Google Colab, users may use Python to implement their programs. For machine learning engineers, this cloud-based platform offers several benefits. It is not viable to install expensive GPUs on personal computers in order to meet industrial requirements or execute time and memory intensive programs. While in Colab, each laptop has access to free GPU, regardless of whose personal computer is being used [15].

2.3. Feature selection

To determine the whether the 8 sensors have impact on 4 gestures (rock, paper, scissor and ok), a one-way Analysis of Variance (ANOVA) tests are conducted. In this test, 8 sensors are the independent variable and the hand gesture classes are the dependent variable.

The hypothesis is defined as:

H_0: *all sensors have equal variance.*

H_1: *At least one sensor is different.*

Then, the dataset is imported in SPSS to perform one-way ANOVA test. SPSS stands for Statistical Package for the Social Sciences and it can perform complex statistical data analysis. Table 3 shows the results from the ANOVA analysis.

Table 3.

ANOVA						
		Sum of Squares	**df**	**Mean Square**	**F**	**Sig.**
1	***2***	***3***	***4***	***5***	***6***	***7***
sensor 1	Between Groups	659.17	3	219.72	0.57	0.63
	Within Groups	11245302.42	29162	385.61		
	Total	11245961.60	29165			
sensor 2	Between Groups	68.05	3	22.68	0.16	0.92
	Within Groups	4144975.82	29162	142.14		
	Total	4145043.87	29165			
sensor 3	Between Groups	7.17	3	2.39	0.09	0.97
	Within Groups	806010.27	29162	27.64		
	Total	806017.45	29165			
sensor 4	Between Groups	33.28	3	11.09	0.17	0.92
	Within Groups	1943582.43	29162	66.65		

1	*2*	*3*	*4*	*5*	*6*	*7*
sensor 4	Within Groups	1943582.43	29162	66.65		
	Total	1943615.72	29165			
sensor 5	Between Groups	1302.44	3	434.15	1.48	0.22
	Within Groups	8570979.07	29162	293.91		
	Total	8572281.51	29165			
sensor 6	Between Groups	3363.11	3	1121.04	1.84	0.14
	Within Groups	17734083.01	29162	608.12		
	Total	17737446.12	29165			
sensor7	Between Groups	52429.58	3	17476.53	17.95	0.00
	Within Groups	28386444.97	29162	973.41		
	Total	28438874.56	29165			
sensor8	Between Groups	1288.82	3	429.61	1.44	0.23
	Within Groups	8725963.81	29162	299.22		
	Total	8727252.62	29165			

The total sum of squares is used in ANOVA test to indicate the entire variation that may be ascribed to multiple variables [21]. Based on the results of ANOVA test, F value needed to be calculated to accept or reject the Null Hypothesis. Even though sensor 7 is shown to be the most significant with the F value 17.95, for this work, all sensor data is used irrespective of the F value since robotic arms data uses all of these readings to decide classification.

2.4. ML Model Training and Testing

In the dataset, 10-fold cross validation is used to evaluate models' accuracy. The dataset is split into 10 parts, train on 7 and test on 3. *StratifiedKFold* is used here to ensure that each fold or split of the dataset will have the same distribution of examples by class as the entire training dataset. *random_state* is set to 1 make sure that it is the same splits of the training dataset when performing each algorithm. To train the dataset, six machine learning models are used for supervised learning, which are Linear Regression (LR), Linear Discriminant Analysis (LDA), K-nearest neighbors (KNN), Classification and Regression Trees (CART), Naive Bayes classifier (NB) and Support Vector Machine (SVM). Among these 6 models, the first two models (LR and LDA) are linear algorithms and the last 4 models (KNN, CART, NB and SVM) are non-linear models. Last, the metric of '*accuracy*' is used to evaluate the performance of the models [22].

Linear Regression is used to find the relationship between the 8 sensors that are given in the dataset and to make a best-fit line for predicting hand gesture classes. The hypothesis function for this model is defined as:

$$y = \theta_1 + \theta_2 \cdot x \qquad (1)$$

where x is the input muscle activity data, y predicts resulted hand gesture classes as a result of the best-fit line, θ_1 is the intercept of the best-fit line and θ_2 is the coefficient of x of the best-fit line.

Linear Discriminant Analysis classifies the dataset with two classes. The classification is done through reducing dimensions and visualizing data. Bayes Theorem is used in this model to make predictions, which use the probability of each class and the probability of data belonging to each class to predict the possible classes for the given input data:

$$P(Y = x \mid X = x) = \left[(Plk \cdot fk(x)\right] / \left[sum(Pll \cdot fl(x)\right] \qquad (2)$$

where x is the input muscle activity data and k are the output hand gesture class. $fk(x)$ is the examined probability of x belonging to class k. Plk is called prior probability which means the base probability of each hand gesture class occurred in the training dataset [20], and it can be defined as

$$Plk = \frac{nk}{n}. \quad (3)$$

The prediction accuracy of this model is 34.8%. The performance is not good mainly because not all of the muscle activity data in sensors has normal distribution. Skewness occurs frequently in each sensor, which drags the prediction accuracy down significantly. Looking at the result of the last model and this model, it can be concluded that this dataset is not suitable for linear prediction.

K-Nearest Neighbors algorithm can be used as classifier and regression problem solver. This model works based on an idea of similarity. After reading the input muscle activity data, it will measure the proximity of this data to the training data and evaluate the most possible hand gesture class for the input data. This model evaluates a prediction accuracy of 65.44%, which is much higher than the last two models. That's probably because this model dose not have many assumptions, which can fit to nearly all of the dataset. However, since the measurement of proximity plays an important role here, the model may be greatly affected by the outliers.

Classification and Regression Trees can be used for both classification and regression problems. In this model, decision trees are used to do the classification. There are two nodes in decision trees: the internal one represents the muscle activity data in training dataset and the outer one(leaf) represents the resulted hand gesture classes. The branches mean the decision rules. This model works by continuing asking questions and making decisions until reaches the outer node. During the process of classification, the model will split the data based on the features to form a suitable tree. The split score is defined as

$$G = sum\left[\rho k \cdot (1 - \rho k)\right], \quad (5)$$

where pk is the percentage of the same input classes that occur in a specific group. A perfect splitting occurs when $G = 0$. The resulted prediction accuracy is 77.41%.

Naive Bayes classifier can be used for binary and multi-class. This model assumes that all sensors are independent and make unique contribution to the hand gesture classes. It is based on Bayes theorem, which calculate the possibility of a hand gesture class occurring based on the muscle activity readings that are already happened. The mathematical formula for this model is defined as

$$P(y|X) = \frac{P(y|X)P(y)}{P(X)}. \quad (6)$$

This formula finds the probability of y, which is the hand gesture class, with input muscle activity data X, which is given true. As a result, this model has a prediction accuracy of 88.51%.

Support Vector Machine also can be used for classification and regression problems. For the dataset that is used in this paper, which is non-linear, this model will project the dataset into higher dimension to make it linearly separable. This is one of the reasons why Support Vector Machine often gives higher accuracies than other models, which is 89.80%. Also, this model uses less time to make prediction and can deal with dataset with large dataset.

2.5 ANN model training and testing

To achieve a higher prediction accuracy, Multi-Layer Perceptrons is applied to the muscle activity dataset, which is a feedforward Artificial Neural Networks (ANN). This paper proposes that using Multi-Layer Perceptron can have prediction accuracy higher than 98%. After the dataset is uploaded in Google Colab, the columns of input and output variables need to be spilt and stored as arrays in variable x and y.

Then Sequential Model is built and layers need to be added to shape the network architecture. There are 3 dense layers in total. The first layer is the input layer. Since there are 64 columns that indicates muscle activity, the first layer should be 64 and use Rectified Linear Activation function, short for relu activation function. That is because when creating multilayer Perceptron, the rectified linear activation is the default activation and the vanishing gradient problem is solved with the rectified linear activation function, allowing models to train quicker and perform better. The next layer

is called first hidden layer and contains 32 nodes. In the beginning, 64 nodes were first set to the first hidden layer and the accuracy was 96.06%. Although this accuracy is higher than all of accuracies of six machine learning models, it still did not meet the goal accuracy. Then, the number of nodes was adjusted to 50 and 40, and the accuracies were around 97%. When the number of first hidden layer was 30, the accuracies rose to 98.44%. After plugging in different node numbers around 30, the results showed that the highest prediction accuracy occurred when the first hidden layer had 32 nodes, which yielded to 99.58%, and the Relu activation function is also used for this layer. The last output layer, is the number of classes that the dataset has, which is 4 classes in this case, and use Sigmoid Activation function since this is a multi-labeled dataset.

After the Sequential Model is defined, it needs to be compiled. For the loss function, Sparse Categorical Crossentropy is chose for the dataset because the dataset has more than two label classes and the classes are integers. Adam is used for optimizer since it is can automatically adjust itself to perform well in a wide range of problems.

The next step is to train the loaded dataset by calling fit function. 10 epochs are used. The number of epochs is a hyperparameter that specifies how many times the learning algorithm will iterate over the full training dataset. Each sample in the training dataset has had a chance to change the internal model parameters once in each epoch [24].

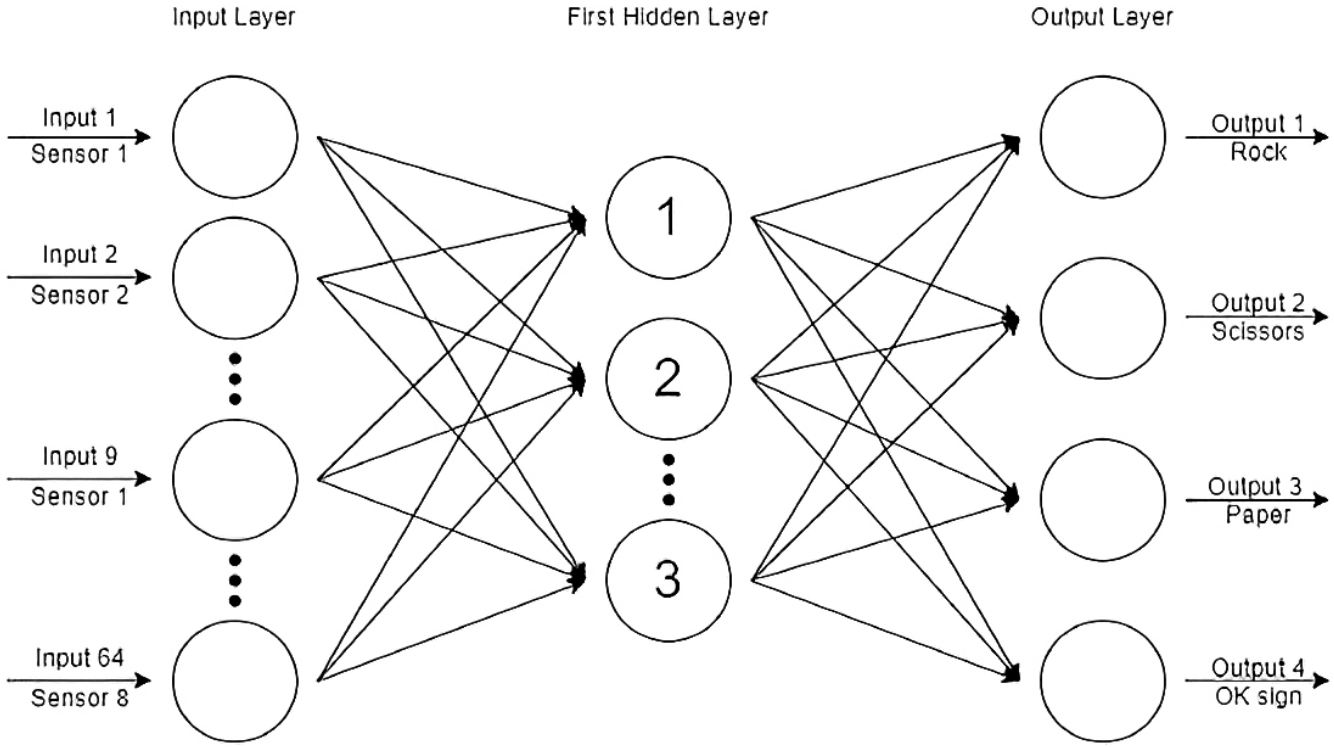

Figure 3. ANN configuration

3. Results and Discussion

3.1. Accuracies of the models

Table 4 shows the accuracies obtained for the different models.

Among the machine learning models, Logistic Regression has the lowest accuracies, which is 34.1897%. Support Vector Machines acquires the highest accuracies, which is 89.7988%. The reason why SVM has highest accuracy is because SVM performs well when the dataset has huge dimensions, has multiple classes to classify and using SVM does not need to worry whether the dataset is linear or not.

Table 4. – Accuracies of the Machine Learning models and Artificial Neural Networks

Machine Learning Models	Accuracies	Neural Networks	Accuracies
Logistic Regression (LR)	34.19%	Multi-Layer Perceptrons (MLP)	99.58%
Linear Discriminant Analysis (LDA)	34.80%		
K-Nearest Neighbors (LDA)	65.44%		
Classification and Regression Trees (CART)	77.41%		
Gaussian Naive Bayes (NB)	88.51%		
Support Vector Machines (SVM)	89.80%		

Although the tradition models already did a good job in classifying gestures, neural networks have a much higher accuracies in classifying, with approximately 99% accuracy. That is because neural networks are outstanding in feature extraction, especially when the dimension of the datasets are large.

4. Conclusion

This paper proposed that applying Artificial Neural Networks instead of Machine Learning models on surgical robotic hands can increase their accuracies in making predictions. At first, six traditional machine learning models are applied to the dataset and the model with highest prediction accuracy is the Support Vector Machine (SVM), which yields 89.80%. A Multi-Layer Perceptron neural network is applied to the same dataset and the accuracy of prediction is 99.58%. The Multi-Layer Perceptron performs better because they have many layers and make interconnections to solve complex problems. Furthermore, the amount of time of Multi-Layer Perceptron need to train and test the data is significantly less than the Machine Learning models. In conclusion, this study highlights the effectiveness and advantages of employing Multi-Layer Perceptron over Machine Learning models to make predictions based on a big dimension dataset, which can play an important role in gesture recognition for similar surgical robotic arms.

Acknowledgements

The author would like to thank Professor Nikhil Yadav.

References:

1. Mujahid A., Awan M. J., Yasin A., Mohammed M. A., Damaševičius R., Maskeliūnas R. & Abdulkareem K. H. (2021). Real-Time Hand Gesture Recognition Based on Deep Learning YOLOv3 Model. Applied Sciences,– 11(9). 4164.
2. Geeksfor Geeks. Top 10 Applications of Robotics in 2020. (2020, November 3).URL: https://www.geeksforgeeks.org/top-10-applications-of-robotics-in-2020/
3. Perkin N. The Limitations of Machine Learning. Only Dead Fish. (2017, January 11). URL: https://www.onlydeadfish.co.uk/only_dead_fish/2017/01/the-limitations-of-machine-learning.html
4. Morrell A. L.G., Morrell-Junior A.C., Morrell A. G., Mendes J. M.F., Tustumi F., De-Oliveira-E-Silva L.G. & Morrell A. The history of robotic surgery and its evolution: when illusion becomes reality. Revista Do Colégio Brasileiro de Cirurgiões,– 48. 2021. URL: https://doi.org/10.1590/0100–6991e-20202798
5. Da Vinci Robotic Surgery.– How Does It Work? – Complications. (2020, July 23). Drug Dangers. URL: https://www.drugdangers.com/da-vinci/robotic-surgery
6. Gao X., Jin Y., Dou Q. & Heng P.-A. Automatic Gesture Recognition in Robot-assisted Surgery with Reinforcement Learning and Tree Search. ArXiv. Published. 2020. URL: https://arxiv.org/pdf/2002.08718.pdf

7. Sarikaya D., Corso J. J. & Guru K. A. Detection and Localization of Robotic Tools in Robot-Assisted Surgery Videos Using Deep Neural Networks for Region Proposal and Detection. IEEE Transactions on Medical Imaging,– 36(7).– P. 1542–1549. 2017. URL: https://doi.org/10.1109/tmi.2017.2665671
8. Vasundhara C. V.S.N. & Sudheer A. P. Design and Analysis of Minimally Invasive Surgical Robot. IOP Conference Series: Materials Science and Engineering,– 1132(1). 2021.– 012037 p. URL: https://doi.org/10.1088/1757–899x/1132/1/012037
9. Thai M. T., Phan P. T. Hoang T. T., Wong S., Lovell N. H. & Do T. N. Advanced Intelligent Systems for Surgical Robotics. Advanced Intelligent Systems,– 2(8). 2020. 1900138. URL: https://doi.org/10.1002/aisy.201900138
10. Sennaar K. Machine Learning in Surgical Robotics – 4 Applications That Matter. (2019, February 3). Emerj. URL: https://emerj.com/ai-sector-overviews/machine-learning-in-surgical-robotics-4-applications
11. Fard M. J. Machine Learning Approach for Skill Evaluation in Robotic-Assisted Surgery. ArXiv.Org. (2016, November 16). URL: https://arxiv.org/abs/1611.05136
12. Radical Prostatectomy Procedure. (2002, February 20). WebMD. URL: https://www.webmd.com/prostate-cancer/guide/prostate-cancer-radical-prostatectomy
13. Hung A. J., Chen J., Che Z., Nilanon T., Jarc A., Titus M., Oh P. J., Gill I. S., & Liu Y. Utilizing Machine Learning and Automated Performance Metrics to Evaluate Robot-Assisted Radical Prostatectomy Performance and Predict Outcomes. Journal of Endourology,– 32(5). 2018.– P. 438–444. URL: https://doi.org/10.1089/end.2018.0035
14. Baraniuk R. The science of deep learning. PNAS. (2020, December 1). URL: https://www.pnas.org/content/117/48/30029
15. Arvindpdmn S. ImageNet. Devopedia. (2021, April 7). URL: https://devopedia.org/imagenet
16. Brownlee J. A Gentle Introduction to the ImageNet Challenge (ILSVRC). Machine Learning Mastery. (2019, July 5). URL: https://machinelearningmastery.com/introduction-to-the-imagenet-large-scale-visual-recognition-challenge-ilsvrc
17. Papers with Code – ImageNet ReaL Benchmark (Image Classification). (n.d.). Peperswithcode. Retrieved July 29, 2021. From URL: https://paperswithcode.com/sota/image-classification-on-imagenet-real
18. Classify gestures by reading muscle activity. (2018, December 9). Kaggle. URL: https://www.kaggle.com/kyr7plus/emg-4?select=1.csv
19. Google Colab. Introduction – Tutorialspoint. (n.d.). Tutorialspoint. Retrieved July 23, 2021. From https://www.tutorialspoint.com/google_colab/google_colab_introduction.htm
20. Raza H. Ph D. An Introduction to Google Colab (Python) – Haider Raza, Ph D. Medium. (2020, September 28). URL: https://medium.com/@sagihaider/benefits-of-using-google-colab-python-8f246c91bc52
21. Sarkar P. What is LDA: Linear Discriminant Analysis for Machine Learning. Knowledgehut. (2019, September 30). URL: https://www.knowledgehut.com/blog/data-science/linear-discriminant-analysis-for-machine-learning
22. Understanding sums of squares – Minitab. (2019). (C) Minitab, LLC. All Rights Reserved. 2019. URL: https://support.minitab.com/en-us/minitab/18/help-and-how-to/modeling-statistics/anova/supporting-topics/anova-statistics/understanding-sums-of-squares
23. Brownlee J. Your First Machine Learning Project in Python Step-By-Step. Machine Learning Mastery. (2020, August 19). URL: https://machinelearningmastery.com/machine-learning-in-python-step-by-step

24. Classify gestures by reading muscle activity. (2018b, December 9). Kaggle. URL: https://www.kaggle.com/kyr7plus/emg-4
25. Brownlee J. Difference Between a Batch and an Epoch in a Neural Network. Machine Learning Mastery. (2019, October 25). URL: https://machinelearningmastery.com/difference-between-a-batch-and-an-epoch

Author

Zijie Liu was born in Shenzhen, China. She played a Chinese traditional instrument, Guzheng, for six years. In high school, she is a programming member of FRC (First Robotic Competition) club and one of the founders of DLR club, which is club that offers free education online for the children who are needed in remote area of China. Zijie plans to attend Universities abroad in next fall. She wants to choose Computer science as her major and she hopes to create a game that most people in the world will enjoy playing.

https://doi.org/10.29013/EJTNS-21-4.5-13-24

Henry Li,
Princeton International School of Mathematics and Science 19 Lambert Dr, Princeton NJ
E-mail: henry.li@prismsus.org
Dr. Chen,
Director, Chinese Academy of Science, Academy of Mathematics and System Science
55 ZhongGuanCun East Road, HaiDian District, Beijing

A NEW DEEP CONVOLUTIONAL NEURAL NETWORK LEARNING MODEL FOR COVID-19 DIAGNOSIS

Abstract. Ever since 2019, people from all over the world are talking about infection with SARS-CoV-2, also known as COVID-19. The symptoms range from asymptomatic conditions to fatal disease, with lung injury most frequently being the result of it. As time flies during the pandemic, the role of medical imaging has been more cortical than ever, with computed tomography being an alternative testing method combined with polymerase chain reaction testing to have a broader role. However, only performing medical imaging testing with suspected patients without classifying whether or not the patient has COVID-19 is not practical. Nevertheless, in many different areas, excellent pulmonology doctors are in extreme shortage for most of the developing counties. Even in developed countries, doctors are too busy with diagnosing and curing patients, so the need for classification for the medical image of patients to see whether they have COVID-19 or not is of high necessity. Moreover, studies of chest radiographs and CT images with applications of artificial intelligence have shown of big importance and necessity. In this paper, we mainly focus on the usage of deep learning and machine learning for categories with findings typical COVID-19 infected images and an application of medical images and testing of the system.

Keywords: SARS-CoV-2, COVID-19, Lung injury, Medical imaging, pulmonology, Computed tomography, Polymerase chain reaction, Imaging classification, Deep learning, Machine learning

1. Introduction

It is generally believed that an infectious disease called COVID-19 was discovered in Wuhan, China in December 2019. The cause of it is generally believed to be Severe Acute Respiratory Syndrome Coronavirus 2 (SARS-CoV-2). In 2020, especially from March to June, the number of people infected with COVID-19 each day has tripled in many European and American Countries. Coronavirus disease is highly contagious. With the increasing number of confirmed cases, how to control this disease is becoming a public health challenge. The World Health Organization (WHO) declared the epidemic as a public health emergency of international concern (PHEIC) on January 30, 2020 [1], and declared it a pandemic on March 11, 2020 [2].

Researchers say that cases of infection can be confirmed by performing a test called reverse transcription-polymerase chain reaction (RT-PCR) [3]. More than 23 million COVID-19 positive cases have been reported until August 2020 [4]. However, the difficulty of quality control during sample preparation has

resulted in a high false-negative rate. Therefore, accurate and fast image processing tools, especially those based on X-ray and computed tomography (CT), can help doctors. Otherwise, even if there are no common COVID-19 symptoms, suspicious patients will be hospitalized or isolated until laboratory test results are clear. The SARS-CoV-2 infection could cause asymptomatic to severe and even fatal diseases. The most common mortality rate is acute lung injury. During the pandemic, the role of imaging has become highly important.

Compared with RT-PCR testing, CT was initially an alternative method and a superior testing method but later evolved into a more limited effect based on specific indications. In the early stages of the pandemic, several chests imaging classification and reporting schemes were developed for patients suspected of COVID-19 to help classify patients with limited RT-PCR testing and unknown performance levels. Some studies have been carrying out observing lung involvement on chest radiographs and CT images, and they indicate that it is related to critical illness. In addition to pulmonary manifestations, cardiovascular complications such as thromboembolism and myocarditis have also been attributed to COVID-19, which sometimes leads to neurological and abdominal manifestations [5]. Finally, artificial intelligence has shown promise that can be used to determine the radiology and CT diagnosis and prognosis of COVID-19 pneumonia [6] Therefore, the collection of chest images such as X-rays and CT scans plays an important role in limiting the spread of the virus and fighting COVID-19 at the appropriate stage of treatment. Artificial intelligence-based technology is used to make quick decisions in saving lives [7]. Among all possible methods, artificial intelligence-based methods tend to help doctors as an effective tool for diagnosing COVID-19. The image acquisition, segmentation, classification, and subsequent diagnosis phases developed between 2019 and 2020 are widely used [8].

2. Deep Learning Network and Models

Deep Learning Networks are AI functions that imitate how the human brain works when processing data and creating patterns for decision making. It is a branch of machine learning of artificial intelligence. Its networks are capable of learning on their own without supervising. To train the network, unstructured or unlabeled data are being inputted. Until then, Artificial intelligence and machine learning technologies improved the accuracy of Covid-19 diagnosis. Also, most of the widely used deep learning models and methods were implemented and a small amount of data was used for COVID-19 diagnosis [9]. However, due to the rapid outbreak of Covid-19, there are not many real data sets available to the community. It is necessary to combine the observation and image information to make diagnoses of COVID-19 [10]. AI can introduce more alternative ways to the medical system, and learn from multi-modal data to capture disease characteristics to obtain reliable results used for COVID-19 diagnosis for timely treatment [9].

2.1 Convolutional Neural Network

One kind of artificial neural network that is most commonly applied to analyze images is convolutional neural networks, which have properties of shift-invariant and space invariant based on the shared-weight structure of the convolution filters that slide along input features and provide translation equivariant responses known as feature maps [11]. Most of the convolutional neural networks are equivariant, which are being applied in for example image and video recognition, image classification, image segmentation, medical image analysis, natural language processing, brain-computer interfaces, and financial time series [12].

Convolutional neural networks were designed base on the biological processes between neurons that resemble the human brain cortex. Individual cortical neurons respond to stimulations only in the receptive field, which is a restricted region of the visual field, and the receptive fields of different neurons partially overlap such that they cover the entire visual field [13].

Convolutional neural networks have multilayer perceptron, which is thoroughly connected networks and every neuron in each layer is connected to all other neurons in the next layer [14]. The property of full

connectivity of these networks makes them capable of processing overfitting data. CNNs take a different approach towards regularization: they take advantage of the hierarchical pattern in data and assemble patterns of increasing complexity using smaller and simpler patterns embossed in their filters [15].

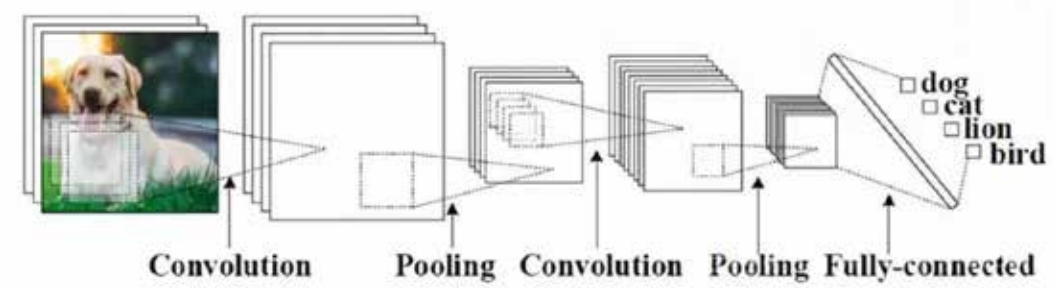

Figure 1. An example of the process of a convolutional network

Convolutional neural networks have a relatively shorter pre-processing procedure compared to other neural networks used for image classification algorithms. This means that the network learns to optimize the filters through automated learning, whereas in traditional algorithms these filters are hand-engineered, and the independence from prior knowledge and human intervention in feature extraction is a major advantage [16].

2.2 U-net

What it takes to train deep convolutional networks are thousands of annotated training samples. An efficient sliding-window convolutional network and training strategy that relies on the strong use of data augmentation to use the available annotated samples more efficiently is named U-net [17].

This network structure consists of a contracting path for capturing contexts as well as the asymmetric expanding path that enables localization precisely, and it is also capable of training an end-to-end result from very few images and outputs the best and prior method and it is also extremely fast. Segmentation of a 512 × × 512 image takes less than a second [17]. In the last few decades, deep convolutional networks have successfully finished a huge amount of visual recognition tasks. One of the most typical applications of convolutional networks is imaging classification, where the output for an image is a single class label. However, in many visual tasks, especially in biomedical image processing, the desired output should include localization [17]. Also, thousands of images used for training are hard to fulfill in the medical task. So, the idea of training a network in a sliding-window set up to predict the class label of each pixel by providing a local patch around that pixel as input has been performed by Ciresan et al, while this network can localize while the training data (counted by patches) much larger than the number of training images [18]. Due to the property of convolution, the output image is smaller than the input images with a constant ratio of border width.

The network structure in (Figure 2) consists of a contracting path, which is on the left side, and an expansive path which is on the right side. The former follows the typical structure of a convolutional network, which consists of the repeated application of two 3x3 unpadded convolutions, each followed by a rectified linear unit (ReLU) and a 2 × 2 max pooling operation with stride 2 for down-sampling [19]. By doubling the number of feature channels for each down-sampling step in the expansive path, which consists of an up-sampling of the feature map followed by a 2 × 2 convolution called "up-convolution" that halves the number of feature channels, a concatenation with the correspondingly cropped feature map from the contracting path with two 3 × 3 convolutions, each followed by a ReLU [20]. At the final layer, a 1 × 1 convolution is used to map each 64-component feature vector to the desired number of classes which in total, the network has 23 convolutional layers [17].

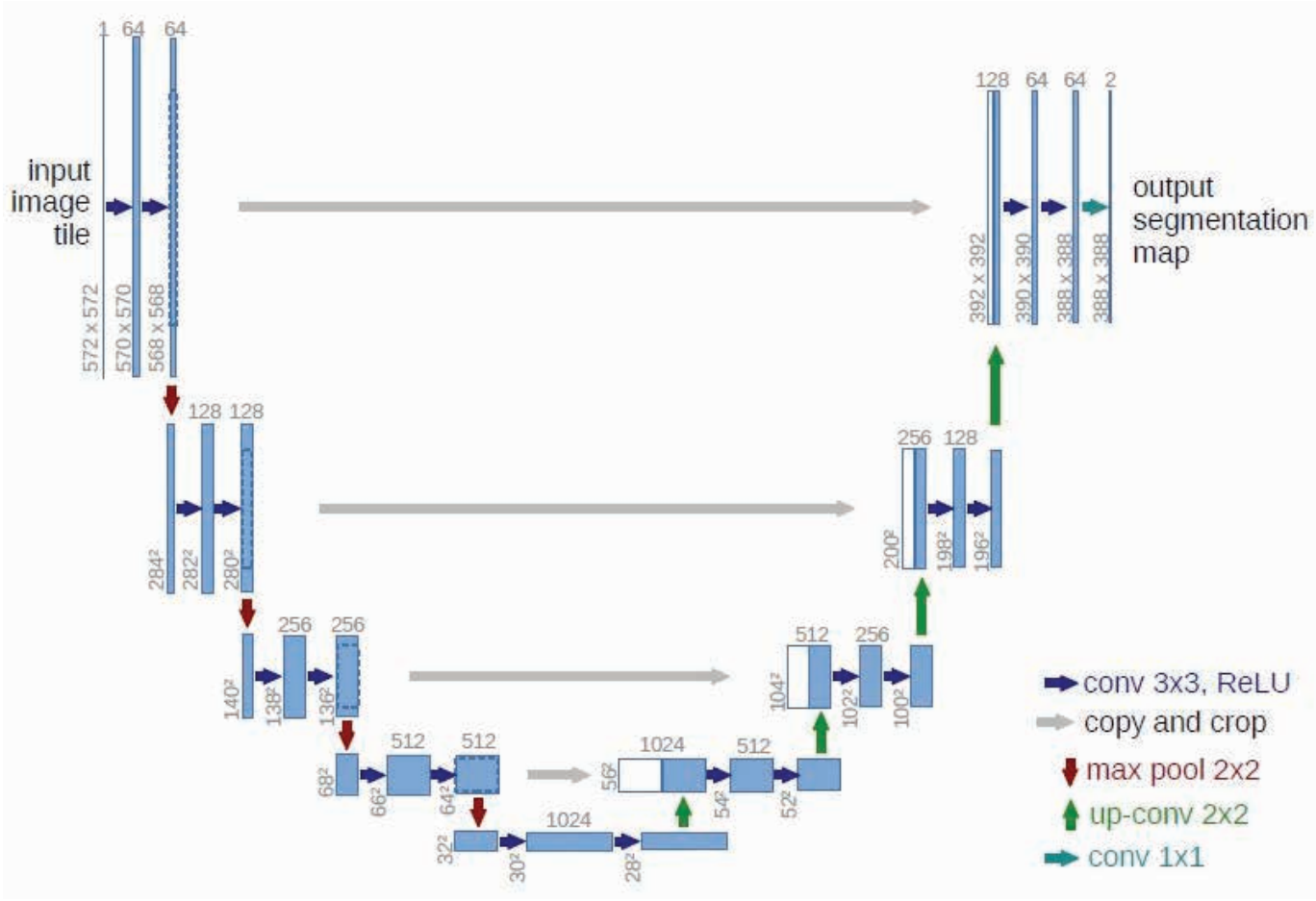

Figure 2. An example of a U-net structure for 32x32 pixels. Each blue box corresponds to a multi-channel map. The number of channels is shown on top of the box while the x-y-size is shown at the lower left edge of the box. White boxes represent copied feature maps, and the arrows denote the different operations [17]

A high momentum of 0.99 is used, as the energy function is defined with a pixel-wise and soft-max with the cross-entropy loss function. The soft-max is defined as

$$p_k(x) = \frac{\exp(a_k(x))}{\sum_{k'=1}^{K}\exp(a_{k'}(x))} \quad (1)$$

where $a_k(x)$ stands for the activation for channel k at the pixel position $x \in \Omega$ with $\Omega \subset \mathbb{Z}^2$, and K is the number of classes and $p_k(x)$ is the approximated maximum function.

The cross entropy then penalizes at each position the deviation of $p_{l(x)}(x)$ from (1) using

$$E = \sum_{x \in \Omega} w(x)\log\left(p_{l(x)}(x)\right) \quad (2)$$

where $l : \Omega \to \{1, \ldots, K\}$ is the true label of each pixel and w: $\Omega \to R$ is a weight map that gives some pixels more importance in the training [17].

By pre-computing the weight map for basic segmentation to recompense the different pixels frequencies from a certain class in the training data set, and also forcing the network to learn small separation borders being introduced between each element, the separation border is computed using morphological operations [21]. The weight map is then computed as

$$w(x) = w_c(x) + w_0 \cdot \exp\left(-\frac{\left(d_1(x)+d_2(x)\right)^2}{2\sigma^2}\right) \quad (3)$$

where $w_c : \Omega \to \mathbb{R}$ is the weight map for balancing the class frequencies, $d_1 : \Omega \to \mathbb{R}$ means the distance to the border of the nearest cell and $d_2 : \Omega \to \mathbb{R}$ the distance to the border of the second nearest cell. In our experiments we set $w_0 = 10$ and $\sigma = 5$ pixels [17]. In a deep network, many convolutional layers could be found with different paths throughout the whole network, which makes a good initialization weight extremely important since parts of the network might give excessive activations, and other parts never contribute otherwise. Ideally, the initial weights should be adapted such that each feature map in the network has approximately unit variance [22]. For a network with alternating convolutional and ReLU layers, this can be achieved by drawing the initial weights from a Gaussian distribution [23].

3. Application of Deep learning models to recognize COVID-19 Infected Lung Images

The main purpose of this research is to train the network to let it recognize the COVID-19 Infected Lung Images. All the images are open-source chest CT images from Società Italiana di Radiologia Medica e Interventistica (Italian Society of Medical and Interventional Radiology) [24], National Institutes of Health (NIH), the Radiological Society of North America (RSNA), [25] the American College of Radiology (ACR), Centers for Disease Control and Prevention (CDC) [26].

3.1 TensorFlow Coding

TensorFlow is Google Brain's second-generation system, it is an open-source software library for machine learning, often focus on the training and inference of deep neural networks. [27] U-net models are available on TensorFlow, which is used to create a virtual environment for the networking building of this learning program.

3.2 Applications and Final Results

The used images are from the website mentioned before to train the network. The images in these websites are typical with labeled information, which is important for the training. We train the training group images by classifying them. In total, there are 1000 images for training the network, and 100 for testing the network, and they are all being concluded into a dataset.

Figure 3. A part of the training image set

So first, inputting the training image data set allows the program to analyze and get a conclusion of the data distribution. We want to put the images into 4 groups, which are train images, train labels, test

images, and test labels. All of the pictures are whether healthy lung chest CT images or COVID-19 infected lung chest CT images. So, these two labels are the ones that the program will be classicizing on.

```
(train_images, train_labels), (test_images, test_labels) = train_image.load_data()

class_names = ['Infected_image', 'Uninfected_image']
```

Before we train the network, we want to see the results of input.

```
train_images.shape
len(train_labels)
train_labels
test_images.shape
len(test_labels)
```

However, the input images are not the same size, so we want to pre-process the images for different images, there is the need to modify them into the same size.

```
plt.figure()
plt.imshow(train_images[0])
plt.colorbar()
plt.grid(False)
plt.show()
```

In order to test the size of the images, we show the first 25 images in the dataset.

```
plt.figure(figsize=(10,10))
for i in range(25):
    plt.subplot(5,5,i+1)
    plt.xticks([])
    plt.yticks([])
    plt.grid(False)
    plt.imshow(train_images[i], cmap=plt.cm.binary)
    plt.xlabel(class_names[train_labels[i]])
plt.show()
```

After all the preparation is done, we will begin to build our deep learning network. The first step is to set up the layers. The basic building blocks of a neural network is layers. Layers can extract representations from the data given.

```
model = keras.Sequential([
    keras.layers.Flatten(input_shape=(28, 28)),
    keras.layers.Dense(128, activation='A'),
    keras.layers.Dense(2)
])

model.compile(optimizer='B',
              loss=tf.keras.losses.SparseCategoricalCrossentropy(from_logits=True
              metrics=['accuracy'])
```

To begin with, the layer: tf.keras.layers.Dense has a parameter that is learned in the process of training. The first layer: tf.keras.layers.Flatten of this network transforms the format of the images from two-dimensional arrays to one-dimensional arrays. Then, after the pixels are flattened, the network consists of

a sequence of two tf.keras.layers.Dense layers will be fully connected neural layers. The first Dense layer has 128 nodes. The second and last layer returns a logits array with a length of 10. Each node contains a score that indicates the current image belongs to one of the 10 classes [28]. In this case, another network is also available.

```
model = tf.keras.models.Sequential([
    tf.keras.layers.Flatten(input_shape=(28, 28)),
    tf.keras.layers.Dense(128, activation='A'),
    tf.keras.layers.Dropout(0.2),
    tf.keras.layers.Dense(2, activation='B')
])

model.compile(optimizer='C',
                              loss='sparse_categorical_crossentropy',
                              metrics=['accuracy'])
```

Training the neural network model requires the following steps: 1) Input the training data into the model, which are train_images and train_labels arrays in this example; 2) The model learns to correlate images and labels. We ask the model to make predictions about a test set – in this example, the test_images array [29]; 3) labels from the test_labels array match the predictions [30]. To start training, we need to call the model.fit method. As the model trains, the loss and accuracy metrics are displayed. This model reaches an accuracy of about 0.89 on the training data [17].

```
model.fit(train_images, train_labels, epochs=10)
```

The accuracy of the testing dataset is not as good as the accuracy of the training dataset, this gap between the training accuracy and the test accuracy is called overfitting [31]. It happens when a machine learning model does not perform as well as on new inputs other than the training data. An overfitted model "memorizes" the noise and details in the training dataset to a point where it negatively impacts the performance of the model on the new data [32]. There are a few ways to prevent overfitting, including 1) Simplifying the model, 2) Early stopping; 3) Use data augmentation; 4) Use regularization and; 5) Use dropouts [33].

```
test_loss, test_acc = model.evaluate(test_images, test_labels, verbose=2)

print('\nTest accuracy:', test_acc)

313/313 - 0s - loss: 0.3333 - accuracy: 0.8809

Test accuracy: 0.8809000253677368
```

After the model is trained, we can then make predictions about our testing group of images. Adding a soft-max layer to convert logits to probabilities will be easier to interpret. After this step, we will make a plot of how the classification class predicts the result.

```
probability_model = tf.keras.Sequential([model, tf.keras.layers.Softmax()])
predictions = probability_model.predict(test_images)
predictions[0]
np.argmax(predictions[0])
test_labels[0]
def plot_image(i, predictions_array, true_label, img):
    true_label, img = true_label[i], img[i]
    plt.grid(False)
    plt.xticks([])
    plt.yticks([])

    plt.imshow(img, cmap=plt.cm.binary)

    predicted_label = np.argmax(predictions_array)
    if predicted_label == true_label:
        color = 'blue'
    else:
        color = 'red'

    plt.xlabel("{} {:2.0f}% ({})".format(class_names[predicted_label],
                                         100*np.max(predictions_array),
                                         class_names[true_label]),
                                         color=color)
```

We can use this model that we trained to first make predictions about some images for the first image in the testing groups, also for prediction array.

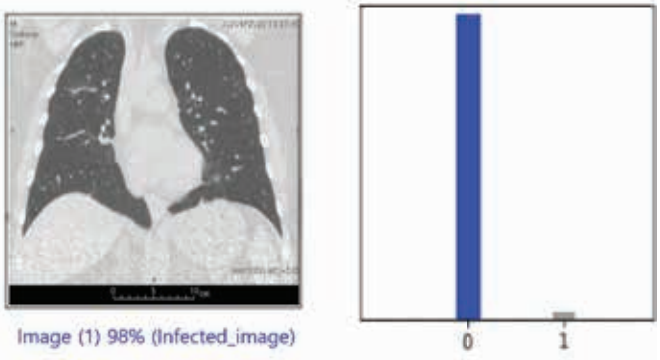

Last but not least, our last goal is to make predictions about a single image based on the trained model. The tf.keras models are optimized to make predictions on a series of examples at once [17]. The method: tf.keras.Model.predict returns a list of lists for each image in the batch of data. In the end, it predicts the correct label as expected.

```
i = 0
plt.figure(figsize=(6,3))
plt.subplot(1,2,1)
plot_image(i, predictions[i], test_labels, test_images)
plt.subplot(1,2,2)
plot_value_array(i, predictions[i], test_labels)
plt.show()
```

```
img = test_images[1]
print(img.shape)
img = (np.expand_dims(img,0))
print(img.shape)
predictions_single = probability_model.predict(img)
print(predictions_single)
plot_value_array(1, predictions_single[0], test_labels)
_ = plt.xticks(range(2), class_names, rotation=45)
np.argmax(predictions_single[0])
```

4. Conclusion

After comparing the characters of the network and the already-known characters of chest CT images with lung affected with COVID-19 [34], the COVID-19 infected lung images characters includes the presence of ground-glass opacities, presence of consolidation, presence of nodules, presence of a pleural effusion, presence of thoracic lymphadenopathy, airways abnormalities that include airway wall thickening, bronchiectasis, and endoluminal secretions, and last but not least, the presence of underlying lung disease such as emphysema or fibrosis [35].

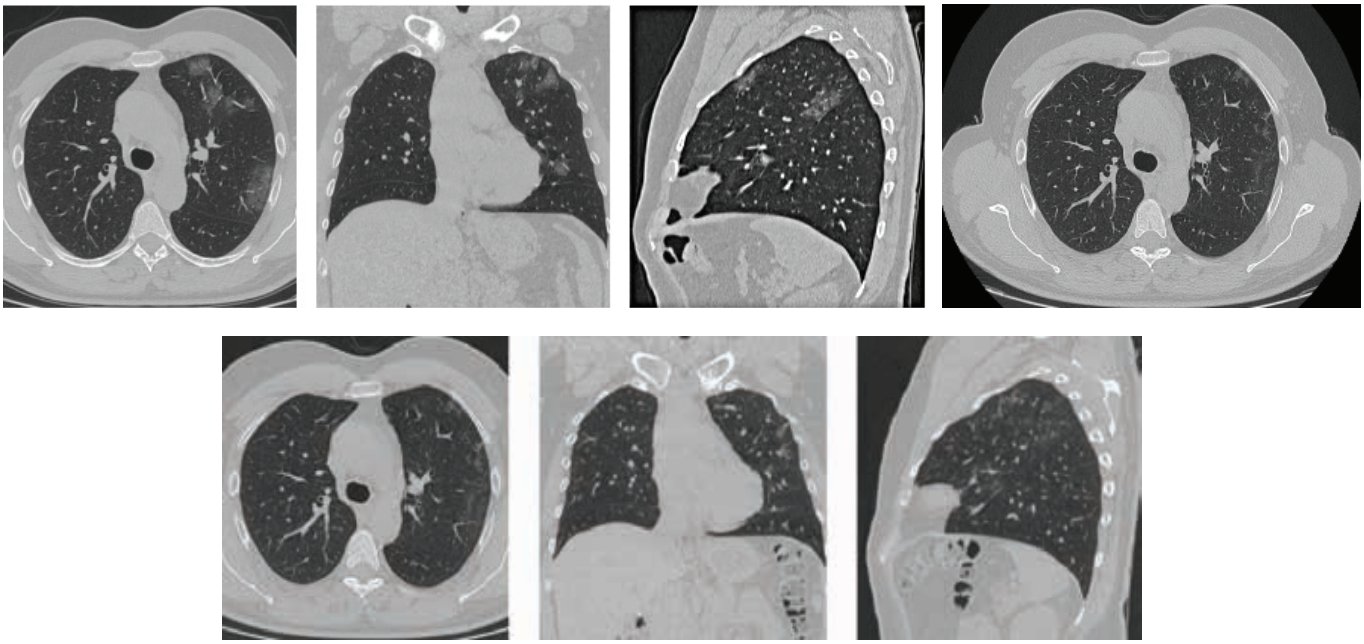

Figure 4. COVID-19 infected chest CT lung Images provided by S. S. Oncological Radiology San Giuseppe Moscati Hospital, Taranto. A patient of a 51-year-old man presented himself to the hospital emergency department with an 8-day fever, chest tightness, and mild dyspnea. The image suggests that this patient with COVID-19 pneumonia manifests at thoracic CT investigation in the form of bilateral subpleural GGO opacities with aerial bronchogram, ill-defined margins, and a slight predominance in the right lower lobe [36]

5. Discussion

The ground-glass opacification is defined as an area of increased lung attenuation with preservation of bronchial and vascular margins [37], in other words, an area of increased hazy lung opacity with vessels and bronchial structures may still be seen. While pulmonary consolidation was defined as opacification with obscuration of margins of vessels

and airway walls [38], in other words, a region of normally compressible lung tissue that has filled with liquid instead of air.

An important direction for future research is to alter the model used in the research to see if the images could also be classified into the correct group. Or using more images to test the stability of the network, maybe actually using it in medical applications. Also, noticing that we have concluded some important characteristics of the COVID-19 infected lung images, we could create more labels that include different kinds of symptoms. For example, labels with ground-glass opacification, or labels of thoracic lymphadenopathy. However, it requires the algorithm and the network to be more complicated, with more layers of convolutional network or more complicated models. Once finished, it would become a more mature neural network.

6. Acknowledgments

I would like to express my gratefulness to my mentor Dr. Chong Chen of Chinese Academy of Science. He has provided guidance and advices. I would also like thank Ms. Betty Wang for providing me this research opportunity. Last but not least, I would like to thank the organizers of the Yau Awards for giving me the platform to show my work.

References:

1. URL: https://www.who.int/publications/m/item/covid-19-public-health-emergency-of-international-concern-(pheic)-global-research-and-innovation-forum
2. URL: https://www.who.int/director-general/speeches/detail/who-director-general-s -opening-remarks-at-the-media-briefing-on-covid-19-11-march-2020
3. Ai T., Yang Z., Hou H. et al. Correlation of Chest CT and RT-PCR Testing for Coronavirus Disease 2019. (COVID-19) in China: A Report of 1014 Cases. Radiology. – 296(2). 2020. – E32–E40. Doi: https://doi.org/10.1148/radiol.2020200642/ Link, Google Scholar
4. Soomro T. A., Zheng L., Afifi A. J. et al. Artificial intelligence (AI) for medical imaging to combat coronavirus disease (COVID-19): a detailed review with direction for future research. Artif Intell Rev (2021). 15 April, 2021. URL: https://doi.org/10.1007/s10462-021-09985-z
5. URL: https://dergipark.org.tr/en/pub/sdutfd/article/902875
6. Kanne J. P., Bai H., Bernheim A., Chung M., Haramati L. B., Kallmes D. F., Little B. P., Rubin G. & Sverzellati N. COVID-19 imaging: What we know now and what remains unknown. Radiology,–3. 2021. – 299p. E262-E279. URL: https://doi.org/10.1148/radiol.2021204522
7. URL: https://mayoclinic.pure.elsevier.com/en/publications/covid-19-imaging-what-we-know-now-and-what-remains-unknown
8. Alexander Selvikvåg Lundervold, Arvid Lundervold. An overview of deep learning in medical imaging focusing on MRI, Zeitschrift für Medizinische Physik,– Vol. 29.– Issue 2. 2019.– P. 102–127. ISSN0939–3889. URL: https://doi.org/10.1016/j.zemedi.2018.11.002; (https://www.sciencedirect.com/science/article/pii/S0939388918301181)
9. URL: http://web.archive.org/web/20210420225353/https://pubmed.ncbi.nlm.nih.gov/33875900
10. Soomro T. A., Zheng L., Afifi A. J. et al. Artificial intelligence (AI) for medical imaging to combat coronavirus disease (COVID-19): a detailed review with direction for future research. Artif Intell Rev. 2021. URL: https://doi.org/10.1007/s10462-021-09985-z
11. Avilov Oleksii, Rimbert Sebastien, Popov Anton, Bougrain Laurent. "Deep Learning Techniques to Improve Intraoperative Awareness Detection from Electroencephalographic Signals". 2020. 42nd Annual

International Conference of the IEEE Engineering in Medicine & Biology Society (EMBC). Montreal, QC, – Canada: IEEE.– July, 2020.– P. 142–145.
12. URL: https://blog.avenuecode.com/using-deep-convolutional-neural-networks-dcnns-for-time-series-forecasting-using-tensorflow-part-1
13. URL: https://github.com/ankit201/cnn
14. Zhang Wei. "Shift-invariant pattern recognition neural network and its optical architecture". Proceedings of Annual Conference of the Japan Society of Applied Physics. 1988.
15. Tsantekidis Avraam, Passalis Nikolaos, Tefas Anastasios, Kanniainen Juho, Gabbouj Moncef, Iosifidis Alexandros. "Forecasting Stock Prices from the Limit Order Book Using Convolutional Neural Networks". July, 2017. IEEE19th Conference on Business Informatics (CBI). Thessaloniki, Greece: IEEE: – P. 7–12.
16. Fukushima K. "Neocognitron". Scholarpedia.– 2 (1). 1717. Bibcode: 2007 SchpJ… 2.1717F. Doi:10.4249/scholarpedia. 1717.
17. Ronneberger 2015 unet, U-Net: Convolutional Networks for Biomedical Image Segmentation, Olaf Ronneberger and Philipp Fischer and Thomas Brox, 2015. 1505. 04597.
18. Ciresan D. C., Gambardella L. M., Giusti A., Schmidhuber J. Deep neural networks segment neuronal membranes in electron microscopy images. In: NIPS, 2012.– P. 2852–2860.
19. URL: https://heartbeat.fritz.ai/deep-learning-for-image-segmentation-u-net-architecture-ff17f6e4c1cf
20. Siddique N. S., Paheding C. P. Elkin and Devabhaktuni V. "U-Net and Its Variants for Medical Image Segmentation: A Review of Theory and Applications". In IEEE Access,– Vol. 9. 2021.– P. 82031–82057. Doi: 10.1109/ACCESS.2021.3086020.
21. Perseus A. I. U-net [Electronic resource]. URL: https://perseusai.blogspot.com
22. Talley Nicholas Joseph. Clinical Examination, a Clinical Guide to Physical Diagnosis, Wiley, 4th ed., 2001.– 121 p. ISBN0632059710.
23. Cornell University, U-net[Electronic resource]. URL: https://arxiv.org/abs/1806.05034
24. Italian Society of Radiology Via della Signora 2 [Electronic resource]. URL: https://sirm.org
25. RSNA, Radiology [Electronic resource]. URL: https://pubs.rsna.org/doi/full/10.1148/radiol.2021204522
26. Imaging Technology News [Electronic resource]. URL: https://www.itnonline.com/content/photo-gallery-how-covid-19-appears-medical-imaging
27. Google (2015). Tensor Flow: Open source machine learning. "It is machine learning software being used for various kinds of perceptual and language understanding tasks".– Jeffrey Dean, minute 0:47 / 2:17 from YouTube clip
28. Tensor Flow [Electronic resource]. URL: https://www.tensorflow.org/guide/keras/train_and_evaluate
29. RICE University [Electronic resource]. URL: https://www.caam.rice.edu/~caam519/notes/module-8/MNIST.ipynb
30. Tensor Flow [Electronic resource]. URL: https://colab.research.google.com/github/tensorflow/docs-l10n/blob/master/site/zh-cn/guide/basic_training_loops.ipynb
31. IBM Cloud Learn Hub [Electronic resource]. URL: https://www.ibm.com/cloud/learn/overfitting
32. The Data Engineering Cloud [Electronic resource]. URL: https://www.kdnuggets.com/2019/12/5-techniques-prevent-overfitting-neural-networks.html
33. Machine Learning [Electronic resource]. URL: https://machinelearningmastery.com/introduction-to-regularization-to-reduce-ovrfitting-and-improve-generalization-error

34. Tensorflow [Electronic resource]. URL: https://colab.research.google.com/github/tensorflow/docs-l10n/blob/master/site/zh-cn/tutorials/keras/classification.ipynb?hl=zh_cn#scrollTo=xvwvpA64CaW_
35. Jerome J. T.J. et al. Perspectives and Consensus among International Orthopaedic Surgeons during Initial and Mid-lockdown Phases of Coronavirus Disease. J Hand Microsurg. Dec,– 12(3). 2020.– P. 135–162. Doi: 10.1055/s-0040–1713964. Epub 2020 Jul 6. PMID: 33408440; PMCID: PMC7773504.
36. Chest CT Findings in Coronavirus Disease-19 (COVID-19): Relationship to Duration of Infection, Adam Bernheim, Xueyan Mei, Mingqian Huang, Yang Yang, Zahi A. Fayad, Ning Zhang, Kaiyue Diao, Bin Lin, Xiqi Zhu, Kunwei Li, Shaolin Li, Hong Shan, Adam Jacobi, and Michael Chung, Radiology,– 3. 2020.– 295p.
37. URL: https://sirm.org/2020/05/31/covid-19-caso-115
38. Differential diagnosis and management of focal ground-glass opacities. Infante M., Lutman R. F., Imparato S., Di Rocco M., Ceresoli G. L., Torri V., Morenghi E., Minuti F., Cavuto S., Bottoni E., Inzirillo F., Cariboni U., Errico V., Incarbone M. A., Ferraroli G., Brambilla G., Alloisio M., Ravasi G. European Respiratory Journal Apr,– 33 (4). 2009.– P. 821–827. DOI: 10.1183/09031936.00047908

Section 2. Mathematics

https://doi.org/10.29013/EJTNS-21-4.5-25-31

Pennington Jeremy,
Hopkins School, New Haven, CT, United States
E-mail: jeremyc1501@icloud.com; szhang2010@gmail.com

STAR CLASSIFIER RESEARCH

Abstract. There are many hundred billion stars in our galaxy alone, and each has a combination of unique factors that define the star itself. Such factors include temperature, relative luminosity, absolute magnitude, spectral class, star color, and star type. By setting these qualities as parameters, we can determine what star type a given star falls under using machine learning models.

Keywords: Stars, temperature, relative luminosity, absolute magnitude, spectral class, star color, red dwarf, brown dwarf, main sequence, supergiant, hypergiant, machine learning, logistic regression, gradient boosting, k nearest neighbors, Python.

Introduction:

Stars are classified using several features, including absolute temperature, relative luminosity, relative radius, absolute magnitude, star color, and spectral class. Each one of these features is individually important in contributing to determine the star type. Absolute temperature, also known as thermodynamic temperature, is measured relative to absolute zero. It is an evaluation of the kinetic energy of individual particles within. An example of this is the kelvin scale, which uses degrees like Celsius. Relative luminosity is a measure of luminance. Luminance is the intensity of light emitted per unit area, determined by the amount of light that passes through, is emitted from, or is reflected by a star. Normalization of the luminance value ranges from 1 to 100. Measuring relative radius considers factors such as angle of rotation and physical size. Absolute magnitude is the luminosity of an object from a standard distance. That distance is defined to be ten parsecs, or 32.6 light-years, without dimming. Star colors include white, red, blue, yellow, and many others, correlating directly with their temperature. For example, blue stars have an approximate temperature of 25.000k, white stars have an approximate temperature of 10.000k, yellow stars have an approximate temperature of 6000k, and red stars have an approximate temperature of 3000k. For comparison, our sun is yellow. Finally, the spectral class includes O, B, A, F, G, and M. Spectral class is a classification of stars based on characteristics such as effective temperature, color, and various other features. Based on the factors above, stars are classified into one of these categories.

Star types in this study include Red Dwarf, Brown Dwarf, Main Sequence, SuperGiants, and HyperGiants. Red Dwarfs are the closest to the sun and have limited radiances. They make up the largest population of stars in the galaxy but cannot be seen with the naked eye. Scientists estimate that twenty out of thirty of the closest stars to the sun are Red Dwarfs, an example being Proxima Centauri, the closest to earth. Brown dwarf stars are failed stars that emit little to no light and size between Jupiter and a small star. A brown dwarf is classified as a brown dwarf if the mass

is 15–75 times that of Jupiter due to being mainly composed of hydrogen gas. The main sequence is an overarching archetype of stars made from dust and gas clouds and can be anywhere from one-tenth to 200 times as massive as the sun. Red dwarfs are a type of main-sequence star, and less massive ones are often considered Brown Dwarfs. SuperGiants are main sequence stars that are enormous in size and are very luminous. For comparison, their diameter is hundreds of times greater than the sun, and their luminosity is estimated to be one million times as significant. They are mostly formed when main sequence stars expend the hydrogen in their cores. Finally, HyperGiants are the most massive and luminous of all stars. One example, R136a1, has a luminosity 8.7 million times the sun and a mass 256 as large. Due to their size and luminosity, hypergiants are very rare.

The main objective of this project is to develop machine learning models to predict star types. The primary means of achieving this intended purpose is using supervised learning. Supervised learning entails the process of learning and developing a function that reasonably assesses data from inputs to outputs. In this process, I analyzed the values of the specific factors listed above and devised a supervised learning model to determine which type of star out of the six given types based on the importance of the factors. My primary tool to accomplish this is the Python programming language in PyCharm, which allows for written code and third-party packages available for Python. After adding in the script and installing packages such as Pandas, NumPy, Matplotlib, Seaborn, and sklearn. The result consists of several graphs and tables. For example, one result was sixteen graphs, comparing temperature, luminosity, radius, and absolute magnitude. Another is a heatmap that shows the correlation between those four facts as well as star type with one another, yielding numerical values from 0.39 to 1.

Data:

First, I imported several third-party packages, including Pandas, NumPy, Matplotlib, Seaborn, and sklearn. I will expand on this topic more in a later paragraph. Additionally, I also imported several CSV files obtained from Kaggle. CSV stands for "comma-separated values" and includes the data that I use. Additionally, I named the Data Frame "stars," which consists of the CSV file. In the Data Frame, the columns are the attributes of each star, and the rows are star samples. The results described output is summarized in the form of raw data after running the program. "Print" is a Python built-in function outside data frame class, and head ( ) is a method associated with the data frame used to display the first five rows. Other categories after "print" include "star type," which serves as a display value, and "unique," which can access the unique values in a column. Finally, "info" shows the general information of the Data Frame.

I then convert the color column to clean up the column's redundant data. Since star color and spectral class are categorical data but should be converted to numeric data types, I encoded them and added them to the data frame. The word "head" displays the first five rows of all columns. Then, I pick all the independent variables and put them in a new data frame named "x." After using the standard scaler to scale the columns in "x," I dropped the original unscaled columns. Finally, I split "x" into a train and test set, where a train set is used to train the model, and a test set is used as a new set of data to gauge the model's performance.

Pandas is a software library that offers tabular data manipulation and analysis. In this project, I used it to create the Data Frame data structure and manipulate data tables. NumPy is a support package that sometimes serves as a library. It can develop arrays and matrices as well as adding support to large amounts of high-level math functions. NumPy is a more quantitative method compared to other packages. Matplotlib is a plotting library that can serve as an added extension onto Python and NumPy. It allows plots to be embedded into other applications. Seaborn is a visualization library based on Matplotlib that provides an interface for highly informative graphs. In this project, seaborn was used to produce

the various graphs referred to as well as the heatmap. Finally, sci-kit learn a learning library based on the three previously described packages. It has classifiers, clustering, and regression algorithms, including logistic regression, decision tree, gradient boosting, and other standard machine learning models.

Methods:

Two diagrams can be produced by utilizing third-party packages for Python such as pandas, NumPy, matplotlib, seaborn, and sklearn in combination with my written code. The first a heat map, which shows a correlation between individual factors (see figure 1). This heat map includes five elements: temperature, luminosity, radius, absolute magnitude, and star type. The correlation values are on a scale from 0 to 1, depending on how related each factor is to the other. For example, every aspect has a correlation value of 1 with itself, which makes sense. The highest correlation value is between absolute magnitude and star type, which has a correlation value of 0.96. This correlation is logical since the absolute magnitude is the luminosity measure from a standard distance, and that is the defining factor of what star type it is. The weakest correlation is between temperature and luminosity and has a value of 0.39. This finding may seem surprising as brightness is often associated with temperature. However, luminosity and temperature are correlated, although weak.

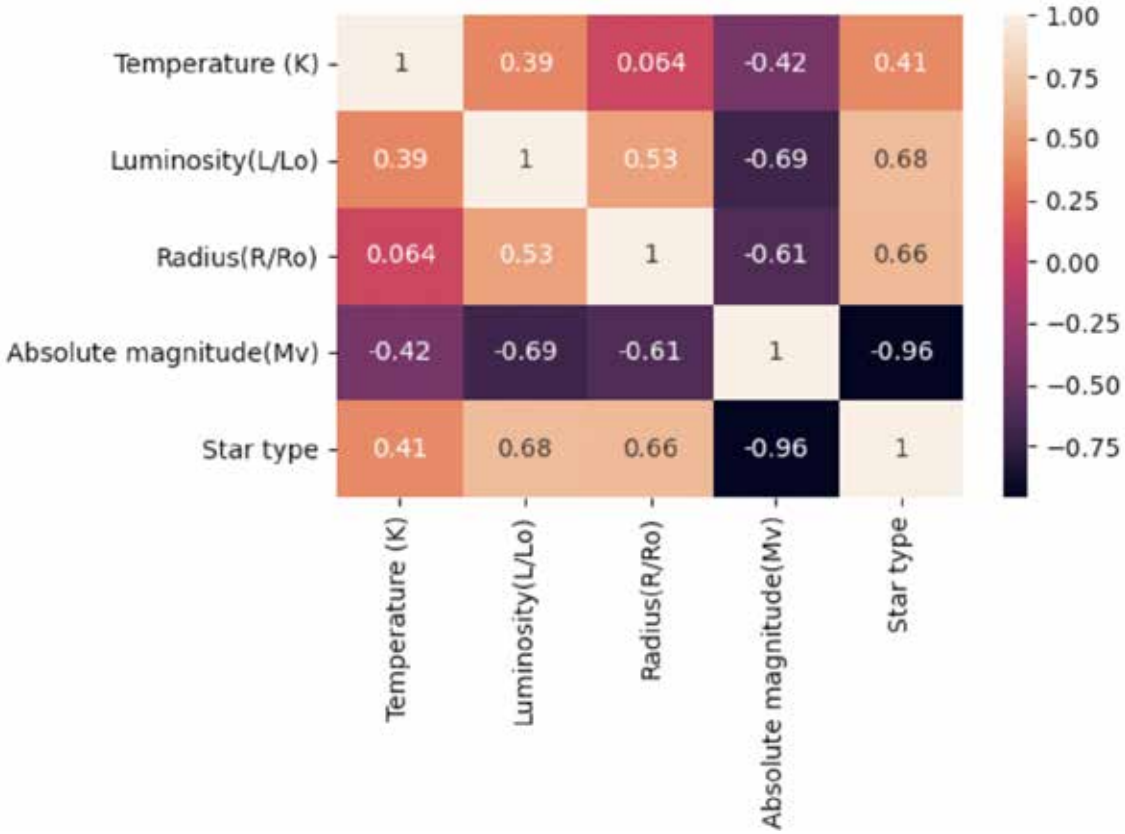

Figure 1. Heat map of feature variable correlations

Other notable correlation values include luminosity, radius, and absolute magnitude, star type, radius and luminosity, and temperature and radius. All these values are between 0.6 and 0.7, which indicates a positive correlation. Absolute magnitude and luminosity have a correlation value of almost 0.69. This finding shows logically that absolute magnitude is essentially luminosity but measured from a fixed distance. The correlation between star type and temperature and luminosity indicates that there is a linear relationship. Another two crucial correlation values are between temperature and star type and absolute magnitude, 0.41 and 0.42, re-

spectively. These values indicate that temperature has a relatively weak correlation between star type and absolute magnitude. This finding is logical since absolute magnitude is not defined by temperature and star type can vary depending on the temperature.

The second diagram produced from the code is a series of graphs showing pairwise relationships. These graphs show the relationship between two factors through plotting points that represent star types. On the chart of temperature vs. luminosity, the type 5 stars are concentrated at luminosities higher than 100000. Additionally, the chart highlights temperatures, some exceeding 30000. At luminosities below 100000, the type of stars are 1 to 4. In temperature vs. radius, a similar pattern occurs. At radii exceeding 500, the star type is 5, but at radii under 500, the star type ranges from 1 to 4. Most of the type 5 stars are at a temperature of close to 0. In the graph of luminosity vs. radius, the almost same scenario occurs, where above a radius of 500, most type 5 stars are seen. However, they are more spread out compared to being concentrated at 0 like the previous graph.

Temperature vs. absolute magnitude has more of a visible pattern. At absolute magnitudes 15–20, all star types are 0 or 1 and are concentrated around 0. From 10–15, the star types are all 1–2 and are concentrated from 0 to 25,000 in terms of temperature. From –5 to 10, all the star types are 3–4 and occur at various temperatures from 0 to 40000. Finally, from –10 to –5 are all type five stars from a range of temperatures. A similar pattern occurs in luminosity vs. absolute magnitude and radius vs. absolute magnitude, where the star type decreases as the total magnitude increases. However, all star types except for five are concentrated at 0. In radius vs. absolute magnitude, type 5 stars are concentrated from a radius of 1000 to 2000.

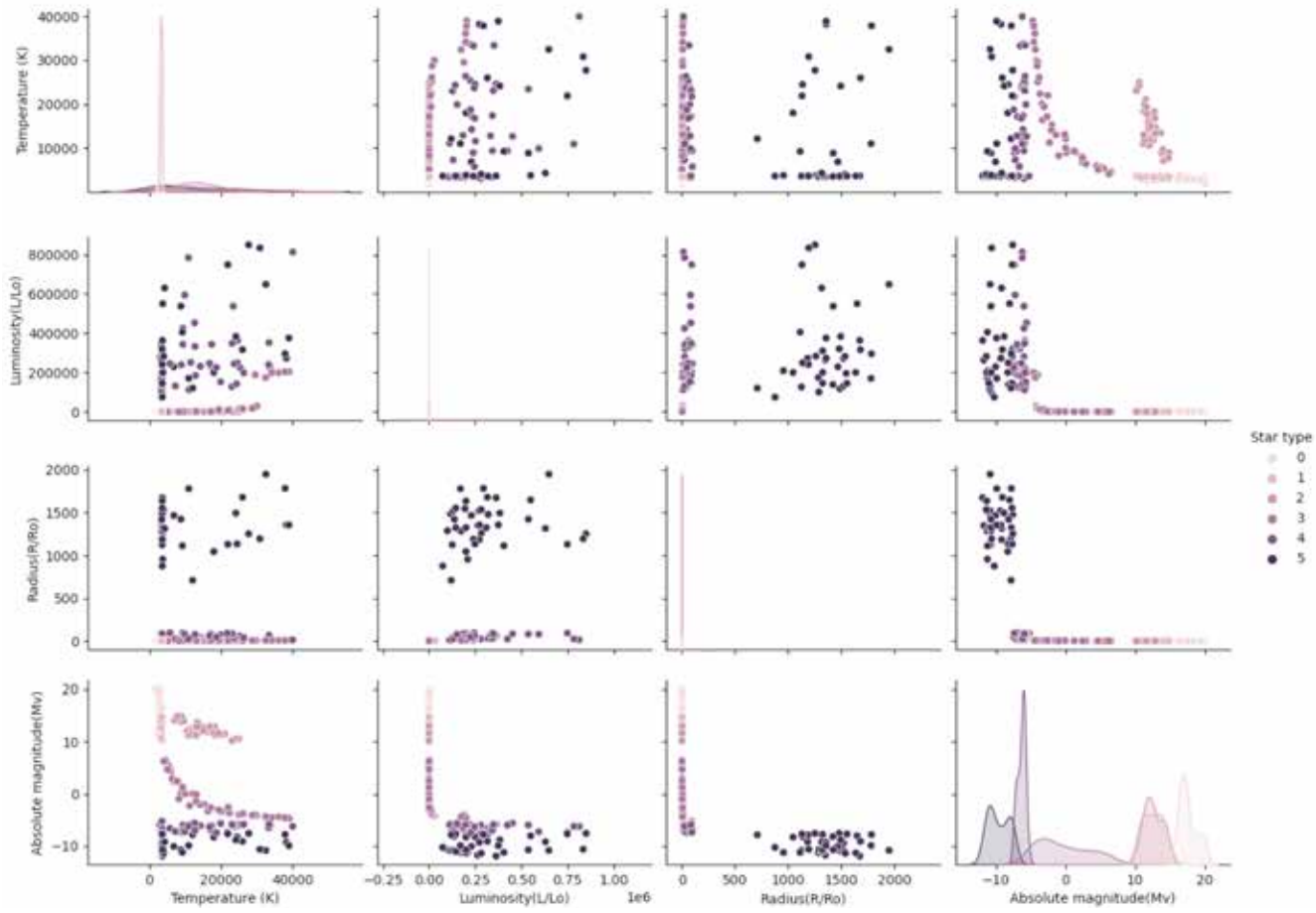

Figure 2. Pairwise relationship graphs

Models:

The machine learning models used include logistic regression, gradient boosting, k-neighbors and the evaluation metrics classification report, confusion matrix, and cross-validation. First, logistic regression is a type of predictive algorithm that is used for classification. Whereas linear regression uses a linear function, logistic uses a logistic function, also known as a sigmoid function, where output values are between 0 or 1. Second, a decision boundary function is centrally created, where all values below are classified at 0. Furthermore, all values above are classified at 1. This 0 or 1 represents the probability that can represent binary classes, such as a "yes" or "no" decision. Third, in linear regression, a cost function is then created to optimize the objective and minimize the error.

Next, the gradient boosting model is used. Gradient boosting trains learners from being weak to strong by implementing predictive models called decision trees. A decision tree is a model that can learn to predict the target variable but has the experience of the original dataset and the observations of the models of previous trees. As the tree number increases, the better the prediction is. By predicting through observation and error, the process can be repeated for a set amount of time, resulting in a final model with the added sum of improvements from the previous trees. The main way errors are identified through the gradients in the loss function ($y = ax + +b + e$), where "e" is the error term. The loss function is based on the margin of error between the correct value and the predicted value. The most essential part about gradient boosting is the optimization of the cost function.

A classification report is a report that shows the main classification metrics include accuracy, precision, recall, f1, and support. Four ways to check if these values are correct, true negative (case negative, predicted negative), true positive (case positive, predicted positive), false negative (case positive, predicted negative), and finally false positive (case negative, predicted positive). Precision is the percentage of correct predictions, also defined as the ratio of true positives to the sum of true positives and false positives. The recall is the fraction of correctly identified positives, which is the ratio of true positives to the sum of true positives and false negatives. . F1 score is the accuracy of positive predictions, times the recall times the precision divided by the sum of the recall and precision. The best score possible is 1.0, while the worst is 0.0. Finally, the support score is just a count of the occurrences of the class and reflects the evaluation process.

A confusion matrix is in the form of a table that describes the performance of a classification model. It compares the actual results to the predicted results, such as "yes" or "no," which yield true and false positives and negatives. Assigning values in category order provides a more quantitative result. The matrix can deliver several results. Accuracy is the ratio of true positives and true negatives to the total. Misclassification rate (also known as error rate) is the ratio of false positives and negatives to the total, one minus the accuracy rate. True positive rate, also known as recall, is the same as mentioned previously in the classification report. True negative rate, also known as specificity, is the ratio of true negatives to actual negatives, which is also one minus the recall. Finally, the precision score is the same as the classification report and prevalence, which is the ratio of actual positives to the total.

Finally, cross-validation is a method of training data in subsets, often a train and test set. Splitting the data is vital since data that is 98 or 99% accurate is not accurate enough. The most common cross-validation technique is the "K-Fold cross-validation". The first step in this technique is to split the data into "k" equal parts. The first part is tested, while the remaining parts with a value of k-1 are used to train the model. Then the trained model is tested on the holdout set, and the process is repeated k times. The yield is a cross-validation score, an average of a list of k accuracy scores.

Results:

Finally, by using the three machine learning models, logistic regression, neighbors, and gradient boosting, we obtained numerical results by classification report under columns of precision, recall, f1-score, and support. The different types of stars are classified under the numbers 0–6, representing Red Dwarf, Brown Dwarf, White Dwarf, Main Sequence, SuperGiants, and HyperGiants, respectively.

In the case of logistic regression, from 0–6, the values of precision were 0.00, 0.44, 0.89, 0.82, 1.00, and 1.00 respectively. Precision means the number of correct predictions, so the most accurate predictions were in the SuperGiants and Hypergiants with a value of 1.00. The lowest value was Red Dwarfs with 0.00, meaning the predictions were not at all correct. Both White Dwarf and Main Sequence were mostly correct since their precision values were close to 0.80. The recall values were 0.00, 1.00, 0.80, 0.90, 0.91, and 1.00 respectively. The recall is the fraction of positives identified correctly, and Brown Dwarfs and HyperGiants had the highest recall value of 1.00. These findings signify the identification of the positives was correct. Main Sequence and SuperGiants also had high fractions with values around 0.90. The lowest value was the Red Dwarf with 0.00, indicating that there was no identification of positives. Finally, the f1-score values were 0.00, 0.62, 0.84, 0.86. 0.95 and 1.00 respectively. F1-score is the accuracy of positive predictions, and HyperGiants had the highest accuracy of 1.00. White Dwarf, Main Sequence, and SuperGiants also had relatively accurate scores. The lowest was Red Dwarfs, with 0.00. In using logistic regression, all values of Red Dwarfs were 0.00 while all values of Hypergiants were 1.00. These results indicate a strong accuracy towards the HyperGiants and a lack of accuracy toward the Red Dwarfs.

By using KNeighbors, from 0–6, the values of precision were 0.63, 0.56, 0.91, 0.88, 0.91, and 1.00 respectively. The HyperGiant was the most accurate with a precision score of 1.00, while Red and Brown Dwarfs had lower values of 0.63 and 0.56. White Dwarfs, Main Sequence, and SuperGiants had relatively correct predictions, with scores of approximately 0.90. The values of recall were 0.86, 0.42, 1.00, 0.70, 0.91, and 0.93 respectively. The highest fraction of correct positives was White Dwarfs at 1, with SuperGiants and Hypergiants close at 0.91 and 0.93. The lowest was the Brown Dwarf at 0.42, which was a relatively low fraction. The values of the f1-score were 0.73. 0.48, 0.95, 0.78, 0.91, and 0.97 respectively. White Dwarfs, SuperGiants, and HyperGiants were all highly accurate with values around 0.90, while all other values were somewhat accurate except Brown Dwarfs at 0.48.

By using Gradient Boosting with Tree, all values of precision were 1.00 except for 0 being 0.88. These results show that utilizing Gradient Boosting yields very accurate results; Brown Dwarf, White Dwarf, Main Sequence, SuperGiants, and Hypergiants all had a value of 1.00, meaning entirely correct. The lowest was the Red Dwarf at 0.88, which is still mostly accurate. The values of recall were all 1.00 except 1 being 0.83. These results show that except for one, correctly identified all the positives. Brown Dwarfs still have a relatively high fraction of positives being identified at 0.83. The values of the f1-score were all 1.00 except for 0 and 1 being 0.93 and 0.91, respectively. All these values were either very high or perfect, so Gradient Boosting indicates high accuracy.

By comparing the three machine learning models, Gradient Boosting is the most optimal. Most of the precision, recall, and f1-scores were all 1.00, meaning 100% accuracy or 100% accurate predictions.

References:

1. What is Absolute Temperature? Universe Today. (December, 25. 2015). URL: https://www.universetoday.com/46840/absolute-temperature

2. Wikipedia contributors. Luminance. Wikipedia. (May 2. 2021).URL: https://en.wikipedia.org/wiki/Luminance
3. Wikipedia contributors. Luminance. Wikipedia. (May 2. 2021a). URL: https://en.wikipedia.org/wiki/Luminance
4. O. (n.d.). Colors of Stars | Astronomy. Lumen Learning. Retrieved September 25, 2021. From: URL: https://courses.lumenlearning.com/astronomy/chapter/colors-of-stars
5. Spectral Classes. (n.d.). Atnf. Retrieved September 25, 2021. From: URL: https://www.atnf.csiro.au/outreach/education/senior/astrophysics/spectral_class.html#:%7E: text=Some%20stars%20exhibit%20spectral%20anomalies%20resulting%20in%20them, zirconium%20oxide%20and%20lanthanum%20oxide.%20More%20items.%20
6. Redd N. T. Red Dwarfs: The Most Common and Longest-Lived Stars. Space.Com.(June 6. 2019). URL: https://www.space.com/23772-red-dwarf-stars.html
7. NASA – Brown Dwarf Detectives. (n.d.). Nasa. Retrieved September 25, 2021. From: URL: https://www.nasa.gov/vision/universe/starsgalaxies/brown_dwarf_detectives.html#:%7E: text=Brown%20dwarfs%20are%20failed%20stars%20about%20the%20size,energy%20source%20and%20emit%20almost%20no%20visible%20light
8. Giant star | astronomy. (n.d.). Encyclopedia Britannica. Retrieved September 25, 2021. From: URL: https://www.britannica.com/science/giant-star

Section 3. Machinery construction

https://doi.org/10.29013/EJTNS-21-4.5-32-39

Kobzar Igor,
SE "Plant" Electrotyazhmash", Head of Scientific-Research and Project Designing Department of Turbogenerator and Hydrogenators, Ukraine
E-mail: ivkobzar@ukr.net

Gakal Pavlo,
Doctor of Technical Sciences, Docent, National Aerospace University "KhAI", Associate Professor at the Department of Aerospace Thermal Engineering, Ukraine
E-mail: pavlo.gakal@gmail.com

Poliienko Vladyslav,
Postgraduate Student, National Aerospace University "KhAI", Ukraine
E-mail: vlad_polienko@ukr.net

Tretiak Oleksii,
Doctor of Technical Sciences,
SE "Plant "Electrotyazhmash", Head of Department, Ukraine
E-mail: alex3tretjak@ukr.net

Tretyak Volodimir,
Ph. D. in Technical Sciences, National Aerospace University "KhAI", Associate Professor at the Department of Aircraft Engine Manufacturing Technologies, Ukraine
E-mail: v.tretyak@khai.edu

FINITE ELEMENT ANALYSIS OF HIGH LOAD THRUST BEARINGS

Abstract. In the presented paper, the main designs of hydrogenerators are considered. It is shown that one of the most loaded units of the Hydrogenerator is the thrust bearing. The analysis of the causes of emergencies in the support unit of a high-power hydrogenerator is carried out taking into account the operating experience. Cause-and-effect relations of origin and development of defects are determined. The existing methods for calculating the stress state of the thrust bearing chambers in the classical setting for a stationary mode of operation are considered. The main features of the operation of the thrust bearing unit are investigated, taking into account the features of the sliding bearings. For the first time, the calculation of the elastic chambers of a thrust bearing was performed in a three-dimensional formulation, taking into account the physical properties of the oil, the material of the chambers, and the unevenness of the acting loads.

Keywords: thrust bearing, fatigue calculation, three-dimensional modeling, fatigue curve.

1. Investigation of the Generator Thrust Units Strength

1.1 Formulation of the Task

A characteristic feature of the design of a vertical Hydrogenerator is availability of a thrust bearing designed for the taking of axial loads of the thrust bearing [1–4]. In the suspended-type generators, the thrust bearing is arranged on the upper cross-piece. In umbrella-type generators, the thrust bearing is arranged on the lower cross-piece, which has the shape of a truncated cone resting on the turbine cover. The axial load from the weight of the rotating parts of the Hydrogenerator and the turbine, as well as from the axial reaction of the water on the blades of the impeller of the turbine act upon the thrust. In large units, the force on the thrust bearing can be up to 2500–3000 tons. These forces are transmitted by the thrust bearing from the shaft to the load-bearing or supporting cross-piece, and then through the stator casing are transmitted to the foundation. For high-power units, two types of thrust bearings are the most common: on adjustable screw supports and on hydraulic supports. Each of them has its advantages and disadvantages.

The thrust bearing is arranged in the oil bath which has water-cooled oil coolers. The movable part of the support structure consists of a hub, which is fit on the upper end of the shaft, and a ring into which the segments are inserted. The lower part of the hub which is equipped with a disk with a polished surface is a thrust bearing mirror.

The oil wedge is created at a certain speed of rotation of the unit on which all design of a thrust bearing is calculated therefore long rotations of the unit at number of turns below the rated one are undesirable. The most dangerous for the unit are starts and stops. To reduce friction in the thrust bearing during the start-up and stop stages, some generators provide additional oil injection under pressure through holes in the segments. For high-power units, it is assumed that the rotor is raised on the brakes before starting the unit, if before that its stop had duration longer than specified.

The main causes of the thrust bearings damage are microroughnesses. They are individual bulges and dents with a distance between them of hundreds of millimeters, located on the mirror surface of the disk in the direction of rotation. When the rotor rotates, these bulges and dents lead to the appearance of additional periodic loads acting on the segment. The causes of microroughnesses are structural defects and peculiarities. For example (e.g.), the thin bottom of the bush of the thrust bearing bends under loads action between the ribs of the bush, causing the emerge of bulges and dents on the attached disk of the thrust bearing; residual deformation of the thrust bushing as a result of hot fit on the shaft, which after attaching the disk to it, causes unevenness on its mirror surface; residual deformations of the disk that appeared during operation or installation; destruction of the gaskets installed between the disk and the bush.

In addition, microroughness leads to deterioration of working conditions of the thrust bearing during starts and stops. At starts the formation of the oil film which is divided on a friction surface becomes complicated and slows down. During emergency shot downs, there is a violation of the oil film, as a result of which the process of direct contact of the friction surfaces is prolonged, there are rubs on the segments, and then the babbit surface of the segments melts, and the thrust bearing loses efficiency. Even distribution of load on all segments is also important for reliable operation of the thrust bearing.

The nut of the screw support is used to adjust and ensure uniform loading of all segments. The load of the segment is controlled by its deflection. Micrometers or strain gauges of a design are used at an estimation of deflections. In the latter case, it is possible to achieve a more even distribution of the load by segments.

The thrust bearing balance is carried out with the help of adjusting screw supports. The screw support is the most loaded part of the thrust bearing, which is a disadvantage of this design. In addition, a significant disadvantage of a rigid thrust bearing is the complexity

and complexity of balancing. As a result of balancing, the difference in load by segments is ± 5–10%, depending on the applied method of measuring deformations.

These disadvantages have been partially overcome in the design of the thrust bearing on the hydraulic support. In it, the segment rests on a powerful steel bellows which is an elastic vessel filled with oil. Bellows of all segments are interconnected by pipelines that provide the same pressure in all bellows and thus the same load of all segments.

The main cause of damage to the bearings of the thrust bearing on the hydraulic support is the depressurization of the chambers, while the thrust bearing from the hydraulic with automatic load balancing between the segments is converted into a thrust bearing on the rigid supports. This is accompanied by a significant adjustment of the load on the segments. When cracks appear in the elastic chamber, it is replaced with subsequent filling of the entire system with oil.

In Figure 1 the Diagram of development of the abovementioned defect of the thrust bearing on the hydraulic support is shown. The causes of the defect (they are shown at the 1-st and 2-nd time levels) are increased pulsation in the thrust bearing or manufacturing defects. In the time levels 3…7 the further development of the emergency situation is shown.

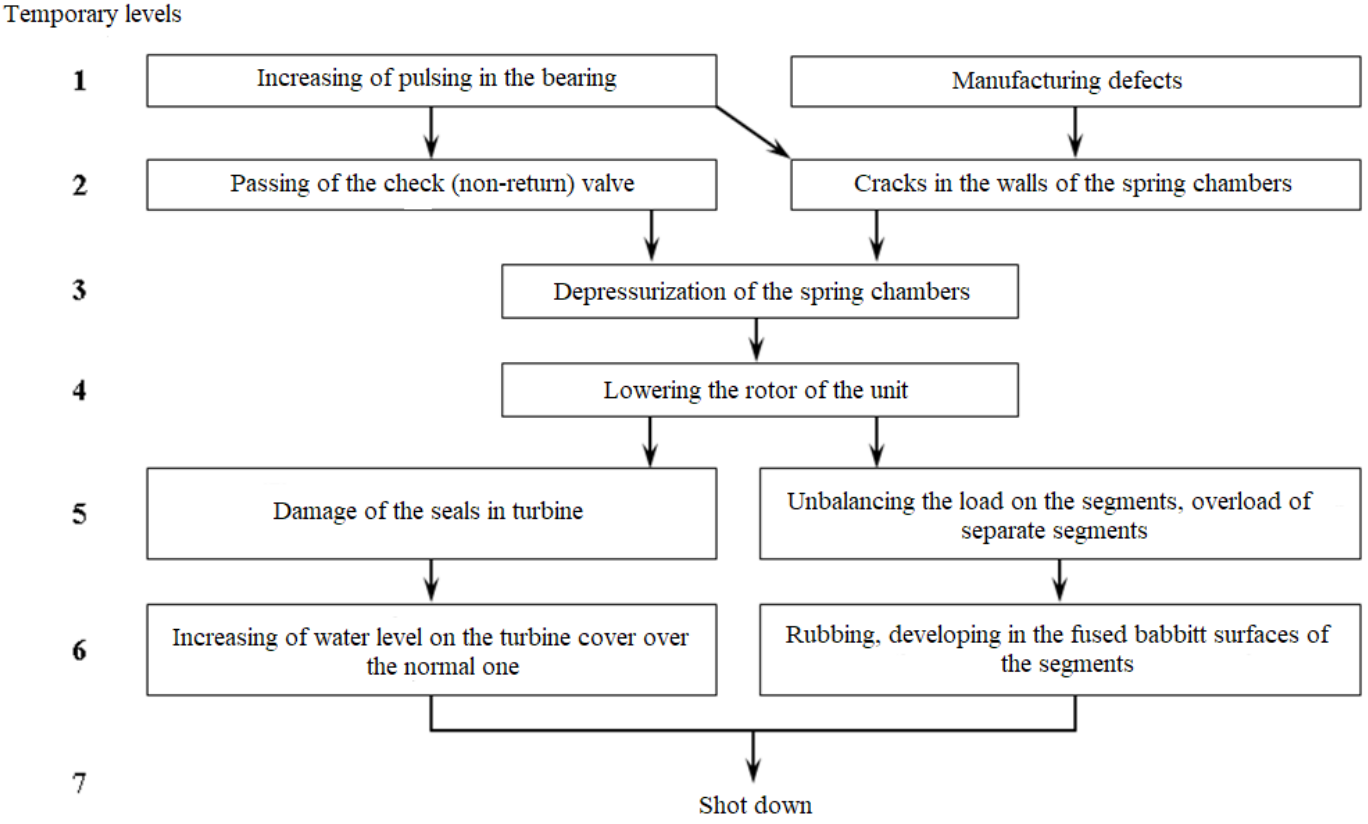

Figure 1. Diagram of Development of The Defects Spring Chambers Of The Thrust Bearing

The thrust bearings in high-power generators are subject to a significant axial load. At operation of Hydrogenerator-Motor rated 330 MW in the generator mode during the start the axial load on to the thrust bearing from the masses of rotating parts of the pump-turbine and water reaction can achieve of 300 tf and total axial load from water pressure and the rotating parts of the Hydro aggregate at rated mode is 2300 tf.

At that, the thrust bearing design shall not allow overheating, vibration, oil spraying and getting into the ventilation duct at all operation modes, including start-ups and stops, as well as operation at maximum runaway rotation speed.

In addition, the vertical vibration of the thrust bearing base (double amplitude) shall not exceed of 0.15 mm.

The segments of the thrust bearing are made with elastic metal-plastic straps (with fluoroplastic coating). At that the specific pressure on to the thrust bearing segments are limited with 6 MPa. The design provides uniform distribution of the load on to the segments with tolerance of ± 10%.

The thrust bearing is arranged in the oil bath protected from water ingress and is self-lubricating. For its lubrication oil of Grade TP-30 is used in accordance with GOST 9972–74 (or its analogue). It is cooled with water circulating through the oil coolers arranged in the oil bath to temperatures corresponding to the established norms.

The thrust bearing provides reliable work in both directions of rotation of the hydraulic unit, and also start of the Hydrogenerator after its long stop without application of special measures.

1.2 Analytical Calculation

As a result of analytical calculation, it was determined that complete stress in the tops of internal roundings of the corrugations of the internal row from the axial displacement and oil pressure is [5]:

$$\sigma_{B1} = \sigma_{B1}(u) + \sigma_{B1}(\rho) = 27.5 + 141 = 168.5 \text{ MPa} \quad (1)$$

where $\sigma_{B1}(u)$ – is the maximum meridional stress at the tops of the internal roundings of the corrugations of the internal row from the action of axial transfer;

$\sigma_{B1}(P)$ – is the maximum meridional stress at the tops of the internal roundings of the corrugations of the internal row from the action of oil pressure inside the chamber.

Complete stress in tops of internal roundings of the corrugations of external row from axial transfer and oil pressure [5]:

$$\sigma_{B2} = \sigma_{B2}(u) + \sigma_{B2}(\rho) = 51 + 102 = 153 \text{ MPa} \quad (2)$$

where $\sigma_{B2}(u)$ – is the maximum meridional stress in tops of internal roundings of the corrugations of external row from the action of axial transfer;

$\sigma_{B2}(\rho)$ – is the maximum meridional stress in in tops of internal roundings of the corrugations of external row from the action of oil pressure inside the chamber.

Thus, the stress level in the corrugations of the thrust bearing does not exceed the allowable values.

1.3 Three-dimensional numerical solution

The three-dimensional computational model of the thrust bearing chamber, which is made by the finite element method (MCE) (SolidWorks Simulation) is considered. In (Figure 2) shows the design grid and the limit conditions of the load of the thrust bearing under the action of the total axial load from the water pressure and the rotating parts of the hydraulic machine, as well as from the mass of the rotating parts of the pump-turbine and the water reaction.

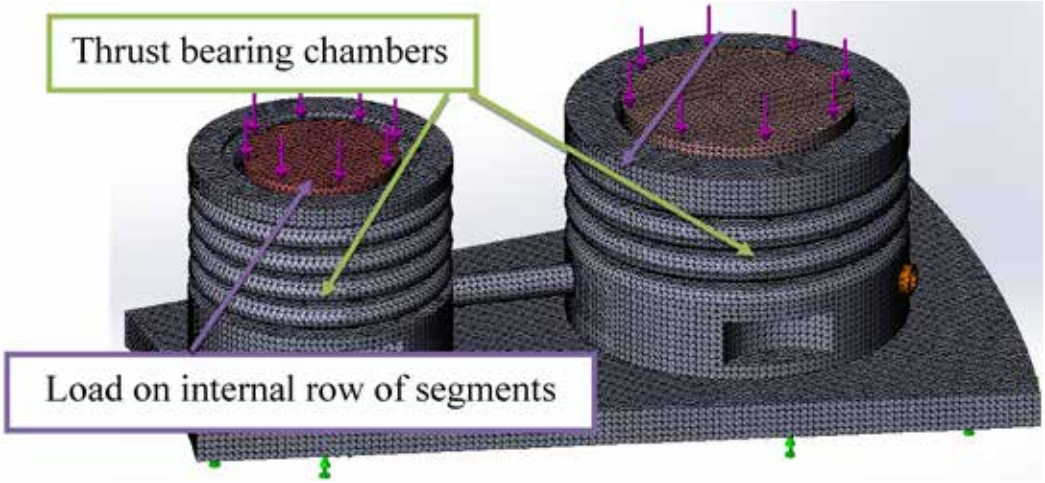

Figure 2. Calculation Diagram and Limiting Conditions of The Thrust Bearing Unit Loading

Table 1.– Parameters of the Grid

Type of the grid	Combined grid
Partition used	Standard grid
Automatic grid thickening	OFF
Switch ON automatic cycles of grid	OFF
Jacobian points	4 points
Jacobian check for the shielding	ON
Dimension of the element	7 mm
Tolerance	0.35 mm
Quality of grid	High
Total quantity of units	2017346
Total quantity of elements	1351299

As it can be seen from Figure 2 the design vessel (the thrust bearing chamber) is closed. It means that the physical properties of oil shall be the same everywhere and, consequently, pressure in all points of the chamber shall be almost constant (P = const).

The successive loading of the thrust bearing was considered at small increments of the load that allowed observing insignificant change in the oil elasticity modulus for each iteration.

In Figure 3 the fields of pressure are given inside the thrust bearing chambers of the sensor at the rated power of the generator.

Calculations are carried out with the help of the Package SolidWorks Flow Simulation. It can be seen from the figure that the oil pressure inside the chambers at rated load equals approximately 9 MPa.

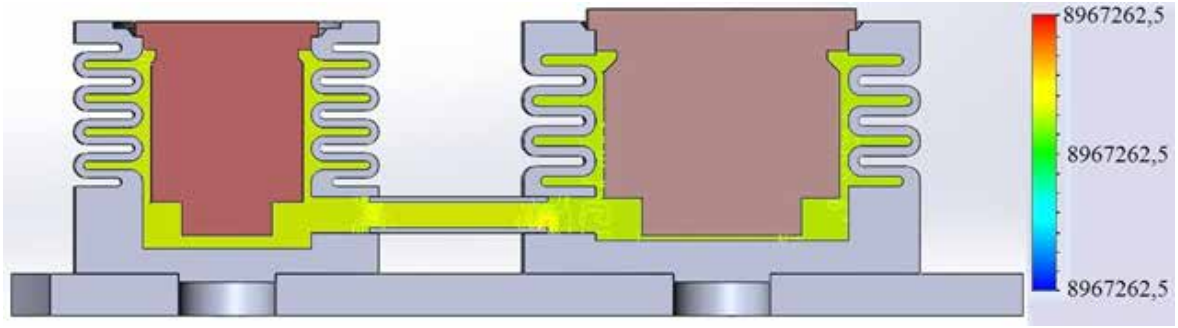

Figure 3. Pressure Fields Inside the Thrust Bearing Chamber, Pascal [Pa]

The stresses distribution on the surface of the corrugated chamber cross section is shown in (Figure 4). A more detailed image of the stress field in the corrugations is given in (Figure 5). All figures show the values of stresses calculated by Mises.

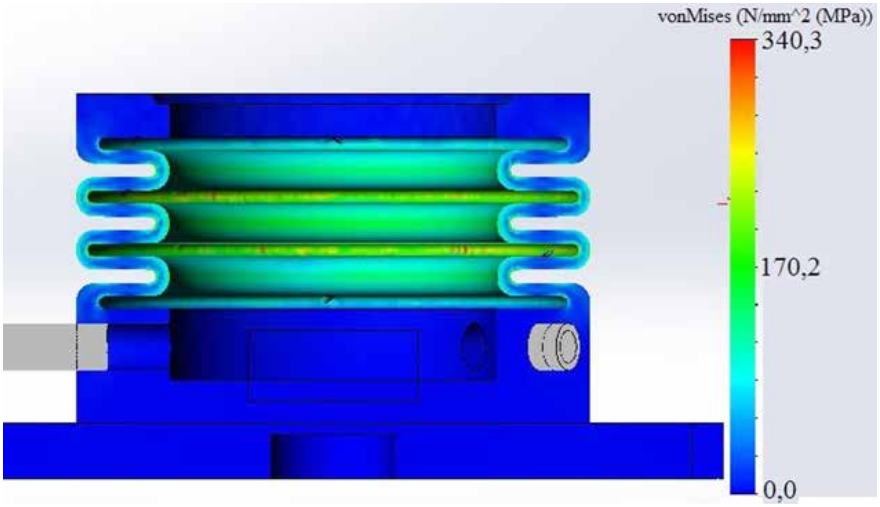

Figure 4. Field Of Stresses in The Cross Section of The Chamber. Liquidity Limit: 220.6 [MPa]

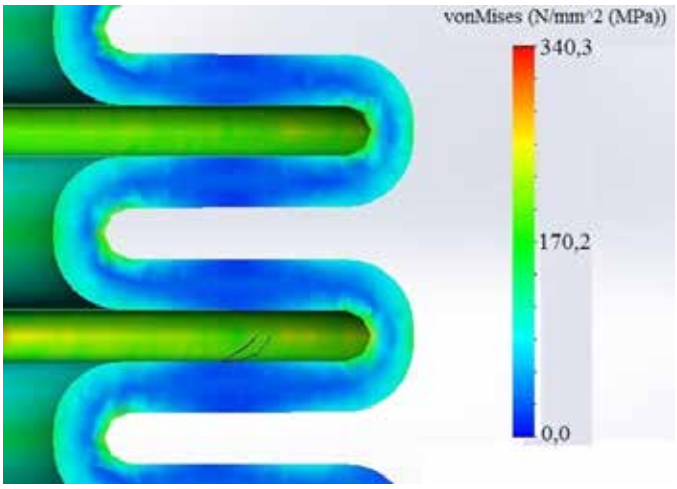

Figure 5. Stress Field in The Corrugations of The Chamber. Liquidity Limit: 220.6 [MPa]

From the calculations shown in (Figure 3–5), it can be seen that the maximum stresses in the chamber of the external row are observed in the top of the internal roundings of the corrugations, where it reaches 170 MPa. These data are qualitatively and quantitatively consistent with the analytical solution, which confirms the validity of the proposed method.

It should be noted that in the analytical calculation, the maximum tensile stresses in the chamber have slightly lower values and are equal to 153 MPa. At that, the analytical method uses a simplified calculation scheme of the chamber, which is based on engineering methods. Therefore, the observed difference of 10% in the values of maximum stresses is explained by a more accurate description of the spatial nature of the deformation of the chamber in the proposed finite-element three-dimensional approach. In all the above results of the calculation of the ITU are the values of not just tensile stresses, but Mises stresses.

Thus, the yield strength beyond the yield strength limit for the thrust bearing is about 1.3, which meets the requirements of TX116M.0133 [6] for structural fatigue and meets the strength standards.

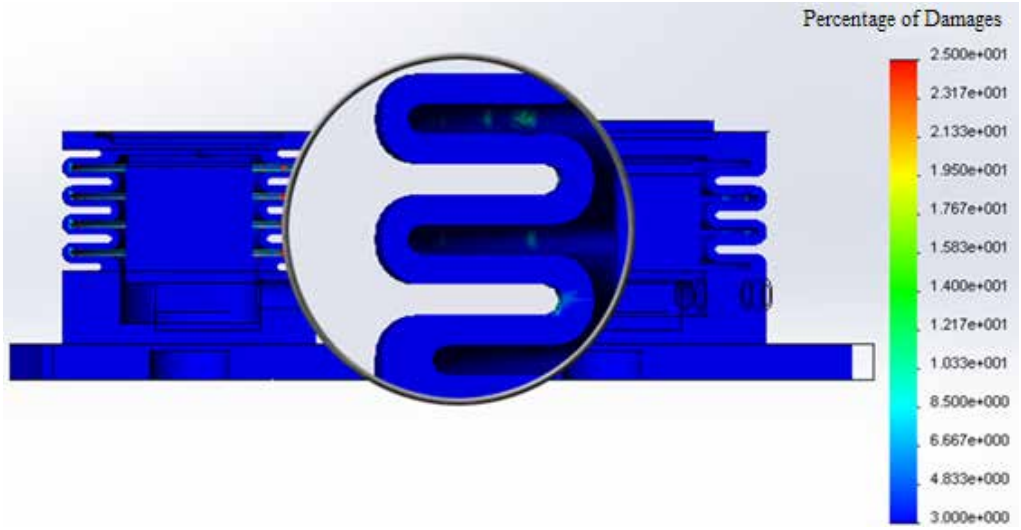

Figure 6. Percentage of Damages of Thrust Bearing Chambers

Due to the fact that hydraulic units shall operate for at least 40 years, and operating conditions require high maneuverability of electric machines, an additional analysis of the operation of the unit on

fatigue was carried out. When carrying out the fatigue calculation, the following factors shall be taken into account:

– technological factor;

– geometrical factor;

– the surface roughness factor (taking into account additional influence of roughness to local stresses and, consequently, on the fatigue strength of the component);

– the influence factor of surface hardening (taking into account influence (residual stress, hardness) of the changed state of the surface to fatigue strength of the corresponding technological procedure).

From the carried-out researches it can be seen (see Figure 6) that development of production wear (wearing out) of a design will occur not earlier than in 100 thousand cycles. This satisfies the requirements of GOST 14965–80, which set the required service life of about 55,000 cycles. Production wear (wearing out) of the structure will be much later than the estimated service life of the structure, which for the generator is 40 years.

Thus, the study of the strength of the thrust chamber of the Dniester HPP under the action of operating loads at rated mode confirmed its strength and the required service life.

1.4 Study of Convergence of Results by HSS Method

In order to exclude the singularity in determining of the stresses of the concentrators by the method of HSS welded joint of sheets, with triangular elements or in the form of a tetrahedron the dimensions of the elements near the place of the weld (stress concentrator) is not over than half the thickness of the sheet t. Stresses are determined at a distance of 0.5t and 1.5t from the weld (Figure 7). If the computational resources allow to model welds, then the stress concentrator shall be arranged near the "foot" (base) of the weld. The interpolation line (AB) shall be arranged perpendicular to the direction of the weld. The grid step is chosen so that the test values of stresses s_0 and s_{15} were calculated in different elements. Rated (geometric) stresses s_0 in the hub are determined by linear interpolation by the formula [8]:

$$\sigma_0 = 1.5\,\sigma_{0.5} - 0.5\,\sigma_{15} = 1.5s_{05} - 0.5s_{15} \qquad (3)$$

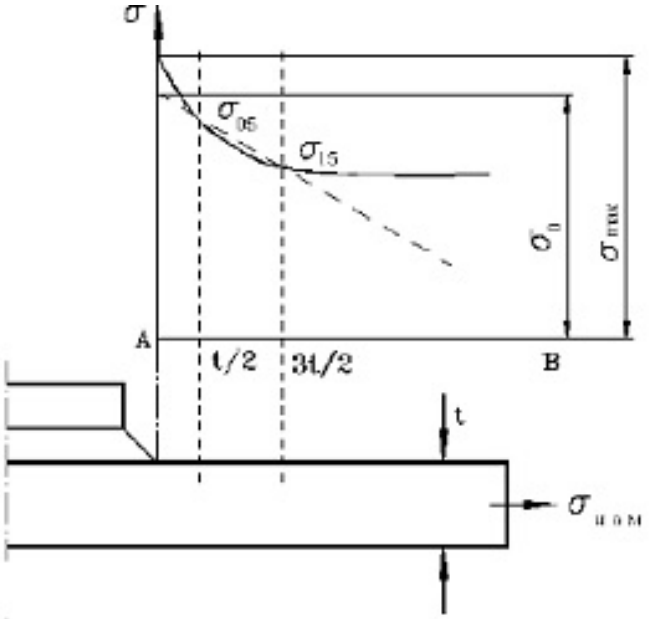

Figure 7. Using of HSS Methods for Determining of Geometrical Stresses

We will carry out an analysis using the HSS method to calculate the thrust bearing chamber, ducts and interpolar jumper. The results of the analysis for the hydraulic chamber of the thrust bearing are shown in Figure 8–9.

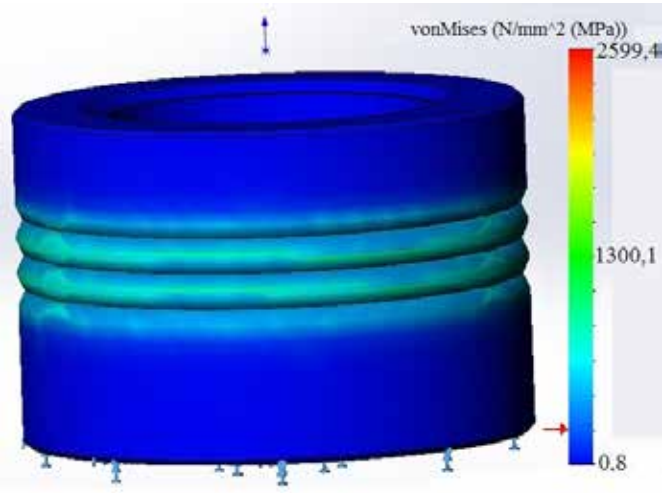

Figure 8. Field of Stresses in Thrust Bearing Chamber. Liquidity Limit: 220.6 [MPa]

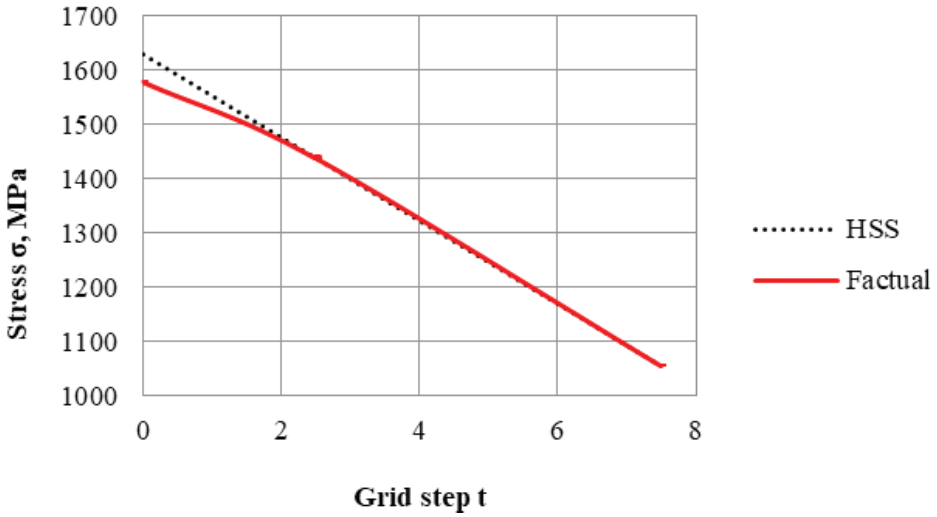

Figure 9. Results of Methods HSS for Determining of Geometrical Stresses in Thrust Bearing Chamber

References:

1. Voldek A. I., Popov V. V. Electric Machines. AC Machines: textbook for high-school.– Sent-Petersburg: Piter, 2010.– 350 p.
2. Hydropower. Construction of HPP Buildings: text book / T. A. Filippova, M. Sh. Misrikhanov, Yu. M. Sidorkin, A. G. Rusina.– Novosibirsk: NGTU, 2011.– P. 435–444.
3. Hydrogenerator Thrust Bearing. URL: https://chebelektra.ru/dvigateli/podpyatnik-generatora/ (date of request: 08.09.2019).
4. Operation of Thrust Bearings and Bearings of Hydrogenerators. URL: http://forca.ru/instrukcii-po-ekspluatacii/raznoe/ekspluataciya-generatorov-sinhronnyh-kompensatorov-3.html/ (date of request: 08.09.2019).
5. TX.116–4304. Technical Parameters of the Thrust Bearing Chamber for Hydro-generator-Motor SV01255/255–40.– Kharkov: SE "Plant «Electrotyazhmash»". 2010.– 5 p.
6. TX116M.0133. Calculation of Fatigue Strength of Chambers of Two-Row Thrust-Bearing of Hydrogenerator-Motor for Dnestrovskaya HAPP SV01255/255–40.– Kharkov: SE "Plant «Electrotyazhmash»". 1980.– 5 p.
7. Biryukov V. P., Petrova I. M., Gadolina I. V., Tatarkin D. Yu. Optimization of la-ser welding deposition modes and selection of nickel-based powders to increase the fatigue limit of specimens and machine parts. Discoveries and achievements of sciences. Collection of Materials of the International Scientific Conference.– Moscow, 30–31 July, 2015.– P. 52–60.
8. OTX.220.660. General Methodology of Calculation of Hydrogenerators.– Khar-kov: SE "Plant «Electrotyazhmash»". 2010.– 15 p.

Section 4. Medicine

https://doi.org/10.29013/EJTNS-21-4.5-40-43

Datsyshyn Pavel,
PhD, in Medicine, docent, Ukraine
E-mail: Ferduk@mail ru

Nikolaenko Oksana,
PhD, in Biology, docent
E-mail: oksnikolaienko@gmail.com; gmail.com
Department of Normal physiology,
Vinnitsa National Medical University
n.a. M. I. Pirogov, Ukraine
E-mail: oksnikolaienko@gmail.com

ON METHODS FOR ASSESSING THE LEVEL OF FORMATION COMPETENCES OF SECOND COURSE STUDENTS OF A MEDICAL UNIVERSITY

Abstract. Evaluation methods of academic achievements of higher school students are considered in the paper from the point of view of competency-based education. Such methods as observation, a questionnaire, appraisal tests, the expert evaluation method, the portfolio method, the case study method and others are proposed as tools of competency formation assessment.

Keywords: universal competencies, professional competencies, evaluation methods, competency formation level, competency formation assessment.

The opposite of a correct saying is
false statement. But the opposite
deep truth, there may be another deep truth.
(Niels Bohr).

The modern educational process is a complex activity aimed at the formation of universal and general professional competencies of university students and, in particular, the second course of a medical university. These professional competencies determine the professional potential of trainees, their ability to effectively and stable life in the modern sociopolitical, economic and communication space.

Thus, the set of competencies mastered by students at different departments represents the results of education, the effectiveness of which is determined by the corresponding pedagogical conditions, the existing educational environment of the university.

Among the signs that signal the formation of competence, the following features stand out: dynamism, interactivity, situationalilly (connection with the context), versatility and consistency. The

contextual nature of competence is manifested in the ability to realize the experience of activity in a specific situation of professional or everyday interaction. In addition, the formation of competencies is associated with the process of development, improvement of skills, skills and abilities, achievement of a certain level of skill and experience.

Based on the characteristics of competencies listed above, we can talk about the appropriate level of their formation and assessment procedures, reflecting the functions and principles of monitoring the formation of the level of competencies.

It is proposed to assess the level of competence formation according to criteria including the following levels: cognitive component (knowledge level), integrative-activity component (level of skills and abilities), personality component; motivational component.

On the basis of the cognitive criterion, the level of knowledge of the theoretical and methodological foundations of the studied discipline, in our case, normal physiology, and the creative abilities of students is determined. At the cognitive level, the degree of formation of the scientific, theoretical and practical readiness for the professional activity of a doctor is also determined.

The integrative-activity component is associated with the mastery of skills and abilities acquired by students in the process of mastering academic disciplines, the ability to apply the theoretical knowledge in professional activities. These are practical skills that students acquire in the classroom.

The personal component of competence contributes to the determination of the level of formation of the individual qualities of students, value-motivational sphere, and communication skills. First, the ability to communicate in a group, which later will help correct communication with patients.

The motivational component guides students towards achieving success in their professional activities [3, C. 81; 4].

The objectivity of assessing the level of competence formation is associated with the selection and systematization of methods for assessing and measuring the results of education. Monitoring of the formation of competencies can be carried out using the following research methods:

– observation (tracking changes in competencies under the influence of the educational process);

– survey methods (obtaining information based on the analysis of written and oral answers to standard and specially selected questions, practical tasks);

– midterm certification tests;

– method of expert assessments, which implies the involvement of experts-experts in the assessment of the level of competence formation: practitioners, employers, representatives of the scientific and pedagogical community (to assess the results of educational professional, research and creative activities of students).

– portfolio (assessment technology aimed at identifying the level of formation of general cultural and professional competencies, and their improvement by making corrections in the educational process);

– case-method (an assessment procedure that uses problematic situations and tasks related to the future professional activity of students and affecting various subject areas);

– method of projects;

– business games and trainings.

Let us dwell on some technologies for assessing the level of competence formation in more detail. So, using the case method, which is used as a diagnostic tool, the ability to effectively apply the acquired knowledge and skills, practical experience, and communication skills in solving practical problems is assessed. Within the framework of this method, it is possible to directly diagnose the level of independence, initiative of trainees, the ability to work in a team, find rational solutions and other analytical abilities. The case-method allows you to obtain a comprehensive assessment of the level of formation of professional competencies [1, C. 227].

The use of various gaming technologies (role-playing games, business games, trainings, intellectual games) in professional education is one of the most promising areas in modern conditions. The high

innovative potential of gaming technologies is determined by the participant's deep immersion in the game situation, extensive use of interactive interaction, and the formation of teamwork skills. Within the framework of the appropriate game technology used by the teacher in the educational process, it is possible to assess the skills of social interaction and management of people, the ability to lead and obey, take responsibility, find ways to interact with partners, take individual and joint actions to solve educational problems.

The design technology is based on the development of the cognitive, creative, analytical abilities of trainees, the ability to independently design their knowledge, navigate the information space, and develop critical thinking. Design technology is always focused on independent activities (individual, pair, group) performed by students for a certain period of time. This approach is organically combined with group work and technology of collective interaction. Project technology contributes to the development of skills for joint activities, develops a sense of individual and collective responsibility, and teaches cooperation. An important component of the project technology is the stage of project defense, during which the teacher assesses the level of formation of the declared competencies. In addition, at this stage, presentation skills and abilities, communicative and interactive competence of students are diagnosed. The results of completed projects should be "tangible", substantive. So, if trainees are working on a theoretical problem, they must present a specific solution to it. The practical task should be focused on practical results, ready for use.

Unlike other methods, the project method carries not only the function of controlling knowledge, but also a significant element of training and developing the thinking of a future doctor. In this method, students can use many medical terms, specific language clichés that the doctor should use in his conclusions and explanations, the formulation of the diagnosis, the connection of pathological changes with clinical manifestations, the solution of medical and diagnostic questions and much other information that helps to develop certain associative connections and improve the quality of memorization of educational material.

Application of the method to control knowledge in practical lessons and, especially, in the final lessons had a higher productivity than the traditional questioning and solving tests. The interview with the students was more meaningful, since it took place on a specific clinical situation and gave the student the opportunity to show his awareness of this issue, draw logical conclusions and show how deeply he understands the problem or situation raised in the problem. In addition, other students can act as consultants, make their own additions, or collectively discuss the situation and, using the method of brainstorming, come to the correct and more complete solution for this particular situation.

A portfolio is a technology for working with the results of educational and cognitive activities of students, used to demonstrate, analyze and evaluate and self-assess the results of educational activities. Diagnostics of the results is carried out on the basis of a collection of individual types of work collected over a certain period (semester, academic year). Assessment is carried out in terms of the formation of competencies acquired within the framework of this technology (professional reflection skills, creativity, self-education skills) [2, C. 14].

References:

1. Бордовская С. Ю. Оценка уровня сформированности ключевых компетенций будущих рабочих с помощью кейс-метода / С. Ю. Бордовская // Вестник ТГПУ (TPSU Bullletin). 2011.– № 13 (115).– С. 226–230.
2. Гущин Ю. В. Интерактивные методы обучения в высшей школе / Ю. В. Гущин // Психологический журнал Международного университета природы, общества и человека «Дубна» (Dubna Psychological Journal). 2012.– № 2.– С. 1–18.

3. Елисеев И. Н. Методология оценки уровня сформированности компетенций студентов / И. Н. Елисеев // Информатика и образование. 2012.– № 4.– С. 80–85.
4. Пахаренко Н. В. Модель определения уровня сформированности общекультурных и профессиональных компетенций / Н. В. Пахаренко, И. Н. Зольникова // Современные проблемы науки и образования. 2012.– № 6.– Режим доступа: URL: http://www.science-education.ru/106-7502

Section 5. Agricultural sciences

https://doi.org/10.29013/EJTNS-21-4.5-44-48

Volokitin Mitrofan Petrovich,
Ph.D., in Agricultural sciences, senior researcher
Institute of Basic Biological Problems, RAS, Pushchino, Russia
E-mail: volokitin1@rambler.ru

IIRRIGATION AND RECLAMATION OF SOLONETS SOILS

Abstract. Research has been carried out to study the effect of irrigation on soil properties. A method for reclamation of solonetz soils is proposed.

Keywords: irrigation, soil properties, saline soils, chemical reclamation.

Волокитин Митрофан Петрович,
канд. с-х. наук, старший научный сотрудник
Института фундаментальных проблем биологии РАН,
г. Пущино, Россия
E-mail: volokitin1@rambler.ru

ОРОШЕНИЕ И МЕЛИОРАЦИЯ СОЛОНЦОВЫХ ПОЧВ

Аннотация. Проведены исследования по изучению влияния орошения на свойства почв. Предложен способ мелиорации солонцовых почв.

Ключевые слова: орошение, свойства почв, солонцовые почвы, химическая мелиорация.

Введение. Орошение является мощным антропогенным фактором, который оказывает значительное влияние, практически, на все элементы окружающей среды. В орошаемом земледелии накоплен большой опыт по орошению сельскохозяйственных культур в различных почвенно-климатических зонах. Однако до сих пор ученые и практики затрудняются однозначно дать ответ на вопрос: Какие земли, как, и в каком объеме нужно орошать? Это, прежде всего, связано с просчетами при строительстве и эксплуатации оросительных гидротехнических сооружений, выбором объекта орошения, с недостаточными знаниями процессов, протекающих в почве, а в последнее время – и с новыми социально-экономическими условиями [2; 3].

Целью исследований являлось изучение возможности вторичного засоления и осолонцевания орошаемых почв, а также выяснение возможности применения технического лигносульфоната аммония (ЛСА) для мелиорации солонцов. Объектами исследований были предкавказские черноземы и солонцы-солончаки (Ростовская обл., Багаевский район), южные солонцевато-глубокосолонцеватые черноземы (Ставропольский край, Андроповский район).

Результаты. Наши исследования показали, что при правильном выборе объекта орошения и соблюдении основ эксплуатации оросительных систем орошение не вызывает существенных изменений в вещественном составе почв. Так, содержание солей, гумуса, обменных катионов после 30 лет орошения предкавказских черноземов (Ростовская обл.) оставалось на уровне их неорошаемых аналогов. Отмечено некоторое увеличение подвижности карбонатов, которые диагностируются морфологическими (белоглазка становится более рыхлой, пятна заметно увеличиваются) и химическими методами. Повышение уровня грунтовых вод не было отмечено.

При орошении почв равновесное состояние ионов устанавливается между твердой фазой почвы и почвенным раствором. Поэтому необходимо учитывать процесс осаждения или растворения кальцита при испарении оросительных вод в результате эвапотранспирации. Исследования показали, что величина коэффициента селективности обмена (К) натрия-кальция на обыкновенных и карбонатных черноземах зависит от степени заполнения почвенно-поглощающего комплекса (совокупность высокодисперсных коллоидных веществ, ППК) обменным натрием. При содержании обменного натрия менее 1% от суммы поглощенных катионов наблюдается большое сродство почвы к натрию, что выражается в увеличении коэффициента селективности. Резкое снижение К с ростом содержания обменного натрия означает, что в первые годы орошения при достижении содержания обменного натрия до 2% адсорбция натрия почвой снижается. Это приводит к накоплению натрия в почвенном растворе, что вызывает повышение пептизируемости органо-минеральных коллоидов, снижение водопроницаемости и слитизации почв. В интервале от 2 до 30% обменного натрия величина коэффициента селективности меняется незначительно. Причем для разных почв эта величина близка.

Среднее значение К при широком соотношении натрия в поглощенном комплексе почвы (sodium adsorption ratio) от 2 до 30% равно 0,14 моль/л. Коэффициент селективности обмена магния-кальция также зависит от содержания обменного магния. При снижении обменного магния в почвах до 7–8% коэффициент селективности возрастает до 2.

Для того, чтобы не допустить нежелательных изменений в составе обменных катионов необходимо оценивать качество воды по активности ионов натрия и кальция в почвенной пасте. Соотношение квадрата активности натрия к активности кальция не должно превышать 0,024.

Нами было показано, что за десять лет орошения водой низкого качества активность иона кальция в пахотном горизонте карбонатного чернозема снизилась с 7,5 до 2,6 мг-экв/л, а активность натрия увеличилась с 0,4 до 17 мг-экв/л. Содержание обменного натрия в карбонатном черноземе увеличилось до 9,7%. В верхней части почвенного профиля образовалась трещиноватая, глыбистая корка мощностью 5–7см.

Наиболее масштабные негативные явления происходят при орошении исходно засоленных и солонцеватых почв. За сравнительно непродолжительный период орошения (12 лет) южных черноземов (Ставропольский край, Андроповский район) без устройства дренажа, так как рассчитывали на естественную дренированность территории, уровень грунтовых вод повысился до 2,0–1,4м. При близком залегании минерализованных грунтовых вод (14 г/л) содержание солей в орошаемом черноземе даже увеличилось. Возросло содержание анионов (Cl^-, SO_4^{2-}), образующих токсические соли. Изучение почвенных растворов орошаемых черноземов показало, что они формируются в зависимости от расположения почв по рельефу. Так, при расположении черноземов на водораздельной части формирование почвенных растворов происходит под влиянием взаимодействия оросительных вод с твердой

фазой почвы. При расположении в пониженной части склона на формирование почвенных растворов оказывают влияние еще и грунтовые воды.

В первом случае происходит рассоление почв в результате снижения солей в почвенных растворах за счет пресных оросительных вод. Сумма ионов в орошаемом черноземе на водоразделе в слое 25–87см в 2,2–4,3 раза была ниже, чем в неорошаемой почве на склоне. Однако, суммарная токсичная щелочность (HCO_3^-, Mg^{2+}, Na^+) ионов почвенного раствора оставалась достаточно высокой, а pH был щелочным. В орошаемом южном черноземе, расположенном на склоне, происходило концентрирование почвенных растворов. Начиная, с глубины 20–45см концентрация почвенного раствора превышала в 3 раза допустимую величину, которая при хлоридно-сульфатном типе засоления не должна превышать 3 г/л. Из-за высокого содержания токсичных солей в почвенном растворе всходы люцерны на значительной площади погибли.

Таким образом, орошение исходно засоленных и солонцеватых южных черноземов, без проведения комплексной мелиорации, не приводит к их рассолению и рассолонцеванию.

Особо следует отметить практику инициативного орошения на местном стоке, осуществляемую в подчиненных и транзитных ландшафтов склонов и в долинах малых рек. Использование на орошение минерализованных и щелочных вод за короткий период привело к засолению и осолонцеванию почв. Сооружение местных водоемов для накопления воды, при незначительной облесенности территории, сопровождается заилением водоемов и аккумуляцией в них загрязняющих веществ. Искусственное зарегулирование стока пагубно сказывается и на экологии пойменных ландшафтов. Подобные последствия орошения отмечаются практически во всех южных регионах.

Таким образом, можно заключить, что процессы деградации почв проявляются на оросительных системах с неудовлетворительными почвенно-мелиоративными условиями. Наличие солей в почвах, или близко залегающих породах, недостаточная естественная дренированность территорий, отсутствие дренажа или его невысокая эффективность сопровождаются подтоплением, засолением и осолонцеванием почв. В результате этого сотни тысяч гектаров земель были выведены из сельскохозяйственного использования.

Солонцы характеризуются высокой дисперсностью коллоидной массы, имеют плотную глыбистую структуру, высокую набухаемость, низкую порозность и водопроницаемость. После иссушения солонцовые почвы становятся очень плотными, трещиноватыми, глыбистыми или столбчатыми. Они с трудом поддаются механической обработке.

Коренным приемом химической мелиорации солонцов является внесение в почвы гипса для замещения обменного натрия, содержащегося в ППК. Для нейтрализации высокой щелочности содовых солонцов применяют кислые химические вещества – железный купорос, серу, серную кислоту, отходы химической промышленности и др. [1]. Помимо снижения щелочности, кислые мелиоранты повышают растворимость соединений кальция в почве.

Большой интерес для мелиорации солонцов и солонцовых почв представляет использование производных лигнина. Лигносульфонаты получают в виде смолоподобного продукта темно-коричневого цвета, при гидролизе древесины на целлюлозно-бумажных комбинатах. Они состоят из смеси сульфолигнина, продуктов разложения целлюлозы и лигнина, содержат различные углеводы, минеральные вещества, свободные серную кислоту и сульфаты.

В данной работе исследовалось влияние технического лигносульфоната аммония на физико-химические, биологические и биохимические свойства солонца-солончака сульфатно-содового. Важно было выяснить продолжительность действия ЛСА как структурообразователя, а также

влияние его метаболитов на микробиологическую и ферментативную активность почвы. Солонцы-солончаки сульфатно-содовые широко развиты на повышенной части поймы р. Дон (Ростовская обл.) с абсолютными отметками 4,3–4,7м. Грунтовые воды залегают на глубине 250–300см, состав их хлоридно-сульфатно-содово-натриевый. В солонцовом горизонте содержание обменного Na^+ составляет 70–85% от суммы поглощенных оснований, реакция сильнощелочная (pH до 9,7). Почвы суглинистые, малогумусные.

В солонце-солончаке сульфатно-содовом обработке ЛСА, предварительно, растворенном в воде, подвергался верхний 10-сантиметровый солонцовый горизонт, обладающий неблагоприятными свойствами. Препарат вносили в дозе 19 и 28т/га. Изучались засоление, состав поглощенных оснований, гранулометрический и микроагрегатный составы, содержание общего гумуса, биологические свойства (численность микроорганизмов, ферментативная активность). В полевых условиях определяли величину плотности сложения почвы.

Результаты гранулометрического и микроагрегатного анализов, через год после внесения ЛСА, показали, что препарат вызывает значительное увеличение водопрочности агрегатов на солонце-солончаке. Доза 28 т/га снизила значение фактора дисперсности (отношение содержания частиц менее <0,001мм микроагрегатного анализа к содержанию частиц менее <0,001мм гранулометрического анализа по Качинскому), в солонце-солончаке почти до уровня черноземных почв (K = 8–26%). В варианте опыта с 19 т/га ЛСА фактор дисперсности равнялся 46,6%, что в 1,4 раза было ниже, чем на контроле (K = 66,0%). Через 2 года после внесения ЛСА верхний слой солонца-солончака, обработанный препаратом, сохранял благоприятную структуру. Следует отметить, что действие препарата на структуру почвы проявляется и в слое 20–30 см, т.е. ниже изначально мелиорируемого слоя. На третий год последействие препарата на структуру почвы несколько снизилось.

Внесение технического лигносульфоната аммония положительно сказалось на ионном составе и содержании легкорастворимых солей в солонце-солончаке, определяемых методом водной вытяжки. При этом эффект от обработки заметен и в нижележащих горизонтах. Уменьшилось содержание гидрокарбонатов. Резко снизилась щелочность от нормальных карбонатов в верхних мелиорированных горизонтах в варианте с 19 т/га ЛСА (с 1,45 до 0,46 мг-экв/100 г. почвы), в варианте с 28 т/га препарата в этих горизонтах ее не обнаружено совсем. Снизилось абсолютное количество легкорастворимых солей натрия, тогда как относительное содержание солей кальция увеличилось. Произошло снижение величины pH с 9,4–9,7 в контроле до 7,9–8,3 в варианте с 28 т/га препарата.

Показательны изменения в составе поглощенных оснований солонца-солончака сульфатно-содового. Величина суммы обменных оснований практически не изменилась, но произошла качественная перестройка почвенного поглощающего комплекса. Абсолютные и относительные количества обменного Ca^{2+} заметно возросли с увеличением дозы ЛСА. Так доля обменного кальция изменилась с 32,7% на контроле до 38,4% в варианте с 19 т/га ЛСА и до 62,0% в варианте с 28 т/га ЛСА (табл. 1). Эти изменения происходят за счет снижения доли обменного натрия в ППК. Отмечается тенденция к увеличению обменного калия с ростом дозы препарата. Положительное действие на состав обменных катионов сохраняется на второй и третий годы с момента внесения препарата.

Изменение физико-химических свойств почвы сопровождается количественной и качественной перестройкой ее микробного ценоза. Увеличение общей численности микроорганизмов характеризует улучшение благоприятных свойств почвы. Через год после внесения ЛСА в солонце-солончаке общая численность микроорганизмов в почве увеличилась в 1,7–3 раза.

Таблица 1.– Содержание гумуса, азота и обменных катионов в солонце-солончаке (через год после обработки ЛСА)

Варианты опыта (дозы ЛСА, т/га)	**Гумус,%**	**Общий азот,%**	**Обменные катионы в% от суммы поглощенных оснований**			
			Ca^{2+}	**Mg^{2+}**	**Na^{+}**	**K^{+}**
Контроль	0,24	0,045	32,7	2,9	62,0	2,4
19 т/га	0,79	0,054	38,4	4,4	54,8	2,5
28 т/га	0,98	0,072	62,1	3,3	31,5	3,1

Заключение. Исходя из этого следует заключить, что технический лигносульфонат аммония в дозе 28т/га можно использовать для улучшения ряда свойств содовых солонцов-солончаков, относящихся к наиболее злостному типу засоления и обладающих в естественных условиях крайне низким плодородием. Надо отметить и другую сторону необходимости широкого использования ЛСА в мелиоративных целях – утилизацию большого количества неиспользованных отходов целлюлозно-бумажной промышленности, что будет способствовать сохранению окружающей среды.

Список литературы:

1. Балакай Г. Т., Докучаева Л. М., Юркова Р. Е. Способы мелиорации орошаемых солонцовых почв.– Новочеркасск, 2011.– 73 с.
2. Каштанов А. Н. Концепция устойчивого развития земледелия России в XXI веке // Почвоведение. 2001.– № . 3.– С. 263–265.
3. Новикова А. Ф. Мелиоративное состояние и деградационные процессы на орошаемых землях России // Почвоведение. 1999.– № . 5.– С. 614–625.

Section 6. Technical sciences

https://doi.org/10.29013/EJTNS-21-4.5-49-57

Dr. Hoang Ngoc Hai,
University of Fire Prevention and Fighting, Vietnam
E-mail: hoanghait34@gmail.com; hung.police114@gmail.com

STATE MANAGEMENT OF FIRE PREVENTION AND FIGHTING FOR HIGH RISE APARTMENT BUILDING IN VIETNAM – THEORETICAL AND PRACTICAL ISSUES

Abstract. Construction and development of high-rise buildings is an inevitable trend, not only in Vietnam but also other countries in the world. The issue of state management of fire prevention and fighting for high-rise buildings is an issue that has always received much attention from countries, especially developing countries. The article analyzes and clarifies theoretical and practical issues of state management of fire prevention and fighting for high-rise buildings in Vietnam; on that basis, draw out solutions to improve the efficiency of state management of fire prevention and fighting for high-rise buildings to meet the requirements of sustainable development.

Keyword: fire prevention and fighting; high rise apartment building; Vietnam.

1. Make a problem

Fire and explosion of high-rise buildings always leave great consequences, causing serious damage to people and property. With the land fund increasingly shrinking, the planning, construction and development of high-rise buildings is an objective necessity. In Vietnam, as of June 2021, there are 3.679 high-rise buildings in 55/63 localities, in which, focusing mainly on socio-economically developed localities such as: Hanoi City; Ho Chi Minh City; Da Nang; Khanh Hoa; Quang Ninh; Nghe An; Hai Phong; … [5]. Like other countries in the world, in Vietnam, high-rise buildings exist with many different uses, can be high-rise condominium, may be hotels, motels high rise, high-rise offices, … each type of facility has different characteristics and properties of fire and explosion hazards. Therefore, the research and management of high-rise buildings in general and state management of fire prevention and fighting for high-rise buildings in particular towards the goal of sustainable development is necessary and meaningful.

2. State management theory on fire prevention and fighting for high-rise buildings

The concept of high-rise buildings in Vietnam is defined as follows: "High-rise buildings are houses and public works with a height of between 25m and 100m (equivalent from 10 floors to 30 floors)" [4]. Thus, to determine whether a building or facility is a high-rise building, it is necessary to rely on the number of floors or the height of the building and the building.

State management of fire prevention and fighting is an organized and regulated influence by state power on the basis of the Law on Fire Prevention and Fighting for fire prevention and fighting activities in agencies, organizations, households and

individuals of competent entities in order to minimize the occurrence of fires and damage caused by fire, contribute to the protection of lives and property of the State, organizations and individuals, environmental protection, security and social order and safety [6]. From that, it can be seen that the goal of state management of fire prevention and fighting is to minimize the occurrence of fires and the damage caused by fires, contribute to protecting human life and health, protecting property of the State, organizations and individuals, protecting the environment, ensuring security and social order and safety; bring all aspects of fire prevention and fighting work step by step to meet the requirements of socio-economic growth and development, effectively serve the cause of industrialization and modernization of the country in each development stage.

With this approach, the concept of state management of fire prevention and fighting for high-rise buildings is understood as follows: "*State management of fire prevention and fighting for high-rise buildings is an organized and regulated influence by the power of the State on the basis of the Law on Fire Prevention and Fighting for fire prevention and fighting activities in high-rise buildings of competent entities, in order to minimize the occurrence of fires and damage caused by fire contribute to protecting lives and property of the State, organizations and individuals, protecting the environment, ensuring security and social order and safety*". From the concept that shows, the goal of state management of fire prevention and fighting for high-rise buildings is in order to minimize the occurrence of fires and the damage caused by fires, contributing to the protection of life and property of the State, of organizations and individuals, protecting the environment, ensuring security and social order and safety.

The legal basis in the state management of fire prevention and fighting for high-rise buildings in Vietnam is system of legal documents, standards and technical regulations in the field of fire prevention and fighting, typically: Law on fire prevention and fighting; Decree No. 136/2020/NĐ-CP dated November 24, 2020 of the Government; Circular No. 149/2020/TT-BCA dated December 31, 2020 of the Ministry of Public Security; TCVN6160:1996 Fire prevention and fighting of high-rise buildings – Design standards; QCVN06:2021/BXD national technical regulations on fire safety for buildings and constructions; …

Contents of state management of fire prevention and fighting for high-rise buildings in Vietnam are: formulating and directing the implementation of strategies, master plans and plans on fire prevention and fighting; promulgate, guide and organize the implementation of legal documents on fire prevention and fighting; propagating, educating and disseminating knowledge about fire prevention and fighting; building a movement of all people to participate in fire prevention and fighting; organize and direct fire prevention and fighting activities; organize training, build forces, equip and manage fire prevention and fighting means; ensure budget for fire prevention and fighting activities; organize fire and explosion insurance associated with fire prevention and fighting activities; appraise and approve projects, design and take over construction works on fire prevention and fighting; technical inspection and testing and certification of conformity for vehicles, equipment, substances and goods subject to strict requirements on fire prevention and fighting; organize the research, application and dissemination of scientific and technological advances in fire prevention and fighting; inspect, examine, handle violations, settle complaints and denunciations about fire prevention and fighting; fire investigation; organize the state statistics on fire prevention and fighting; international cooperation on fire prevention and fighting for high-rise buildings.

On the basis of the provisions of law, Contents of state management of fire prevention and fighting for high-rise buildings are organized and deployed from the central to local levels with the core management subject being police force for fire prevention, fighting and rescue. In addition, all violations of the law in the state management of fire prevention and fighting for

high-rise buildings, The Vietnamese state has strict and thorough sanctions in accordance with the 2012 Law on Handling of Administrative Violations (amended and supplemented in 2020) and guiding documents.

3. State management of fire prevention and fighting for high-rise buildings in Vietnam today

3.1. Advantages

High-rise buildings in Vietnam have been invested heavily in construction in recent years. As of June 2021, there are 3,679 high-rise buildings in Vietnam, concentrated in some cities with fast socio-economic development, as shown in (Figure 3.1) [5].

Table 3.1.– Statistics on the number and percentage% of high-rise buildings

Numerical order	Local	Number of high-rise buildings	Percentage%
1	Hanoi City	1.272	34.6
2	Ho Chi Minh City	1.107	30.1
3	Da Nang city	270	7.3
4	Khanh Hoa province	203	5.5
5	Quang Ninh Province	104	2.8
6	Nghe An province	85	2.3
7	Hai Phong city	60	1.6

Thus, Hanoi and Ho Chi Minh City in Vietnam are the two cities with the highest density of tall buildings. Thereby, it shows that the development and urbanization speed in the two cities have far exceeded that of other provinces and cities. In addition, high-rise buildings also develop very diversely with all types, specifically as shown in (Figure 3.2) [5].

Table 3.2.– Statistics type high-rise and percentage%

Numerical order	Type of high-rise building	Quantity	Percentage%
1	Apartment	1.106	30.57
2	Hotels, motels	935	25.84
3	Office house	747	20.65
4	Mixed house	594	16.42
5	Educational institution	56	1.55
6	Hospital	64	1.77
7	The house has other functions	116	3.21

The highest proportion of high-rise apartment buildings (30.57%) shows that the demand for housing is very large. The development of high-rise buildings as well as the diversity of uses have attracted a large number of people to choose to live, work and work. At the same time, this development and diversity also poses certain difficulties and challenges in the state management of fire prevention and fighting for high-rise buildings today.

Recognizing the importance of state management of fire prevention and fighting for the sustainable development of high-rise buildings, at the same time, in order to organize the effective implementation of the provisions of law, contents of state management on fire prevention and fighting for high-rise buildings, The Prime Minister of Vietnam issued Directive No. 29/CT-TTg on October 9, 2018 In terms of strengthening the effectiveness of state management over the operation, management and use of apartment buildings, this is the type of high-rise building that accounts for the highest proportion in Vietnam. Simultaneously, the Fire Prevention

and Fighting and Rescue Police force of local units in Vietnam organized the synchronous implementation of management measures, obtained the following results:

– Consolidate, build and promote the effective operation of advanced models and examples of fire prevention and fighting safety such as: "Apartment is safe for fire prevention and fighting"; "Safe residential cluster for fire prevention and fighting"; "The collective house is safe for fire prevention and fighting"; …, thereby, creating a change in awareness and implementation sense of the heads of facilities and people in high-rise buildings; Party committees and local authorities have paid attention to, led and directed the work of fire prevention and fighting for high-rise buildings.– Conducted safety inspection on fire prevention and fighting 5,398 times of establishments, detected 5,002 shortcomings and violations and issued 964 petition documents; fined 419 cases with an amount of more than 3,252 billion VND, temporarily suspended operations for 43 cases, suspended operations for 55 cases, and publicized the violating establishments on the mass media [5].

3.2. Limitations, difficulties

– The investor, the head of the facility has not fully performed the fire prevention and fighting responsibilities as prescribed, such as: put the works into operation but have not yet been accepted for fire prevention and fighting or arbitrarily build more work items, renovate or change the use properties of items and areas in the facility but fail to comply with regulations on design appraisal, approval, acceptance of fire prevention and fighting; failure to implement or incompletely implement the compulsory fire and explosion insurance regime; has not maintained the organization of propaganda and dissemination of laws and knowledge on fire prevention and fighting, practice fire fighting plans, inspect and maintain fire prevention and fighting systems and equipment periodically according to regulations.

– Records of monitoring and management of fire prevention and fighting activities of the facility have not been updated or supplemented to ensure components during operation, such as: there are no internal rules and regulations on fire prevention and fighting promulgated by the head of the establishment; have not updated or supplemented the components and contents of the rescue file; In the fire fighting plan, the typical fire and explosion situations are not assumed.

– Traffic conditions for fire fighting, fire prevention and fighting safety distances, fire fighting water sources are still inadequate, fail to meet the requirements for fire fighting vehicles to deploy, fail to maintain a safe distance of fire prevention and fighting between items and surrounding facilities, such as: building more work items, allowing cars, motorbikes or businesses and services to encroach on traffic roads or in fire prevention and fighting distances between buildings, the system of fire-fighting water supply posts outside the houses of urban centers, establishments, and natural water sources must not be maintained.

– Conditions for preventing fire spreading in the house have not been maintained regularly or become ineffective during operation, such as: at locations where channels, wells, technical shafts and pipes of the technical system pass through fire-blocking walls and floors, the requirements for preventing smoke and fire spread are not met; arbitrarily opening doorways, openings, technical pipes on walls, fire partitions; dismantling or replacing the wrong type of fire door and failing to maintain the normally closed state of the doors on the fire prevention wall; the water curtain system to prevent fire is not maintained to function properly.

– Conditions for roads and exits in the house have not been maintained regularly and are as common as: arrange and place goods and items on the road and escape route; inserting, locking or invalidating the doors on the emergency exits, the doors entering the stairwells; emergency lights, emergency exit lights have not been installed in sufficient quantity, not in accordance with specifications and many

lights are damaged; parking vehicles on the escape route, blocking the escape route at the garage, affecting the safe escape activities for people.

– Fire prevention and fighting systems and equipment, technical systems related to fire prevention and fighting equipped at establishments that have been put into operation for many years, establishments that have not been appraised, approved and accepted for fire prevention and fighting, etc., often do not meet regulations, equipment quality does not meet requirements, installation is not suitable for fire fighting area, failure to maintain the periodic inspection and maintenance of fire prevention and fighting equipment, leading to a situation after a period of improper operation.

– The grassroots fire prevention and fighting force has not yet ensured the number and staffing according to regulations, team members have not yet grasped the knowledge and skills of fire prevention and fighting, mainly security and operational technicians, residents and workers who join the grassroots fire prevention and fighting force but do not regularly participate in fire prevention and fighting activities; are not trained, trained in fire prevention and fighting periodically, etc., The operation is still formal, confusing in deploying forces and means of fire fighting, rescue and rescue according to hypothetical situations.

3.3. Causes

a) Objective causes

High-rise buildings have been in operation for many years, mini-apartments, offices, hotels, high-rise motels, etc., converted from separate houses or built improperly according to planning, construction permits often fail to meet fire safety requirements and the equipment and systems of fire prevention and fighting do not meet current regulations; used electrical systems and equipment are not inspected and maintained and there is an increase in consumption of equipment but the electrical system is not renovated; Damaged systems and equipment lead to the risk of unsafety in terms of fire prevention and fighting. At the same time, due to lack of synchronization in construction planning, the construction of works adjacent to the facility, leading to failure to ensure the conditions of traffic, safe distance for fire prevention and fighting, and water source for fire fighting.

The implementation of regulations of laws, standards and technical regulations still has some difficulties and problems such as: (1) There are no regulations on fire safety for buildings over 150m high, some regulations are still inconsistent or difficult to apply to high-rise buildings; (2) It is very difficult to apply current regulations when renovating or changing the use of houses and works (difficult to meet regulations on roads for fire engines, arrangement of roads, exits, stairs, etc.); (3) Regulations on implementation of fire and explosion insurance regime are still problematic for establishments with many owners (apartment buildings, mixed-use buildings, ...); (4) Regulations on management and use of apartment buildings such as: establishment, capacity conditions of the Management Board, funding sources for maintenance and maintenance of fire prevention and fighting activities, the investor's responsibilities in handing over the works, management and operation of the shared and private ownership portions of the apartment building are not specific, unified and difficult to implement; (5) sanctions for handling violations of fire prevention and fighting have not yet met management requirements, and there have been no radical handling measures for high-rise buildings that do not ensure fire prevention and fighting safety or refuse to comply with decisions on temporary suspension or suspension of operations or sanctions issued by state management agencies.

b) Subjective causes

A part of the investor and the head of the facility has not strictly performed their fire prevention and fighting responsibilities, leading to violations such as: (1) arbitrarily put the works into operation without being tested and accepted for fire prevention and fighting or building, expanding, expanding, renovating, changing the use properties of items or facilities

in the course of operation without carrying out the procedures for appraisal, approval and collection of fire prevention and fighting according to regulations; (2) extending the time to hold the apartment building meeting to establish the Management Board or having a dispute or disagreement on the management of the area under common ownership, private ownership,... the management and operation are loose and not tight, leading to violations of regulations on fire prevention and fighting; (3) not focusing on fire prevention and fighting, but also focusing on economic goals, cutting investment costs for fire prevention and fighting, equipping and installing fire prevention and fighting systems and equipment at a minimum level, failing to ensure quality and technical requirements and failing to regularly maintain fire prevention and fighting safety conditions of the facility; (4) has not yet secured the nominal funding for fire prevention and fighting activities; (5) do not buy compulsory fire and explosion insurance according to regulations [2].

The knowledge and sense of compliance with the law on fire prevention and fighting of a part of employees and people is still limited, failing to comply with the rules and regulations on fire prevention and fighting, causing many violations such as: damage or inactivate the fire prevention and fighting system; leaving items on the corridor, in the stairs; insert, block the exit door; installing more power-consuming equipment, using fire and heat sources that do not ensure fire prevention and fighting safety; do not know how to use fire prevention and fighting means originally equipped for fire fighting; not actively supervise the implementation of responsibilities of the investor and the management and operation unit.

A part of leaders of departments, branches and People's Committees of districts and communes have not yet fulfilled their responsibilities in directing, inspecting, supervising and performing the state management of fire prevention and fighting. The coordination between sectors is still formal, not consistent in the appraisal, appraisal, approval, construction without permits and does not meet the requirements on fire prevention and fighting; There is no synchronous planning for the construction of condominiums and high-rise buildings, so many works are built alternately in residential areas, fail to meet safety requirements on fire prevention and fighting, causing difficulties in handling violations of violating works that have been put into operation.

The coordination between units of the police in some localities is not consistent and close leading to failure to provide timely information about the establishment's violations to take appropriate and timely measures to prevent the risk of fire, explosion, incidents and accidents. In addition, the professional qualifications of a part of staff are limited, lack skills and experience or have not fulfilled their responsibilities in performing their duties, leading to the following characteristics: (1) a number of facilities have been accepted and put into use, but with recommendations on fire prevention and fighting that are difficult to overcome; (2) the inspection content is incomplete as prescribed, focusing on testing fire prevention and fighting systems and equipment, not carefully checking other conditions such as: traffic for fire engines, layout of premises, use functions, prevention of fire spread,...; (3) the detection of violations on fire prevention and fighting and the implementation of penalties is still low, due to the lack of resoluteness in handling violations, at the same time, there is a situation where violations are recorded as existing, omissions or not recorded in the inspection report or petitioned many times but did not carry out sanctions, in many cases wrongly identified violations, incorrectly recorded the contents of the violation minutes; ...

4. Solution

High-rise buildings will continue to be strongly planned and developed, to improve the efficiency of state management of fire prevention and fighting for high-rise buildings, contributing to the successful implementation of the goal of minimizing fires, explosions and damage caused, as well as the goal of

sustainable development. As the core force in performing the function of state management of fire prevention and fighting for high-rise buildings. The police force for fire prevention, fighting and rescue needs to do well a number of the following contents:

– Assume the prime responsibility for, and coordinate with functional units under relevant ministries and branches in, continuing to research, advise and propose amendments and supplements to the provisions of legal documents, construction, fire and explosion insurance and other relevant regulations to ensure consistency in management and implementation organization; to develop national technical regulations on fire prevention and fighting for buildings with a height of over 150m; promulgate a resolution guiding the criminal handling of crimes specified in Clause 4, Article 313 of the Penal Code 2015 (amended and supplemented in 2017); regulations on responsibility, management and inspection of safety assurance in electricity installation and use at establishments and households. To advise and develop documents to guide and direct professional activities and organize professional training and inspection for officials performing the work of appraisal, approval, management and safety inspection of fire prevention and fighting, investigate and deal with fire and explosion, handle violations; guide measures to organize fire fighting for high-rise buildings, gathering situations in basements, crowded public service floors and upper floors; organize the inspection of the implementation of the state management of fire prevention and fighting for high-rise buildings by the local police.

– Advise the People's Councils and People's Committees of provinces and centrally run cities to issue documents directing the enhancement of the effectiveness of state management of fire prevention and fighting for high-rise buildings, focus on thoroughly handling establishments that do not meet the requirements, In the immediate future, it is necessary to direct and immediately handle the works that have been put into operation but have not been appraised, approved and accepted according to regulations, there are many problems and violations that pose a risk of fire and explosion, fail to ensure the conditions for preventing fire spread and safe escape for people of the facility; for existing establishments, violations cannot be remedied, It is necessary to coordinate with functional ministries and branches to agree on a solution and take measures to ensure the lives of people in buildings that do not meet fire prevention and fighting safety conditions when they are shut down. To ensure the level of local budget expenditure to support fire prevention and fighting activities for establishments that are unable to secure funding for implementation; equip fire prevention and fighting means and equipment, maintain the operation of the civil defense force; take responsibility for compulsory fire and explosion insurance for establishments that are headquarters of local state agencies.

– To step up the propaganda on fire prevention and fighting, to renovate the contents, forms and methods of propaganda, in which, focus on disseminating measures and skills for escape and initial handling when a fire occurs. Instruct the investor, the head of the facility, the management board of the apartment building to deploy the daily propaganda using the sound system, the advertising screen that is available in the building. Review and guide the establishment and maintenance of operation, ensure funding and operating means for grassroots fire prevention and fighting teams and periodically organize practice of fire fighting plans for high-rise buildings.

– Regularly update new regulations related to design appraisal and acceptance, fire prevention and fighting works. In particular, the application of standards and technical regulations on fire prevention and fighting in design appraisal and approval must be fully and accurately applied, suitable to the scale and nature of the works, but must comply with the provisions of law [1]. Actively follow up, grasp the situation, conduct basic investigation on the construction investment of projects, works and high-rise buildings in operation, properly assess the current situation of

fire prevention and fighting to serve the management and come up with a fire fighting plan suitable to the situation and characteristics of each high-rise building. To guide research institutions and implement a number of measures to increase efficiency in fire fighting and rescue and rescue for high-rise buildings such as: clearly determine the location for the ladder truck, the fire truck to park and the position to open the glass panes on the outside of the house to serve the ladder truck to approach and deploy fire fighting, rescue and rescue activities; arrange refuges and equip necessary means and equipment for fire fighting, rescue, rescue and first aid; renovating the pipeline of the waiting throat system for professional fire forces to connect with fire engines and supply water to the upper floors of high-rise buildings.

– In the construction of apartment buildings and high-rise buildings, it is necessary to comply with the provisions of the law right from the stage of site approval, appraise and approve the design of fire prevention and fighting, invest in construction until the work is accepted and put into use. The law on fire prevention and fighting specifies these contents very specifically, therefore, investors, design consultants and construction contractors need to strictly abide by them when implementing them; resolutely not to accept and put into use the works that do not ensure the safety of fire prevention and fighting according to regulations [3]. Carry out safety inspection on fire prevention and fighting in accordance with the procedures, sequence and content and ensure the number of times as prescribed, strengthen irregular inspection of establishments with many shortcomings and violations but have not yet been remedied; determine the responsibility of each violator in order to make recommendations and offer effective remedial solutions. The inspection record made must fully record the inspection contents, omissions, violations, recommendations for measures, time to remedy, terminate the status of recording violations to "existence, omission" or no error recognition. Resolutely deal with the acts of arbitrarily renovating, changing the nature of use, building more work items; failing to maintain conditions for preventing fire from spreading, escaping, operating the fire prevention and fighting system, etc.; ensuring that 100% of detected administrative violations must be handled in accordance with the provisions of law and decisions on sanctioning of administrative violations must be strictly implemented, ensuring within the prescribed time limit.

– Assign officers to perform the management and safety inspection of fire prevention and fighting to ensure that they fully meet the prescribed standards and meet the requirements on qualifications and experience to effectively implement the management of high-rise buildings; organize professional training and retraining for inspection staff, resolutely do not arrange cadres whose professional examination results are unsatisfactory. Review, revise and promulgate regulations on decentralization of management for police forces of fire prevention, fighting and rescue, provincial-level police, district-level police, professional process in accordance with the provisions of law and the guidance of the Ministry of Public Security of Vietnam. Strictly comply with the provisions of law and the direction of the Ministry of Public Security on assignment of tasks and coordination in investigation and handling of fire and explosion, to ensure that all fires and explosions must be investigated, clarified and completely dealt with without leaving a long backlog.

5. Conclusion

Each country has different conceptions, management and administration in the field of state management of fire prevention and fighting in general and for high-rise buildings in particular. With an approach from theory to practice of state management of fire prevention and fighting for high-rise buildings in Vietnam today, along with that is a system of logical and scientific solutions that contribute to improving the efficiency of state management of fire prevention and fighting for high-rise buildings. Each solution has a scientific basis and feasibility when applied in practice, however, the study and application of these

solutions in the state management of fire prevention and fighting for high-rise buildings for each country requires a clear study of the subjects, the subject and especially the characteristics and organizational model of each country must be suitable, only then can the solution be effective.

References:

1. Trinh The Tuan. Fire prevention in design appraisal, acceptance and acceptance of works in Hanoi city, Fire prevention and fighting magazine – Hanoi.– No. 93. 2017.– Tr. 38–39.
2. Hoang Ngoc Hai, Trinh The Tuan, Le Quang Hai. Monograph "State management of fire prevention and fighting for high-rise apartments of the Fire Prevention and Fighting Police force in the current period". Transport Publishing House,– Hanoi. 2018.
3. Trinh The Tuan, Thieu Thanh Thuan. Ensuring fire safety in the construction and development of apartment buildings and high-rise buildings in the current period, Journal of Construction and Urban – Hanoi.– No. 64. 2019.– Tr. 55–59.
4. TCVN6160:1996 Fire prevention and fighting of high-rise buildings – Design standards.
5. Ministry of Public Security. Notice No. 09/2021/TB-BCA-C07 dated March 15, 2021 of the Ministry of Public Security on the results of safety inspection of fire prevention and fighting for high-rise buildings,– Hanoi. 2021.
6. Dao Huu Dan, Hoang Ngoc Hai. Textbook of State management of fire prevention, fighting and rescue, People's Public Security Publishing House,– Hanoi. 2020.

Section 7. Chemistry

https://doi.org/10.29013/EJTNS-21-4.5-58-63

Ming Albert,
Princeton Day School, High School Senior
United States of America
E-mail: albertming88@gmail.com

PREDICTING DAILY AVERAGE PM 2.5 MOVEMENT USING MACHINE LEARNING MODELS

Abstract. The article discusses the implementation of multiple machine learning algorithms on particulate matter data. The models were assessed on the ability to predict if the average particulate matter concentration for the succeeding day would increase or not.

Keywords: Particulate matter; Machine learning; ARIMA; Linear regression; Logistic regression; Random forest.

1. Introduction

Air is one of the most important aspects to our survival; without it, humans are not able to survive. However, due to the lingering problem of pollution, society must be aware of its actions that impact the quality of air we breathe. Ever since the industrial revolution, pollution has damaged the well-being of planet Earth, whether it be through gas emissions or through chemical reactions between gases in the atmosphere. In recent years, the issues of air pollution and global warming have become imminent in society. Although there has been some misunderstanding on the state of climate change, the consensus in the scientific community is that the Earth's climate has been continually affected by humans [4]. With advocates such as Greta Thunberg and Al Gore, world leaders have felt the need to strengthen their climate policies in order to preserve the environmental safety of the Earth.

One of the most prevalent catalysts in the air pollution process are particles called *particulate* matter *(PM)*. These particles are a mixture of small solids and liquid droplets in the air that once inhaled, can cause serious health problems in the future. The two different types of particulate matter are classified by the diameter of the particles themselves; they are called PM2.5 and PM10, containing particles with diameter less than 2.5 micrometers and particles with diameter less than 10 micrometers respectively [6]. Generally, particles falling under the PM2.5 category are more dangerous to the human body because they can build up more efficiently inside the lungs, weakening the breathing system [6]. Both types of particulate matter form most prominently through the emission process of gasoline, oil, or wood. Additionally, they can also be formed naturally in the air through gaseous reactions between particles like sulfur dioxide or nitrogen oxides, both of which indirectly accelerate the process of greenhouse gas emissions.

Specifically in Beijing, China, the concentrations of particulate matter have always been hazardously high. After the initial COVID-19 swarm throughout the country, air pollution began to return to its nor-

mal level. These high levels of air pollution not only have damaged the environment but have also caused the citizens to suffer dramatic health problems. More than a million deaths could have been prevented with more attentive care to fossil fuel emissions, and with China and India accounting for more than half of the global PM2.5 death toll, it is clear that the country must play a part in reducing its particulate matter and gas emission levels. Additionally, there has been a lack of comparison between different predictive methods of forecasting. Therefore, being able to predict the concentration of particulate matter in the atmosphere poses clear benefits to society. We look at four different machine learning methods, ARIMA, Logistic Regression, Linear Regression, and Random Forest in our procedure for tackling this research problem.

Firstly, in section 2.1, a brief overview of the dataset itself is explained. Then in section 2.2, the entire plan of analysis is revealed, starting with filtering and cleaning the data, to the way the predictive power of each model was assessed. The establishment of the prediction accuracy is important because it must remain the same for each of the four different models. Sections 3.1–3.4 outline the models themselves and the way they are applied into the PM2.5 dataset. Finally, sections 4 and 5 report the results, summarize the findings, and add more points of discussion about the state of air pollution in the world.

2. Methodology

2.1 Data Set

The dataset used in this research paper is a part of the Beijing Multi-Site Air Quality Data Set found through the University of California-Irvine Machine Learning Repository [5]. The chosen dataset was centered around the ChangPing district in Beijing and included hourly data values for "6 different main air pollutants and 6 different meteorological variables." For the purposes of this research, only the PM2.5 (measured in μg/m^3) column was examined, and daily average particulate matter concentration levels were calculated to predict air pollution levels from day to day. Figure 1 shows the daily fluctuation of the average readings.

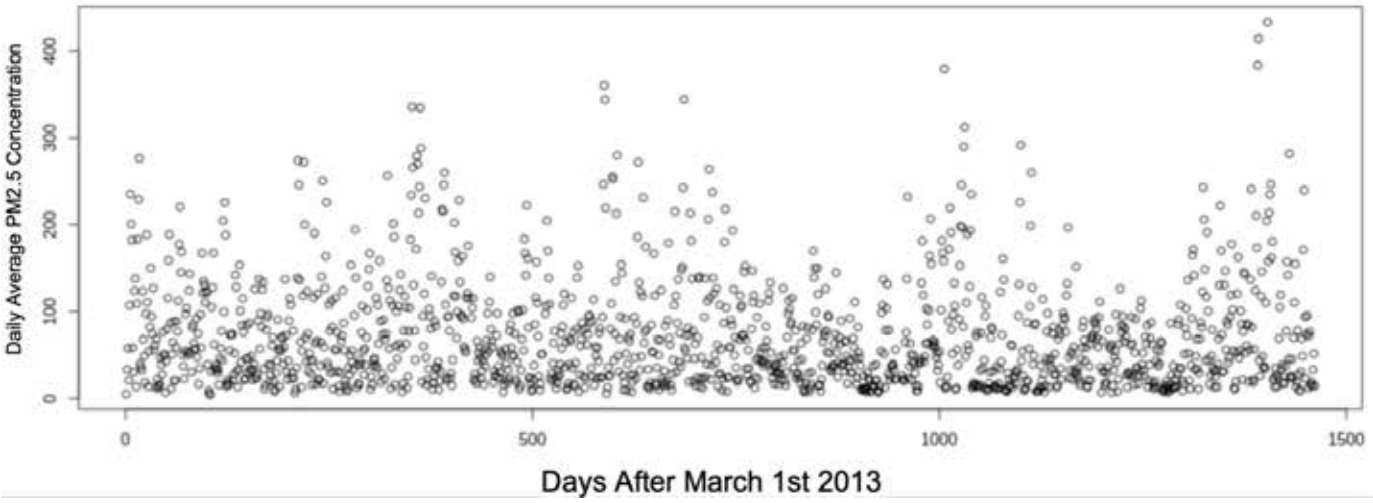

Figure 1. Plot of daily average PM2.5 concentration

2.2. Research Plan

1. Extract the PM2.5 column from the dataset.

2. Calculate the average PM2.5 concentration for each day available in the dataset. This was done by using the data value at each hour of the day and computing the mean. There were hours for which no PM2.5 concentration was recorded; these hours were excluded from the calculation of the daily average PM2.5 concentration.

3. Run the new, cleaned data through each of the models to test for predictive accuracy. The four types of models used in this research paper were ARIMA, Logistic Regression, Linear Regression, and Random Forest.

4. Obtain the prediction accuracy of each model and compare. Graphs and visuals are also produced in this step of the process.

The prediction process is inspired by Shannon's MindReader Game. In 1953, Claude Shannon sought to create a machine that could accurately predict the patterns of a human. To play the game, a user must choose either "left" or "right," and the machine will make a prediction either "left" or "right" as well. If the computer can predict the same side as the user, that is if both the user and the machine selected "left" or if both the user and the machine selected "right," then a point is given to the machine for its correct guess. On the other hand, if the machine and the user do not predict the same side, that is to say if both "left" and "right" appear in a single round, then a point is awarded to the user.

Table 1.– Summary of Possible Algorithm Outcomes

		Actual Reading	
		Increase	Decrease
Model Prediction	Increase	Correct	Incorrect
	Decrease	Incorrect	Correct

For this research, the list of actual PM2.5 daily average concentrations and the lists of PM2.5 predictions were converted into lists of 1's and –1's, with the 1's representing an increase in the daily average concentration from one day to the next and the –1's representing a decrease in the daily average concentration from one day to the next. If there exists an instance where both the predicted and actual PM2.5 concentration change indicate a 1 or a –1, then the algorithm is rewarded for guessing correctly. However, if the predicted and actual PM2.5 concentration changes differ, then the algorithm has guessed incorrectly and is not rewarded.

3. Models

As mentioned before, four different methods were used throughout the whole research process. Time series analysis, logistic regression, linear regression, and random forest models were put up against each other to determine the most efficient method for analyzing and predicting this air quality dataset. All coding for the models and their analysis was completed in RStudio.

3.1 Arima

Times series analysis using ARIMA is a popular and effective method for prediction. It is generally thought of as an augmentation of ARMA with its ability to make trends stationary [3]. The function auto.arima in R from the "forecast" library was used to select the proper parameters for the time series, while the predict function appended the predicted PM2.5 value to a list. Those predictions were then used to produce a predictive percentage.

3.2 Logistic Regression

Logistic Regression is an efficient method for modeling binary outcomes. It can produce a predictive, directional probability of an event happening. In the case of this research paper, the events are either the PM2.5 concentrations will increase, or it will decrease. The logistic regression prediction for a given day was completed based on the lagged data of steps one through five for all the days leading up. If the generated probability was greater than 0.5, the algorithm correlated this to an increase in the PM2.5 concentration, and if the generated probability was less than 0.5, the algorithm correlated this to a decrease in the PM2.5 concentration. The function used to complete this task was the glm function found in R.

3.3 Linear Regression

Linear regression is another useful predictive tool used for modeling due to its simplicity in nature. However, instead of outputting a probability, linear regression models output a continuous variable, which can be more useful visually speaking. Much like logistic regression, the linear regression prediction for a given day was completed based on the lagged data of steps one through five for all the days leading up. The function used to complete this task was the lm function found in R.

3.4 Random Forest

Random Forest is one of the most popular machine learning methods to use for modeling and prediction. It is very versatile, as it can handle both classification and prediction problems. In addition to this flexibility, the model gets more and more accurate as the number of trees increases [2]. Using the randomForest function from the "randomForest" library, decision trees were made based on the lagged data of steps one through five. Then, the function automatically counted and determined the highest voted "prediction target" to use as the overall prediction of PM2.5 concentration change. For the purpose of this research paper, 100 trees were used during the random forest modeling process.

All models started their prediction process from day 100 to ensure adequate amount of data in each step of the prediction process.

4. Results and Discussion

The results from all the models are shown below in tables 2–5 in the form of two-way tables. In each of these tables, *Actual* represents the movement in the actual PM2.5 concentration data after transformation, while *Predicted* represents the movement in the predictions of PM2.5 concentration data generated by each of the models after transformation *(For details of how the PM2.5 concentrations were converted into 1's and –1's, please refer back to section 2.2)*. Each box within the two-way table receives a tally based on the movement of both the actual and predicted daily average PM2.5 concentration for a given day; the table gets filled up once the last day that is featured in the dataset is covered.

The formula for prediction accuracy is then defined to be the proportional percentage of the number of correct predictions [1]. In other words, this is the count of the number of times where the prediction and actual movements are –1 plus the number of times where prediction and actual movements are 1, divided by the total number of occurrences. All prediction accuracies are then rounded to five significant figures with three numbers after the decimal.

Table 2.– Results of ARIMA Model on PM2.5 Data

ARIMA		Actual	
		-1	1
Predicted	-1	328	172
	1	271	579

Table 3.– Results of Linear Regression on PM2.5 Data

Linear Regression		Actual	
		-1	1
Predicted	-1	377	283
	1	222	468

Table 4.– Results of Logistic Regression on PM2.5 Data

Logistic Regression		Actual	
		-1	1
Predicted	-1	296	168
	1	303	583

Table 5.– Results of Random Forest on PM2.5 Data

Random Forest		Actual	
		-1	1
Predicted	-1	293	215
	1	306	536

Table 6. – Summary of models and their prediction accuracies broken down

Models	Prediction vs Actual				Prediction Accuracy
	Agreement		Disagreement		
	[1,1]	[-1, -1]	[1, -1]	[-1, 1]	
ARIMA	579	328	172	271	67.185%
Linear Regression	468	377	283	222	62.593%
Logistic Regression	583	296	168	303	65.111%
Random Forest	536	293	215	306	61.407%

Table 6 compares the overall prediction accuracies of the models. All the prediction accuracy values hovered roughly between 60% and 70%, with the ARIMA model performing the best with an accuracy of 67.185%. Interestingly, we observe that the models had the most success predicting correctly when the daily average PM2.5 concentration would increase. This is likely due to the fact that the daily average PM2.5 concentration was increasing more often than not. For example, in the case of ARIMA, the model gave a positive one prediction 850 times out of 1350. When the models predicted incorrectly, there seemed to be no clear trend.

We notice that the data created happened to be a time series with one observation per day. Therefore, the result of the model comparison is interesting because it may have indicated that the PM2.5 dataset has satisfied the assumptions of the ARIMA model. We suspect that ARIMA may be the best option for this type of analysis because certain hidden factors affecting particulate matter may have been stationary. With that being said, the predictive power that this procedure has to offer may prove to be rather beneficial. Using ARIMA, we would be able to predict the movement of particulate matter concentrations in any region with up to almost 70% accuracy. Politicians may gain a better sense of the state of pollution in their country, while companies may seek new locations for venues that they may not have considered in the past for the safety of their employees.

Additionally, we recognize a few areas for improvement, including potential next steps for further research. One idea we can explore is adding more columns of data to analyze for the purpose of gauging the dangers of global warming. In addition to analyzing particulate matter concentration, it is possible to analyze categories of data such as temperature, greenhouse gas emissions and fossil fuel consumption. Together, these sets of data can be combined to provide a more reliable outlook when it comes to understanding the level of danger that global warming has on the world and how soon effects may take place.

5. Conclusion

In this research paper, multiple predictive models are implemented in order to better estimate the daily average concentrations of PM2.5 levels in ChangPing district of Beijing from 2013–2017. ARIMA, logistic regression, linear regression, and random forest models were implemented to predict the exact concentration value or if the concentration would increase or decrease based on all the preceding days. Prediction accuracies were then assigned based on the number of times a given algorithm was able to correctly predict whether the daily average PM2.5 concentration would increase or decrease. Afterward, these results were compared in order to satisfy the goal of finding the best method of predicting movement of the daily average PM2.5 concentration. The findings of this paper conclude that the ARIMA time series method yields the best predictive accuracy for forecasting PM2.5 levels on the ChangPing air quality dataset out of the four models used.

References:

1. Suganya S. & Meyyappan T. Forecasting And Prediction of Air Pollution Levels To Protect Human Beings From Health Hazards. International journal of scientific & Technology research,– 9(1). 2020. URL: http://www.ijstr.org/final-print/jan2020/Forecasting-And-Prediction-Of-Air-Pollution-Levels-To-Protect-Human-Beings-From-Health-Hazards.pdf
2. Doreswamy Harishkumar K. S., Yogesh K. M., Ibrahim Gad. Forecasting Air Pollution Particulate Matter (PM2.5) Using Machine Learning Regression Models, Procedia Computer Science,– Vol. 171. 2020.– P. 2057–2066. ISSN1877–0509. URL: https://doi.org/10.1016/j.procs.2020.04.221; (https://www.sciencedirect.com/science/article/pii/S1877050920312060)
3. Sánchez Lasheras F., García Nieto P. J., García Gonzalo E. et al. Evolution and forecasting of PM10 concentration at the Port of Gijon (Spain). Sci Rep 10.– 11716. 2020. URL: https://doi.org/10.1038/s41598-020-68636-5
4. Oreskes N. The Scientific Consensus on Climate Change. Science,– Vol. 306. 2004.
5. Zhang S., Guo B., Dong A., He J., Xu Z. and Chen S. X. Cautionary Tales on Air-Quality Improvement in Beijing. Proceedings of the Royal Society A,– Vol. 473.– No. 2205. 2017.– 457 p.
6. Kate Adams, Daniel S. Greenbaum, Rashid Shaikh, Annemoon M. van Erp & Armistead G. Russell. Particulate matter components, sources, and health: Systematic approaches to testing effects, Journal of the Air & Waste Management Association,– 65:5. 2015.– P. 544–558. DOI:10.1080/10962247.2014.1001884

https://doi.org/10.29013/EJTNS-21-4.5-64-72

Tianrui Tan,
Experimental High School Attached to Beijing Normal Universit, China
E-mail: thomastianruitan@gmail.com
Xiyan You,
Experimental High School Attached to Beijing Normal Universit, China

IMMOBILIZATION OF C@TIO$_2$ IN CALCIUM ALGINATE HYDROGEL FOR PHOTODEGRADATION OF ORGANIC POLLUTANTS

Abstract. Nano titanium dioxide is a widely used photocatalyst, but there are still two problems with it. On the one hand, nano titanium dioxide can only absorb ultraviolet rays, so the utilization rate of sunlight is relatively low. On the other hand, it is not easy to recycle, which will cause secondary pollution. In response to the above problems, this study prepared polyvinyl alcohol coated nano titanium dioxide by simple solution mixing. By controlling the thermal degradation of polyvinyl alcohol on the surface of nano titanium dioxide into carbon, a carbon coated nano titanium dioxide composite photocatalyst was made. The carbon coating on the surface is about 2.5 nm, and the carbon content is about 3.1%. A supported photocatalyst was prepared by embedding carbon coated nano titanium dioxide in calcium alginate hydrogel. The calcium alginate/carbon coated nano titanium dioxide composite hydrogel has good photocatalytic activity and is easy to recycle.

Keywords: carbon coating; titanium dioxide; hydrogel; visible light photocatalyst.

1. Introduction

According to the World Health Organization (WHO), 80% of human diseases are related to water pollution, and more than 800000 people die of diarrhea caused by unsafe water every year [1]. At present, titanium dioxide is regarded as one of the best white pigments. It is broadly utilized in coatings, plastics, papermaking, synthetic fibers and cosmetics. In 1972, Fujishima and Honda discovered that titanium dioxide (TiO_2) can absorb ultraviolet light and decompose water catalytically to produce hydrogen, which has attracted widespread attention [2]. The photocatalysis principle of TiO_2 is shown in (Figure 1) [3]. When TiO_2 is exposed to sunlight, especially ultraviolet rays, the electrons in the valence band will be triggered and move to the conduction band, no matter in water or in the air, to generate free electrons-hole pairs. Free electron-hole pairs possess strong redox ability, which is able to activate oxygen and water in the air to generate active oxygen and hydroxyl radicals. When benzene, toluene, formaldehyde, bacteria, viruses and other pollutants are adsorbed on the surface of TiO_2, they will combine with free electrons or holes, causing redox reactions and being decomposed into carbon dioxide and water. At present, nano titanium dioxide are utilized in great scale in air purification, sewage treatment, hydrogen production (by water splitting), CO_2 reduction, and dye-sensitized solar cells [4; 5].

While using TiO_2, people discovered that there were two problems with the titanium dioxide photocatalyst.

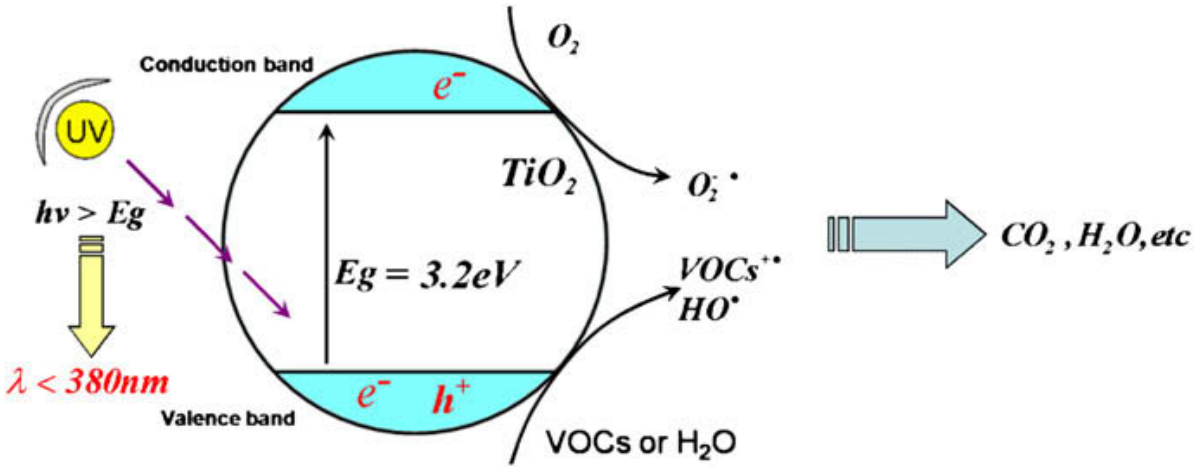

Figure 1. Schematic diagram of TiO_2 catalytic degradation of pollutants under UV irradiation [3]

On one hand, because of the relatively large forbidden band width of TiO_2, about 3.2 eV (Anatase), and the wavelength of light is inversely proportional to the energy, titanium dioxide can only absorb ultraviolet (UV) below 388nm, while in the sunlight spectrum, the ultraviolet light content is about 4%. Therefore, TiO_2 almost absorbs no visible light, hardly has photocatalytic activity in regions with visible light, and has a poor utilization rate of sunlight [6]. On the other hand, with the continuous reduction of TiO_2 particle size, the specific surface area of TiO_2 increases, Therefore, the TiO_2 used for photocatalysis is all nano TiO_2. However, a problem emerges when using nano TiO_2: the separation and recycle of nano TiO_2 is hard. If it cannot be recycled, the loss of nano TiO_2 particles into the natural environment will pose a potential threat to the ecosystem and human health [7].

In order to improve the visible light absorption performance of TiO_2, a lot of attempts have been made, including doping with a variety of metals and nonmetals, supporting precious metal particles, and coupling with narrow bandgap semiconductors, etc [8]. In recent decades, the grafting of materials containing conjugated structures on the surface of TiO_2 nanoparticles has attracted more and more interest. This is mainly because the conjugated structure can capture visible light and inject excited electrons into the conduction band of TiO_2, thereby improving the photocatalytic activity of TiO_2. Therefore, many materials containing conjugated structures, such as graphene, fullerene, carbon nanotubes, chlorophyll, fluorescein, etc., have been used to improve the visible light catalytic activity of TiO_2 [9]. However, scientists have found that only by building a bridge capable of transporting electrons between the conjugated structured material and the TiO_2 can the photocatalytic activity of TiO_2 be greatly improved [10].

In terms of improving the recyclability of nano TiO_2, the most effective method currently is to load or wrap nano TiO_2 particles in a large size solid carrier to prepare a supported nano TiO_2 photocatalyst [11]. Carriers supporting nano TiO_2 can be divided into inorganic carriers and organic carriers. Inorganic carriers mainly include glass beads, ceramics, clay and aluminum foil, etc., and organic carriers mainly include polyethylene terephthalate, polypropylene, cellulose and activated carbon [12]. However, many carriers themselves absorb and block light, which significantly reduces the photocatalytic activity of nano TiO_2.

Therefore, there are still many challenges to develop a cheap and environmentally friendly method for preparing efficient and easy-to-recover TiO_2 composite photocatalysts. This study proposes a

simple, effective, and capable of large-quantities manufacturing method to synthesize carbon coated TiO_2 nanoparticles ($C@TiO_2$), and then embed the carbon coated nano titania in calcium alginate hydrogel to prepare a supported photocatalyst. The composite photocatalyst has good photocatalytic activity and easy recovery.

2. Experimental

2.1 Materials

Polyvinyl alcohol (PVA, average degree of polymerization 1750 ± 50), sodium alginate (analytical grade), and calcium chloride (analytical grade) were purchased from Sinopharm Reagent Co., Ltd. Nano-TiO_2 (P25, 20% rutile and 80% anatase) with an average particle size of 21nm was purchased from Evonik Industries. Methyl orange (MO) manufactured by Yongjia Fine Chemical Plant in Zhejiang, China was used as a model pollutant. All chemicals were not further purified.

2.2 Synthesis of Carbon Coated Nano Titanium Dioxide ($C@TiO_2$)

2g PVA was added to 98g deionized water, then the temperature was raised to 95 °C, and the mixture was stirred for 1 hour to obtain a clear and transparent PVA solution with a concentration of 2%. 15g nano titanium dioxide and 30g of deionized water was added into a beaker. Then, 40g of the PVA solution mentioned above was added. The mixture was ultrasonically dispersed for 10 minutes, magnetically stirred for 1 hour, then poured into a watch glass and placed in an oven at 80 ˚C for 10 hours to obtain PVA coated nano titanium dioxide. The PVA coated nano titanium dioxide was put into a muffle furnace, calcined at 230 °C for 3 hours, and grounded to obtain brown carbon coated nano titanium dioxide powder.

2.3 Synthesis of Calcium Alginate/ $C@TiO_2$ (Ca-Alg/$C@TiO_2$)

0.8g $C@TiO_2$ was added to 392 g of deionized water. The mixture was ultrasonically dispersed for 10 minutes, then stirred for 2 hours to obtain a brown solution with a concentration of 0.2%. 8 g sodium alginate was added to the $C@TiO_2$ dispersed solution mentioned above. The mixture was stirred for 1 hour to obtain sodium alginate/$C@TiO_2$ mixed solution. 16 g anhydrous calcium chloride was added to 384 g of deionized water, and stirred to obtain clear and transparent calcium chloride solution with a concentration of 4%. Sodium alginate/$C@TiO_2$ mixed solution was drawn by a 5ml medical syringe and slowly dripped into the stirred calcium chloride solution at a distance of about 15cm. The mixed solution solidified into small pellets immediately after it was dripped into the calcium chloride solution. After 2 hours of cross-linking, the obtained Ca-Alg/$C@TiO_2$ pellets were rinsed three times with deionized water.

2.4 Photocatalytic Degradation

15mg of methyl orange was added to a 1L volumetric flask. Water was added to the mark. The mixture was then shaken to dissolve to obtain an orange-red methyl orange solution with a concentration of 15mg/L.

50g Ca-Alg/$C@TiO_2$ pellets was added to a bottle containing 400g methyl orange solution. Then the bottle was placed under sunlight. Every 3 days, samples were taken to test the concentration of the methyl orange solution.

2.5 Characterization

Transmission electron microscope (TEM) and scanning electron microscope (SEM) were used to observe the morphology of the sample. The acceleration voltage of the scanning electron microscope (SU8020, Hitachi) was 15 KV. In order to prepare of the sample of scanning electron microscope, nano titanium dioxide was diluted with alcohol and dropped on the sample stage. After the diluted nano titanium dioxide was dry, gold was sprayed on the surface. Then the sample was ready for observation. In order to prepare the sample of the projection electron microscope sample, nanometer titanium dioxide was diluted with alcohol and dropped on the supporting carbon net. The sample was ready for observation after drying. The Fourier Transform

Infrared Spectroscopy (FTIR) analysis of the sample was conducted with the Nicolet Smart Orbit Accessory (Thermo Fisher Scientific) of the Nicolet Avatar 6700 Fourier Transform Infrared Spectrometer of Thermal Fisher Company, the wave number range was 4000~650 cm^{-1}, and the resolution was 4 cm^{-1}. A sample was scanned for 32 times. The thermal weight loss analysis (TGA) under air atmosphere was conducted with the Perkin-Elmer TGA-7 series thermal analysis system, the temperature range was 100 °C to 700 °C, the heating rate was 20 °C/min, and the air flow rate was 20 mL/min. The absorbance of the methyl orange solution (MO) solution at the maximum absorption wavelength of 465 nm was measured with an ultraviolet-visible absorption spectrometer (Lovibond, ET99731). The measurement was repeated for three times, and the average value was calculated. The degree of degradation of MO was described by C_t/C_0 ($=A_t/A_0$). The C_t/C_0–t curve was plotted.

3. Results and Discussion

Light absorption range is one of the key factors affecting the photocatalytic performance of TiO_2 photocatalyst. As shown in Figure 2 (A), pure nano TiO_2 is white powder, which hardly absorbs visible light, so the photocatalytic activity of pure TiO_2 in the visible light region is very low. The C@TiO_2 is dark brown powder, indicating that the organic polyvinyl alcohol material has undergone thermal degradation on the surface of nano-TiO_2 and formed carbon coated nano TiO_2. It also shows that the nanoparticles can absorb visible light. Therefore, we tested the light absorption range of nano TiO_2 with Uv-Vis Spectrometer. The results are shown in Figure 3. Pure nano TiO_2 has obvious absorption of ultraviolet light below 400 nm and basically no absorption of visible light above 400 nm, the C@TiO_2 nanoparticles can not only absorb ultraviolet light below 400 nm, but also absorb visible light above 400 nm.

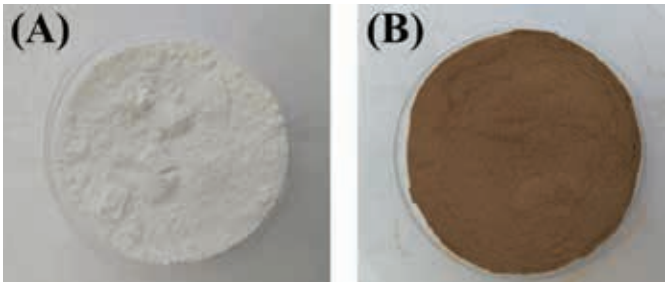

Figure 2. Photos of TiO_2 (A) and C@TiO_2 (B)

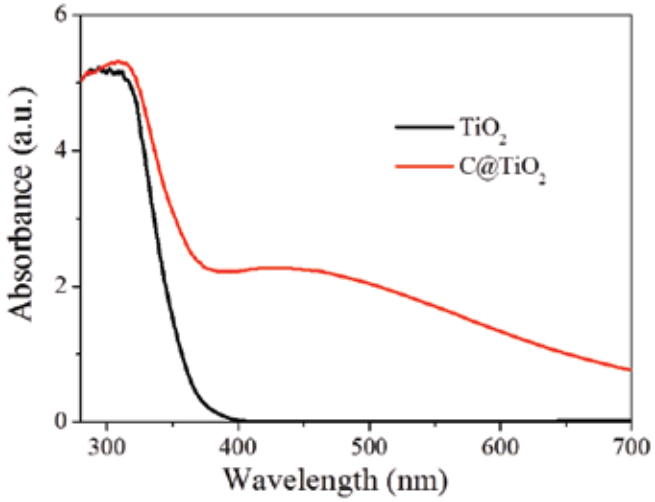

Figure 3 UV–Vis diffuse reflectance spectra of TiO_2 samples

We observed the morphology of nano TiO_2 by scanning electron microscope. The photo in Figure 4 shows that the pure nano TiO_2 particles have good dispersion, the particle size is less than 100nm, and the C@TiO_2 nanoparticles have obvious aggregates, but there are many voids on the surface of the aggregates, indicating that the carbon material slightly adheres the nano TiO_2 particles together. The element scanning function (EDX) of SEM was used to scan C@TiO_2 nanoparticles, as shown in the photo in Figure 5, the distribution of C, O and Ti is basically consistent with the shape of C@TiO_2 nanoparticles, the distribution of in nanoparticles The shape of nanoparticles is basically the same, indicating that the carbon material formed by thermal degradation of polymer is successfully coated on the surface of nano TiO_2, rather than the simple mixing of carbon and nano TiO_2.

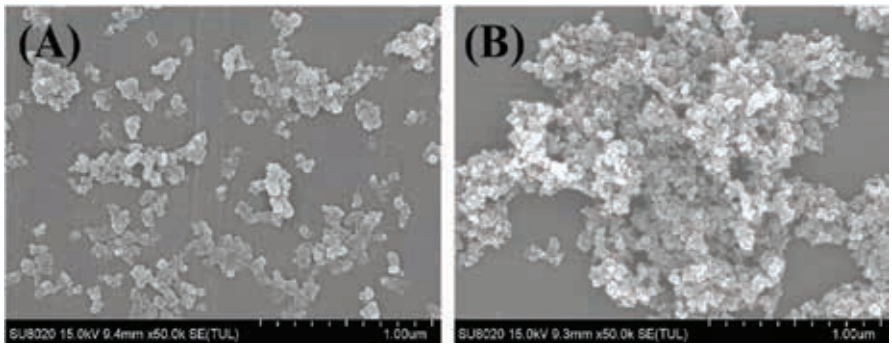

Figure 4. SEM images of TiO_2 (A) and C@TiO_2 (B)

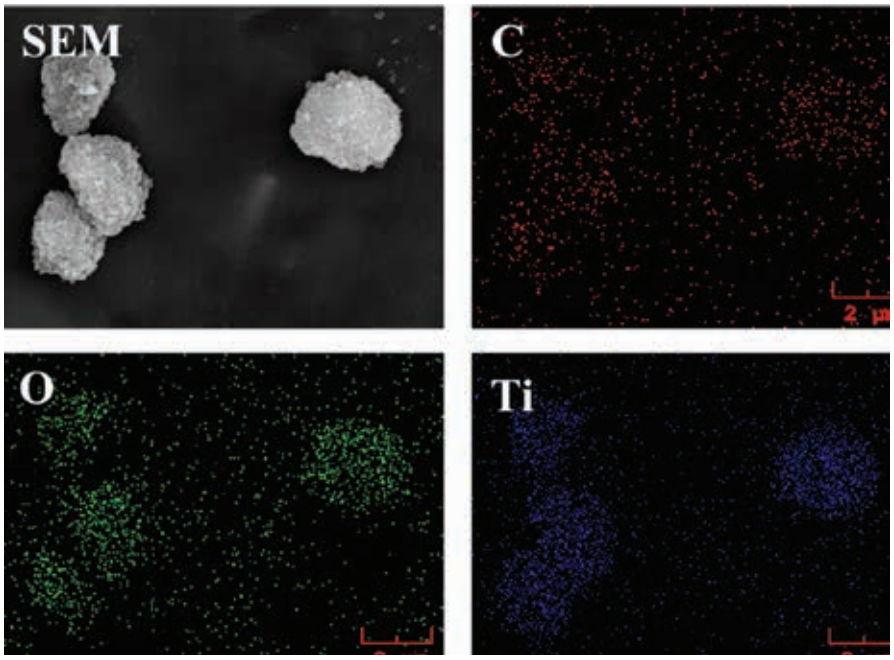

Figure 5. SEM and EDX images of TiO_2 and C@TiO_2

Pure nano TiO_2 and nano C@TiO_2 nanoparticles were further studied by TEM. The photo in Figure 6 show that the surface of pure nano TiO_2 is smooth and the particle size is about 20 nm. However, a fuzzy coating layer can be seen on the surface of C@TiO2 nanoparticles. The coating layer is evenly distributed and dense. The thickness of the coating layer is about 2.5nm. It can be concluded that the coating layer is a carbon material produced by thermal degradation of polymers, indicating that we have successfully prepared carbon coated nano titanium dioxide nanoparticles.

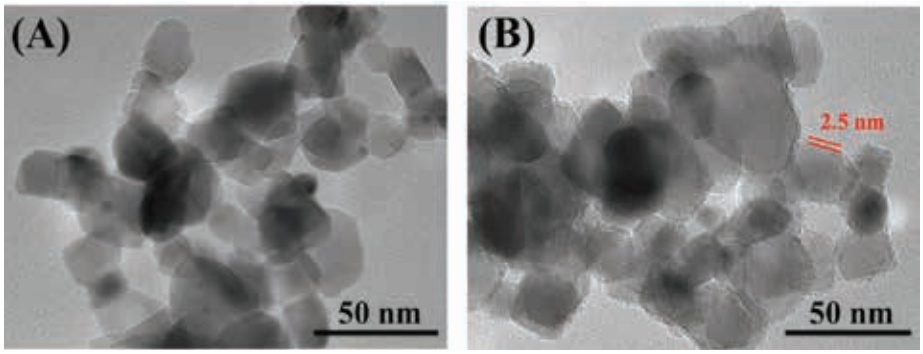

Figure 6. TEM images of TiO_2 (A) and C@TiO_2 (B)

The content of carbon in C@TiO_2 nanoparticles characterized by TGA, which is shown in Figure 7. Nano TiO_2 has good heat resistance, and does not contain organic substances. When heated to 600 °C, there is only 1.3% weight loss. These thermal weightlessness is mainly caused by the removal of adsorbed water on the surface of nano TiO_2. It is worth noting that, there is obvious thermal weight loss of C@ TiO_2 nanoparticles at 450 °C, which is mainly caused by the oxidation of carbon materials. The weight of TiO_2 and C@TiO_2 nanoparticles above 500 °C is basically unchanged,

The average weight is basically unchanged above 500 °C, indicating the carbon material on the surface of C@TiO_2 nanoparticles has been completely decomposed. At 600 °C, the weight loss of nano TiO_2 and C@TiO_2 nanoparticles is 1.3% and 4.4% respectively. So, the weight of carbon material coated on the surface of TiO_2 is about 3.1% in C@TiO_2 nanoparticles.

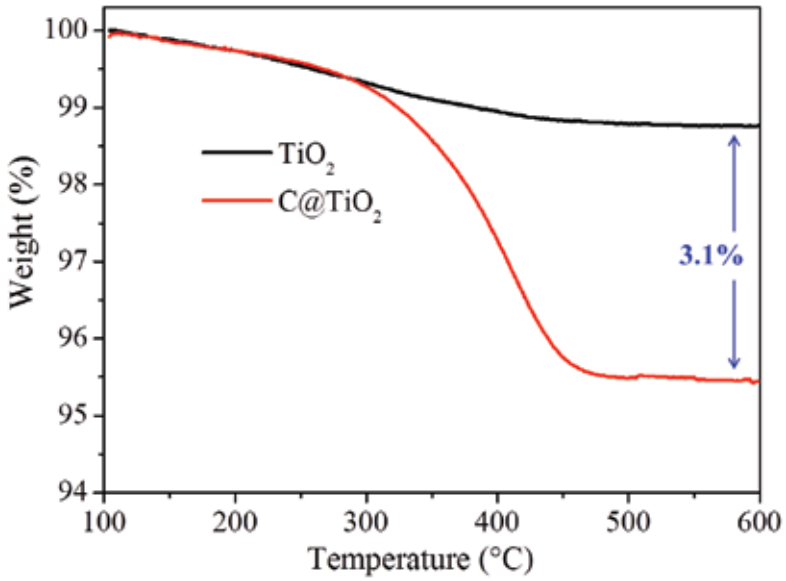

Figure 7. TGA of TiO_2 and C@TiO_2

The Fourier transform infrared spectrometer was used to further characterize the structure of C@TiO2 nanoparticles. According to the FTIR of nano TiO_2, the absorption peaks at 3270 cm^{-1} and 1643 cm^{-1} are attributed to the stretching vibration and bending vibration of OH, indicating that there is adsorbed water on the surface of nano TiO_2, which is consistent with the results of TGA. In C@TiO_2 nanoparticles, the absorption peaks at 3240 cm^{-1} and 1609 cm^{-1} are attributed to the absorption of OH, indicating that there is also adsorbed water on the surface of C@TiO_2 nanoparticles. But in C@TiO_2 nanoparticles, several

new absorption peaks have been observed, 2925 cm^{-1}, 1706 cm^{-1} and 1417 cm^{-1}. These peaks correspond to the stretching vibration of CH2, C=C double bond stretching vibration and CH2 bending vibration, indicating that the polymer is degraded into carbon on the surface of nano TiO_2, and formed C=C double bonds, which have been proved to be beneficial to the transmission of electrons[13; 14].

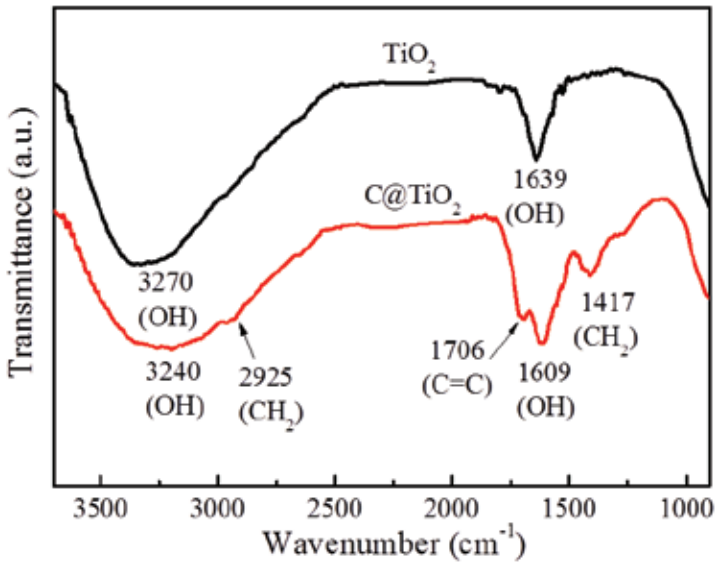

Figure 8. FTIR of TiO_2 and C@TiO_2

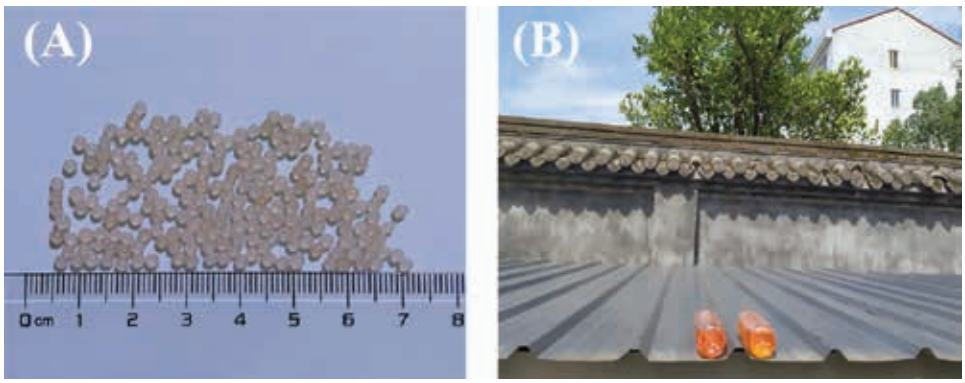

Figure 9. Photos of Ca-Alg/C@TiO_2 hydrogel pellets and photocatalysis under sunlight

Figure 9 shows the Ca-Alg/C@TiO_2 hydrogel pellets that we prepared, the diameter of pellets is about 2mm and color is brown. It shows that C@TiO_2 is more uniformly dispersed in calcium alginate. We mix the Ca-Alg/C@TiO_2 hydrogel pellets with the methyl orange solution, put them in a transparent bottle, and place them in a place where the sunlight can reach, and take samples every three days to test the concentration of pollutants. The results are shown in Figure 10, the methyl orange solution is orange-red, without the photocatalyst, the concentration of the methyl orange solution is almost unchanged after being irradiated by sunlight for 18 days, merely degraded about 3%. However, under the catalysis of Ca-Alg/C@TiO_2 hydrogel beads, the concentration of methyl orange solution decreased significantly. But as time passed, the decrease rate of the concentration of methyl orange solution slowed down. This is because that the photocatalytic process reaction is a first-order reaction, and as the solubility of the dye decreases, the contact efficiency between the photocatalyst and the pollutants decreases. Under the sunlight, the Ca-Alg/C@TiO_2 composite photocatalyst degraded about 96% of the methyl orange pollutants after 18 days. The color of

the solution was really close to colorless and transparent, and the appearance of hydrogel pellets did not change significantly, and the composite photocatalyst was easy to separate from pollutants.

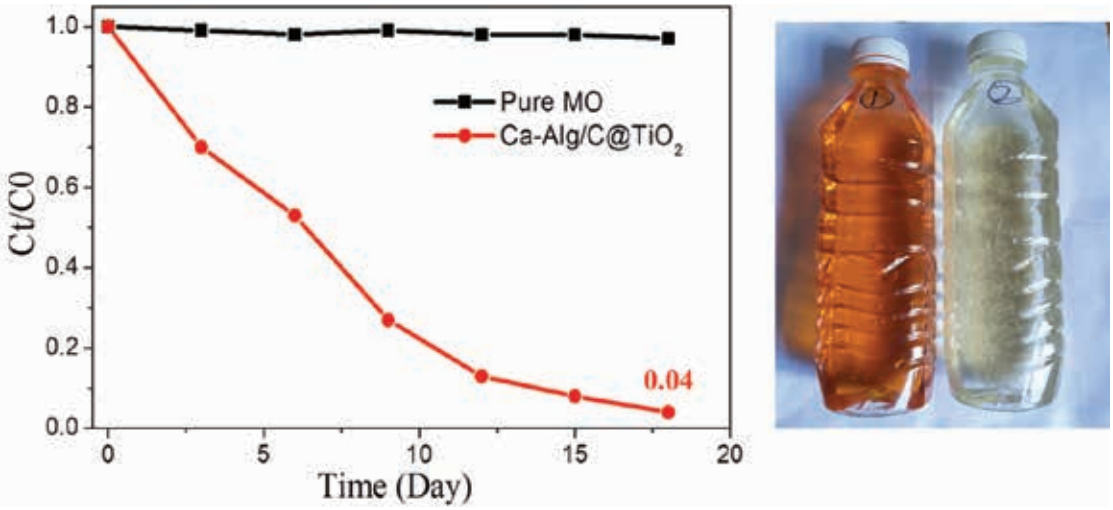

Figure 10. Photocatalytic degradation of Methyl orange solution by Ca-Alg/C@TiO_2 hydrogel pellets

4. Conclusion

Aiming at the problem that nano titanium dioxide cannot absorb visible light and is not easy to recycle, this paper proposes a simple and effective solution. Polyvinyl alcohol coated nano titanium dioxide was prepared by solution mixing, and the coating amount of polymer was easy to adjust. Then, by controlling the thermal degradation of polyvinyl alcohol on the surface of nano titanium dioxide to carbon, a dark brown carbon coated nano titanium dioxide composite photocatalyst was prepared. The carbon coating layer on the surface of nano titanium dioxide is about 2.5 nm, and the carbon content is about 3.1%. The structure of carbon material made by thermal degradation contains a large number of CH_2 and C = C chemical bonds. By embedding the carbon coated nano titanium dioxide in calcium alginate hydrogel, a supported photocatalyst with a diameter of about 2 mm was prepared. This Ca-Alg/C@TiO_2 composite hydrogel pellets have relatively good photocatalytic activity, which catalyzed about 96% of the pollutants under the sunlight in 18 days. In addition, these composite hydrogel pellets are easy to recycle.

References:

1. URL: https://www.who.int/health-topics/water-sanitation-and-hygiene-wash, in.
2. Lei P., Wang F., Zhang S., Ding Y., Zhao J., Yang M. Conjugation-grafted-TiO(2) nanohybrid for high photocatalytic efficiency under visible light, ACS applied materials & interfaces,– 6. 2014.– P. 2370–2376.
3. Mo J., Zhang Y., Xu Q., Lamson J. J., Zhao R. Photocatalytic purification of volatile organic compounds in indoor air: A literature review, Atmos. Environ.,– 43. 2009.– P. 2229–2246.
4. Zhang H., Lv X., Li Y., Wang Y., Li J. P25-Graphene Composite as a High Performance Photocatalyst, ACS Nano,– 4. 2010.– P. 380–386.
5. Li G., Wang F., Liu P., Chen Z., Lei P., Xu Z., Li Z., Ding Y., Zhang S., Yang M. Polymer dots grafted TiO_2 nanohybrids as high performance visible light photocatalysts, Chemosphere,– 197. 2018.– P. 526–534.
6. Li S., Li G., Chen Q., Wang F. Facile green synthesis of Degraded-PVA coated TiO_2 nanoparticles with enhanced photocatalytic activity under visible light, J. Phys. Chem. Solids,– 129. 2019.– P. 92–98.

7. Lei P., Wang F., Gao X., Ding Y., Zhang S., Zhao J., Liu S., Yang M. Immobilization of TiO_2 nanoparticles in polymeric substrates by chemical bonding for multi-cycle photodegradation of organic pollutants, J. Hazard. Mater., 227–228. 2012.– P. 185–194.
8. Martins N. C.T., Ângelo J., Girão A. V., Trindade T., Andrade L., Mendes A. N-doped carbon quantum dots/TiO_2 composite with improved photocatalytic activity, Applied Catalysis B: Environmental,– 193. 2016.– P. 67–74.
9. Tian J., Leng Y., Zhao Z., Xia Y., Sang Y., Hao P., Zhan J., Li M., Liu H. Carbon quantum dots/hydrogenated TiO_2 nanobelt heterostructures and their broad spectrum photocatalytic properties under UV, visible, and near-infrared irradiation, Nano Energy,– 11. 2015.– P. 419–427.
10. Yu X., Liu J., Yu Y., Zuo S., Li B. Preparation and visible light photocatalytic activity of carbon quantum dots/TiO_2 nanosheet composites, Carbon,– 68. 2014.– P. 718–724.
11. Hashemizad S., Montazer M. A. Rashidi, Influence of the surface hydrolysis on the functionality of poly(ethylene terephthalate) fabric treated with nanotitanium dioxide, J. Appl. Polym. Sci.,– 125. 2012.– P. 1176–1184.
12. Yao S., Li J., Shi Z. Immobilization of TiO_2 nanoparticles on activated carbon fiber and its photodegradation performance for organic pollutants, Particuology,– 8. 2010.– P. 272–278.
13. Sudhagar P., Herraiz-Cardona I., Park H., Song T., Noh S. H., Gimenez S., Sero I. M., Fabregat-Santiago F., Bisquert J., Terashima C., Paik U., Kang Y. S., Fujishima A., Han T. H. Exploring Graphene Quantum Dots/TiO_2 interface in photoelectrochemical reactions: Solar to fuel conversion, Electrochim. Acta,– 187. 2016.– P. 249–255.
14. Zhao L., Chen X., Wang X., Zhang Y., Wei W., Sun Y., Antonietti M., Titirici M. M. One-step solvothermal synthesis of a carbon@TiO(2) dyade structure effectively promoting visible-light photocatalysis, Adv. Mater.,– 22. 2010.– P. 3317–3321.

Contents